Major volatiles in the Earth's mantle beneath mid-ocean ridges and intraplate ocean islands

Rajdeep Dasgupta, Cyril Aubaud

1.1. Major volatiles in the Earth's mantle beneath mid-ocean ridges and intraplate ocean islands

Rajdeep Dasgupta[1]

Cyril Aubaud[2]

[1]Department of Earth, Environmental and Planetary Sciences, Rice University, 6100 Main Street, MS 126, Houston, TX 77005, USA

[2]Université Paris Cité, Institut de Physique du Globe de Paris, CNRS, Laboratoire de Géochimie des Isotopes Stables, 1, rue Jussieu - 75238 Paris cedex 05, France

Abstract

Composition of the Earth's ocean-atmosphere system is maintained over geologic timescale via outgassing of volatile elements from the Earth's mantle. Two major settings where volcanic outgassing takes place from the oceanic mantle are the mid-ocean ridges (MORs) and intraplate ocean islands (OIs). The outgassing flux of various volatiles such as water (H_2O), carbon dioxide (CO_2), sulfur (S), nitrogen (N), and halogens (e.g., chlorine, Cl) depend on their abundances, storage mechanisms, and fates during mantle partial melting and magma emplacement in the crust. In this chpater, we synthecize existing constraints on the major volatiles in the mid-ocean ridge basalts (MORBs) and ocean island basalts (OIBs) and their mantle sources. We present and discuss various techniques and approaches used to gather concentration, speciation, and elemental and isotopic compositions of carbon (C), hydrogen (H), sulfur (S), nitrogen (N), and halogens in submarine glasses, melt inclusions, and mantle-derived gases. We summarize literature estimates of elemental concentrations and isotopic compositions of the volatiles for MORB and OIB source mantles as well as the flux estimates of these volatiles from these mantle domains. To gain process-level understanding of extraction of the major volatiles from MORB and OIB source mantles, we also evaluate the storage mechanisms in the mantle, and the fates and inflluence of different volatiles during mantle melting. We discuss the relative efficiencies of release via mantle melting and exsolution for each of the major volatiles and how the redox states of the mantle impact such processes. Finally, we provide a perspective for open questions and challenges in the knowledge of volatiles and volatile-involved melting for the MORB and OIB source mantles from the Hadean to present.

Keywords: MORB, OIB, volatiles, water, carbon dioxide, sulfur, nitrogen, halogens, mantle, redox, oxygen fugacity, partial melting.

Key Points:

● The bulk silicate Earth (BSE) volatile budgets and compositions are largely influenced by the mid-oceanic ridge (MOR) and ocean island (OI) basalt source mantle compositions.

● Elemental and isotopic compositions of major volatiles in the oceanic mantle are learned from the submarine glasses, melt inclusions, derivative fluids at MOR and OI settings.

● We provide a brief overview of analytical techniques used to measure volatiles.

● We present an overview of the concentration and stable isotopic ratios of volatiles in MORB and OIB melts and sources.

● Deeper OIB source mantles appear more volatile-rich and isotopically distinct compared to the MORB source mantles in terms of C, H, and N.

● The outflux of H_2O, CO_2, N, and S through MOR and OI settings can be understood by the storage mechanisms, partitioning behavior during mantle melting, and the extent of fluid exsolution during magma emplacement.

● Hydrogen and nitrogen gets released from nominally volatile-free silicates whereas carbon and sulfur gets released via dissolution of trace accessory phases.

● Hotter and perhaps more oxidized OIB source mantles lead to deeper melting-induced release of C and H_2O compared to that from the MORB source mantles.

● Uncertainties in the oxygen fugacity, fO_2 with depth in the oceanic mantles affect the exact depth of C-induced mantle melting and the magnitude of release of all volatiles.

● Understanding the influences of major volatiles in the MORB and OIB source melting domains through deep time would require coupling redox and thermal evolution of the mantle and evolution of its convective vigor and mode.

1.1.1. Introduction
1.1.2. Volatile abundance of the oceanic mantle – Constraints from natural samples
    1.1.2.1. Submarine glasses
    1.1.2.2. Melt inclusions
1.1.3. A brief overview of the techniques used to measure volatiles in glasses and melt inclsions
    1.1.3.1. Dissolved volatiles
        1.1.3.1.1. Electron Probe Micro Analyzer (EPMA)
        1.1.3.1.2. Ion microprobe/Secondary Ions Mass Spectrometry (SIMS)
        1.1.3.1.3. Fourier Transformed Infrared (FTIR) Spectroscopy
        1.1.3.1.4. Incremental step-heating technique with manometry and mass spectrometry
        1.1.3.1.5. Wet chemistry
        1.1.3.1.6. Other techniques
    1.1.3.2. Measurement of the gas phase
        1.1.3.2.1. Crushing under vacuum

1.1.3.2.2. Calculation of the vesicle gas content based on vesicularity and an equation of state
1.1.3.2.3. Determination of the total gas content in melt inclusions
1.1.4. General behavior of volatiles in magmas
1.1.5. Carbon, water, sulfur, nitrogen, halogens inventories of the Earth's oceanic mantle (MORB and OIB sources)
1.1.5.1. Carbon
1.1.5.1.1. Measurement of the carbon concentration dissolved in basaltic glasses
1.1.5.1.2. Simultaneous measurement of the carbon content and carbon stable isotope coupled with a mass balanced degassing model
1.1.5.1.3. Carbon scaled to He
1.1.5.1.4. Carbon scaled to a trace element (Nb or Ba)
1.1.5.1.5. Carbon estimated from major element systematics
1.1.5.1.6. Summary of elemental and isotopic composition of MORB and OIB source carbon
1.1.5.2. Water
1.1.5.3. Sulfur
1.1.5.4. Halogens
1.1.5.4.1. Chlorine
1.1.5.4.2. Fluorine
1.1.5.4..3. Bromine
1.1.5.4.4. Iodine
1.1.5.5. Nitrogen
1.1.6. Isotopes of C, H, S, N and halogens in the oceanic mantle
1.1.6.1 Carbon isotopes
1.1.6.2. Hydrogen isotopes
1.1.6.3. Sulfur isotopes
1.1.6.4. Halogen (chlorine) isotopes
1.1.6.5. Nitrogen isotopes
1.1.7. Summary of global concentration and stable isotope distribution in MORB and OIB source
1.1.8. Storage mechanisms of volatiles in the MORB and OIB source mantles
1.1.8.1. Water storage
1.1.8.2. Carbon storage
1.1.8.3. Sulfur storage
1.1.8.4. Nitrogen storage
1.1.9. The fate of volatiles during MORB and OIB source melting
1.1.9.1. The roles and fates of water during MORB and OIB source melting
1.1.9.2. The roles and fates of carbon during mantle melting
1.1.9.3. The combined roles of CO_2 and H_2O during MORB and OIB source melting
1.1.9.4. The fate of sulfur during MORB and OIB source mantle melting
1.1.9.5. The fate of nitrogen during mantle melting
1.1.10. Fluxed melting in the MORB and OIB sources and flux of volatiles through MOR and OI settings
1.1.10.1. Modern Earth
1.1.10.2. The effects of redox and compositional heterogeneity
1.1.10.3. Ancient Earth MORB and OIB source melting

1.1.11. Outlook
Acknowledgements
References

1.1.1. Introduction

Earth's mantle is the largest terrestrial reservoir by mass. Because of this, the mantle contains the greatest inventory of many trace elements (i.e., elements present in concentration <0.1 wt.%). Some of the most important trace elements in the mantle are the major volatile elements such as carbon (C), hydrogen (H), sulfur (S), and nitrogen (N). These elements are also essential for life as we know it. Although these elements are atmophile and are concentrated in in the Earth's atmosphere and surficial reservoirs such as oceans and crusts, because of the large reservoir sizes, either the core or the mantle of the Earth is the largest terrestrial reservoir for these elements (e.g., Bajgain et al., 2021, Dasgupta, 2013, Dasgupta and Hirschmann, 2010, Johnson and Goldblatt, 2015, Plank and Manning, 2019). Between the two deep reservoirs, i.e., the core and the mantle, the mantle's volatile budget is of greater importance because this reservoir exchanges volatiles with the crust-ocean-atmosphere system via volcanism and tectonic recycling over geologic time (e.g., Dasgupta, 2013, Fuentes et al., 2019, Lee et al., 2019, McGovern and Schubert, 1989, Sleep and Zahnle, 2001). Therefore, the abundance of the major volatiles in the mantle reservoirs and their spatio-temporal evolution are also intimately linked to the long-term chemical habitability of the planet Earth. Furthermore, many of these volatile elements, in various forms, significantly influence the geophysical, geochemical, and rheological properties and processes in the Earth's interior. For example, carbon in the form of carbonates and water in the form of fluid or hydrous phases or trace constituents in minerals, lower the melting temperatures of and partial melt compositions of mantle rocks (e.g., Asimow and Langmuir, 2003, Dasgupta, 2018, Grove et al., 2006, Lara and Dasgupta, 2023, Sun and Dasgupta, 2019, Ulmer, 2001). Water in the form of hydrous defects affect elastic and rheologic properties of nominally anhydrous mantle minerals (e.g., Hirth and Kohlstedt, 1996, Jacobsen et al., 2008). The presence of dissolved water and CO_2 in mantle melts affect electrical and transport properties of mantle domains (e.g., Gaillard et al., 2008, Ni et al., 2011) as well as mantle-derived melts (Ghosh et al., 2007, Karki et al., 2021, Kono et al., 2014). Sulfur in the form of sulfides or sulfates affect partitioning and mobility of key ore-forming elements (e.g., Chowdhury et al., 2022, Ding and Dasgupta, 2017, Lee et al., 2012, Li and Audétat, 2015).

Given the bulk silicate Earth (BSE) abundance of volatile elements are largely controlled by the inventories of the volatile elements in the Earth's mantle, any models that attempt to explain the origin of volatiles on Earth or more specifically in the BSE also need to rely heavily on the estimates of volatiles in BSE (Blanchard et al., 2022, Grewal et al., 2019a, Grewal et al., 2021, Grewal et al., 2019b). The estimated abundance of volatiles in the Earth's oceanic mantle also is used heavily in all models of the origin of Earth-Moon system and for comparison with other rocky planets (Ding et al., 2018, Saal et al., 2008, Saal et al., 2013). Therefore, reliable

estimates of the Earth's oceanic mantle volatile budgets are important for a number Earth and planetary science disciplines including astrobiology and origin of life on Earth.

The biggest challenge in constraining the major volatiles in the mantle is that most part of the mantle is inaccessible for direct sampling. Furthermore, even if some mantle domains are accessed via rare, direct samples, such samples may not preserve the original abundance of the elements of interest, because of their volatility. The question therefore is how and how well we know the mantle budget of the major volatiles. There are two main approaches that can be taken to constrain the abundance of volatile elements in the mantle.

The first is a forward approach, which traces the fate of various volatiles during formation of the Solar System, its planets, and early differentiation of the rocky bodies including Earth. This approach provides insightful, process-level understanding of the range of possibilities in establishing the volatile inventory of Earth's major reservoirs. This approach also provides suggestions as to how and when various volatiles may have come in to Earth and how their abundance may have changed during the formative years of the planet. An advantage of probing the mantle volatile abundance via this forward approach is that bulk mantle inventories may be constrained that are otherwise difficult to bracket through other means. However, in this forward approach, the range of possibilities remains too large to quantify the mantle abundance of volatiles in the modern Earth. This is owing to the uncertainties in many factors, including but not limited to, the compositions primary terrestrial building blocks (e.g., Dauphas, 2017, Piani et al., 2020), the nature of processing of such feedstocks prior to accretion (Grewal et al., 2021, Grewal et al., 2019b, Li et al., 2023), and the effects of early terrestrial differentiation (e.g., Boujibar et al., 2014, Chi et al., 2014, Clesi et al., 2018, Dasgupta and Grewal, 2019, Grewal et al., 2019a, Hirschmann, 2016, Keppler and Golabek, 2019, Li et al., 2016, Li et al., 2023).

The second approach takes advantage of direct observation based on natural, mantle-derived samples (e.g., Cartigny et al., 2008, Marty, 2012, Marty et al., 2020, Saal et al., 2002). The advantage of this approach is that it provides direct constraints on the volatile abundance of the present-day mantle domains from which they derive. A limitation of this approach, however, is that the whole-mantle volatile inventory may be difficult to reliably constrain because the deep mantle is rarely sampled. Also, the abundance and chemistry of the present-day volatile inventory of the mantle may not tell us about their origin and evolution.

In this chapter, we discuss the available constraints for the major volatiles – their abundance, elemental and isotopic chemistry, and influence on melting and magmatic release – in the Earth's convective mantle. Given the Earth's convective mantle is chiefly accessed via generation and sampling of mid-ocean ridge basalts (MORBs) and intraplate ocean island basalts (OIBs), we focus on volatiles in MORBs and OIBs and their source regions. Given the paucity of samples that allow direct probing of the mantle source abundance of volatiles, most constraints come from basaltic glasses and melt inclusions and occasionally from bulk extrusive rocks. However, using basalts to back track mantle inventories require a good understanding of the fate of various volatiles during various processes leading to basalt petrogenesis and sampling. These processes include mantle partial melting, melt percolation and emplacement, magmatic differentiation including fractional crystallization and degassing. Many of these processes are

understood based on laboratory experiments and thermodynamic and geochemical models based on such data. Hence in this chapter, we will discuss constraints based on both natural samples' and experimental studies.

1.1.2. Volatile abundance of the oceanic mantle – Constraints from natural samples

Obtaining unmodified direct samples from the mantle, especially the asthenospheric or convective mantle, is virtually impossible. The composition of peridotites that are accessible at the surface is modified by various primary and secondary processes that are problematic for preservation of primary volatiles (Canil, 1990). Geochemists have found that magmas erupted from volcanoes are natural windows to probe the mantle composition (Dasgupta et al., 2010). For volatile species, the task is complicated by degassing processes that lead to partial to near-complete loss of volatiles from magmas. Researchers have established that natural volcanic glasses (rapidly quenched melts) are the best recorders of volatiles. This was first understood by noble gas geochemists in the 1970s and subsequently adopted by researchers on other major volatile species (CO_2, H_2O, F, S, and Cl) (Sobolev and Chaussidon, 1996). There is, therefore, a large database on these species in submarine volcanic glasses and glassy melt inclusions (from subglacial and submarine volcanoes, and also from subaerial volcanoes under the condition that the erupted tephras belong to rapidly cooled products such as scoria and not to slowly cooled massive lava flows).
For these reasons, in this chapter we focus on submarine glasses and melt inclusions. Each of these sample type has advantages and caveats.

1.1.2.1. Submarine glasses

<u>Advantages:</u>
- Large amount of material available (several grams), which allows some bulk analysis to be made.
- Fairly representative of the erupted melt.
- Weakly contaminated by the local environment at the eruption setting; if contamination is present, it occurred before the melt is quenched.

<u>Problems:</u>
- The melts are already significantly degassed, particularly in CO_2.
- They are quenched or rapidly cooled products so the gas phase is modified by cooling (Javoy and Pineau, 1991). The dissolved phase may also be affected by quenching (see the debate on the speciation of water and carbon dioxide in melt and glass, e.g. Nowak et al., 2003; Cody et al., 2020);
- There is an unavoidable sampling bias for the gas phase called vesicle bursting (Burnard, 1999) or also called the popping rock effect (Hekinian et al., 1973). The natural glasses are sampled at relatively high pressure (generally hundreds of bars) and brought to the surface where the ambient pressure is lower (one atmosphere). Then, the glasses are put under vacuum (10^{-9} bars)

for analysis. These two decompression steps lead to some extent of vesicle bursting, a phenomenon that is sometimes spectacularly observed on the deck of sampling vessel during scientific cruises (the so-called popping-rocks) (Hekinian et al., 1973, Jones et al., 2019, Sarda and Graham, 1990). This bursting effect is due to the difference between the pressure inside the vesicles and the ambient pressure and to the low strength of glass sample especially those containing dissolved H_2O (Romano et al., 1996).

The direct consequence of this process is that the gas content that is extracted by crushing is lower than the amount of gas present at eruption. The original gas concentration can be reconstructed on the basis of vesicularity measurements and a gas equation of state (Gerlach, 1990; (Javoy and Pineau, 1991, Jones et al., 2020). There is, however, a debate on the correct procedure to adopt in order to give accurate gas contents (Jones et al., 2020)(see next section).

- Because the sampled glasses are aggregated melts, they are the result of some homogenization effect that may erase some degree of source heterogeneity.
- Gas dilution/accumulation of a magma that has degassed in closed system can decrease or increase (respectively) the total gas content of a melt. For example, the reconstructed total gas content (mostly CO_2) of the popping rock 2πD43 is considered by Javoy and Pineau (1991) as the true original gas content of the primary melt. Other workers consider that this sample suffered from accumulation of gas in a magma chamber and that its original total gas content is lower (Jones et al., 2019). We note here that some pieces of the 2πD43 samples are characterized by a lower vesicularity (5 vol% for the pieces analyzed by Burnard et al., 1999) than the pieces analyzed by Sarda and Graham (1990) and Javoy and Pineau (1991).
- The glasses may be supersaturated in volatiles and may not give accurate pressure when used as a paleobarometer.

1.1.2.2. Melt inclusions

<u>Advantages:</u>

- The main advantage of melt inclusions is that they allow sampling of melts from pressures higher than the eruption pressure of submarine glasses. Thus, they represent earlier stages of degassing and generally give higher CO_2 contents than submarine glasses.
- The melt inclusions may sometimes record melt compositions before mixing at shallow level and thus give a better idea of source heterogeneity and/or complexity of processes occurring in the plumbing system.

<u>Problems:</u>

- The inclusions are not always quenched to glasses. Rehomogeneization by heating and quenching needs to be applied in such cases. Rehomogeneization at high pressures has sometimes been used (Mironov et al., 2015).
- Diffusion through the host mineral can modify the volatile content of a melt inclusion. This principally affects hydrogen, which can diffuse in and out of the inclusion through olivine (e.g., Bucholz et al., 2013, Chen et al., 2011, Gaetani et al., 2012, Hanyu et al., 2020, Kent, 2008). For geobarometers based on CO_2+H_2O solubility, this can alter the resulting calculated pressure.

- Cooling leads to post-entrapment crystallization, pressure decrease, thermal contraction of the melt and the formation of shrinkage bubble. Fe-loss can also occur (Danyushevsky et al., 2000). The melt composition is modified and the true CO_2 content needs to be reconstructed taking into account the vapor phase (Hanyu et al., 2020, Wallace et al., 2015).
- Melts that are trapped in melt inclusions are already degassed (Matthews et al., 2021). CO_2 vapor loss before entrapment can occur because CO_2 saturation happens deep in a magmatic system (Schiano et al., 1998).
- Procedure for correction of post-entrapment crystallization is well-established for olivine. For other minerals (e.g., plagioclase, clinopyroxene, spinel), no standardized procedure exists so few or no correction is applied.
- Mixing: final melts are generally aggregated melts from fractional melting. It is a general case that depleted and enriched melts mix prior to eruption influencing, for example, CO_2 to trace elements ratios (Matthews et al., 2021, Matthews et al., 2017).
- Melt inclusion decrepitation (in one or multiple events) or CO_2 vapor loss after entrapment: a mineral can hold an overpressure but its capacity to do so is not infinite. When the pressure inside a melt inclusion is too high compared to the pressure of the surrounding melt, the inclusion will decrepitate and be re-annealed. For example, Wanamaker et al. (1990) showed that an olivine may support overpressures of up to 2.2 kbar. For Iceland melt inclusions, Matthews et al. (2021) found that the maximum saturation pressure in olivines is 3 kbar suggesting that there is a limit to what an olivine can record in terms of pressure (equivalent to volatile content). Matthews et al. (2021) accordingly concluded that almost all Icelandic melt inclusions are decrepitates.
- Regassing of a melt in CO_2 can occur if, for example, CO_2 fluxing in a magmatic system is pervasive (e.g., van Hinsberg et al., 2016).
- Melt inclusions are too small for bulk extraction techniques (step heating technique) and only point analyses (SIMS or FTIR) can be performed). These techniques cannot measure isotopes or are not precise enough for $\delta^{13}C$ measurements, for example.

1.1.3. A brief overview of the techniques used to measure volatiles in glasses and melt inclusions

1.1.3.1. Dissolved volatiles

1.1.3.1.1. Electron Probe Micro Analyzer (EPMA)

This technique is routinely used to measure the concentrations of S, F, and Cl. The technique can achieve low detection limits and good precision. They require a polish section of the sample. Spatial resolution is typically 1 micron for conventional instrument with W- of LaB_6-filaments and sub-micron for field emission instrument (FE-EPMA). This allows diffusion experiment to be undertaken. CO_2 and H_2O cannot be measured by this technique except high water and/or CO_2 contents that can be estimated by difference of the analytical total from 100 wt.% (e.g. Hughes et al., 2019, Lane and Dalton, 1994, Saha and Dasgupta, 2019, Sun and Dasgupta, 2019).

1.1.3.1.2. Ion microprobe/Secondary Ions Mass Spectrometry (SIMS)

This technique is now routinely used to measure the concentrations of H_2O, CO_2, S, F, Cl (e.g. Hauri et al., 2002) with good precision both in submarine glasses and MIs. The only requirement is to have standards already characterized for the species of interest in samples with a matrix similar to the unknowns. Carbon isotope measurement in natural glasses has been attempted (e.g., Hauri, 2002) but few data have been produced and they are plagued with poor precision. The spatial resolution is typically 30 μm. The nanoSIMS can also be used for such measurements with 1 μm spatial resolution. These techniques require a polished section.

1.1.3.1.3. Fourier Transformed Infrared (FTIR) Spectroscopy

Since the 1980s, FTIR spectrometers have been used to measure CO_2 and H_2O in submarine glasses and glass inclusions. With excellent limit of detection (1 ppm) and precision. Accuracy is dependent on an independent calibration by another technique (step-heating/manometry or nuclear reactions) (e.g., Ihinger et al., 1994). This technique requires doubly polished thick sections because the measurement is made in transmission through the sample. Typical beam size is 100 μm and can be reduced down to 30 μm but with signal loss and lower signal to noise ratio. Mapping capabilities is a new feature of recent spectrometers (von Aulock et al., 2014, Wysoczanski and Tani, 2006). A synchrotron energetic source can reduce the beam size down to 1 μm (Guilhaumou et al., 2005). FTIR spectroscopy also measures speciation of both CO_2 and H_2O (Stolper, 1982; Fine and Stolper, 1985), which provides information about post-quenching water diffusion into the glass (e.g. Wallace, 1998) and the timescales of quenching (Newmann et al., 1988).

1.1.3.1.4. Incremental step-heating technique with manometry and mass spectrometry

With this technique, CO_2 and H_2O concentrations can be obtained and it is currently the sole technique able to measure carbon isotopes (expressed as $\delta^{13}C$-values) of dissolved carbon (Des Marais and Moore, 1984, Macpherson and Mattey, 1994, Mattey et al., 1984, Pineau and Javoy, 1994). Some significant amount of sample is required, however, i.e., from a few tens of milligrams for static mass spectrometry to up to 300-1000 mg for dynamic mass spectrometry. It can achieve low detection limit (a few ppm by weight CO_2) and a good precision both on concentrations (lower than 10% relative 1σ and ±0.2 ‰ for $\delta^{13}C$ value).

1.1.3.1.5. Wet chemistry

For some peculiar applications like isotopic measurements, wet chemistry is used to extract volatiles from a natural glass. This is the case for chlorine stable isotopes (Bonifacie et al., 2007) and sulfur stable isotopes (Labidi et al., 2012).

1.1.3.1.6. Other techniques

Nuclear techniques can also be used but are less common due to restricted access and cost. They have been mostly used to calibrate other techniques (Bureau et al., 2009).

1.1.3.2. Measurement of the gas phase

1.1.3.2.1. Crushing under vacuum

This technique consists of crushing a sample under vacuum to release gases enclosed in vesicles. The gases are then purified, cryogenically separated and the amount is measured by manometry (either with a mercury manometer or a membrane capacitance barometer). The purified CO_2 is measured by mass spectrometry to obtain the $\delta^{13}C$-values. However, the measured vesicle gas concentration is always biased to low values due to vesicle bursting as described in the previous section.

1.1.3.2.2. Calculation of the vesicle gas content based on vesicularity and an equation of state

The principle of the calculation using this approach is to obtain the vesicle total gas content (essentially CO_2 in most scenarios) on the basis of vesicularity and an equation of state.

Sarda and Graham (1990), in their discussion on the vesicle gas content, considered only the measured gas content obtained by another study (0.21 wt%, Javoy et al. 1986). Gerlach (1991), however, pointed out that popping of the rocks decreased their measured vesicle gas content and that the real total gas content should be calculated on the basis of vesicularity. This calculation relies of the perfect gas law at the temperature of glass transition taken to be 1000 °C (1273 K) by Gerlach (1991) and at the pressure of eruption of the melt. He obtained calculated CO_2 concentrations of 0.8-1.0 wt%, about five times the measured CO_2 amount. This calculation was confirmed by Graham and Sarda (1991), who also considered a rigid temperature of 1000 °C.

A similar calculation is conducted by Javoy and Pineau (1991) for the popping rock 2πD43. However, these authors consider a temperature of rigidity of 1000 K, a temperature significantly different from the one taken by Gerlach (1991) and Graham and Sarda (1991). Although they did not discuss the choice of this temperature, 1000 K is a better choice than 1273 K because, as a rule of thumb, the temperature of the glass transition of a melt is 2/3 of the melt temperature (Richet and Polian, 1998). The calculation of Javoy and Pineau (1991) was subsequently reused by several studies (e.g., Aubaud et al., 2004c, Hekinian et al., 2000, Pineau et al., 2004).

In all these studies, it is assumed that equilibrium prevails (the pressure of glass transition at which the bubble size is fixed is taken as that of the collection pressure). However, in general, MORB are supersaturated with respect to CO_2. Even the popping rock 2πD43 show slight CO_2 supersaturation (Pineau and Javoy, 1994). Therefore, in the calculation, the pressure that should be used is the saturation pressure that is generally higher than the collection pressure due to supersaturation. In this case, the calculated vesicle CO_2 amount is larger than that reported in the studies on the subject.

Recently Jones et al. (2020) has challenged the approach of Gerlach (1991) and Javoy and Pineau (1991) to calculate the vesicle CO_2 content. They suggest that previous calculations are in error for two reasons:

(1) The assumption of ideality is incorrect. It is more accurate to use a modified Redlich-Kwong equation of state instead of the perfect gas law.

(2) The temperature that should be used in the calculation is not the temperature of the glass transition (726 °C in Jones et al., 2020) but the magmatic temperature (1200 °C, Jones et al., 2020). The reason invoked for this choice is that if the temperature of glass transition is chosen, this would imply a gas CO_2 density in vesicles that is too high compared to what is actually measured by Raman spectroscopy (see the discussion in their section 5.3, Jones et al., 2020).

Regarding the first point, the assumption of ideality is not a major source of error because at hundreds of bars, deviation from ideality is not large and should be considered negligible. Calculation of the data presented by Jones et al. (2020, their figure 8) with the equation of Javoy and Pineau (1991) indicates that the difference in calculated gas content is essentially caused by the difference in the temperature chosen to make the calculation (point 2). We note that Jones et al. (2020), similarly to previous workers, also perform their calculation considering the pressure of eruption and not the saturation pressure. This choice could also be a source of error if the sample is supersaturated in CO_2 at the point of eruption. Systematic and accurate measurement of vesicle CO_2 density by Raman could potentially resolve this issue in the future.

1.1.3.2.3. Determination of the total gas content in melt inclusions

Although the measurement of dissolved CO_2 (and other volatiles) in melt inclusions are common, the determination of the total CO_2 content must often be completed with the determination of the amount of CO_2 in the vapor phase present in the melt inclusion (the shrinkage bubble). This quantitative measurement has been recently tackled by different methods (Cannatelli, 2015, Gerlach, 1991, Lowenstern, 2015) that are briefly summarized here.

(1) The first method is called rehomogeneization. It consists in heating the MI to re-dissolve the bubble and to quench it in order to maintain the volatiles dissolved in the melt (glass). The dissolved volatiles are then measured by FTIR or SIMS (e.g. Wallace et al., 2015). This technique has some problems, however: to limit H_2O loss it is necessary to heat quickly at high temperature. This leads to partial dissolution of the olivine host and another correction is necessary. Despite this procedure, a bubble can still form during quenching and some amount of CO_2 can be unaccounted for (Wallace et al., 2015).

(2) Calculate the CO_2 of the bubble and add it to the dissolved CO_2 in the glass measured by a conventional technique (SIMS or FTIR). The most common technique is to measure the CO_2 density and to measure the bubble volume fraction in the inclusion. The CO_2 content in wt.% is then:

458 $[CO_2]$ = CO_2 density × bubble_fraction / glass density (1)
459
460 The CO_2 density is commonly obtained by Raman spectroscopy (Aster et al., 2016, Esposito et
461 al., 2011, Moore et al., 2015). It requires accurate calibration, which can vary from one
462 instrument to another due to various factors (Lamadrid et al., 2017). Vesicle size fraction can be
463 obtained by optical measurements with a microscope of by μX-Ray tomography (Hanyu et al.,
464 2020).
465
466 **1.1.4. General behavior of volatiles in magmas**
467
468 Each volatile in magmatic system has its own behavior depending on its properties and
469 concentration. This will dictate the phase where the gas is present and the techniques that can be
470 used to measure it. These are summarized in Table 1.
471
472 **Table 1.** Summary of typical behavior of volatiles in MORB and OIB submarine glasses and
473 melt inclusions and their most common measurement techniques
474

Volatile species	Phase where it is present	General behavior	Technique of measurement of concentration
CO_2	Vesicle and Glass MIs: glass and shrinkage bubble	Major volatile; Very low solubility in silicate melts. Generally highly degassed except in rare undegassed samples or in vesicles-rich popping rocks (where exsolved CO_2 is kept)	Vesicles: by crushing in vacuum Glass, MIs: FTIR, SIMS, incremental step-heating/manometry Shrinkage bubble:size by microscopic technique and micro X-ray tomography Concentration by Raman
H_2O	Mainly dissolved in glass and MIs present in vesicles only for water rich systems (OIB) and/or at shallow depths	highly soluble in silicate melts; prone to diffusion in and out of the mineral host in MIs	Glass: FTIR, SIMS, step-heating, Raman MIs: FTIR, SIMS
S	Glass and sulfide precipitates, partly in vesicles in some OIBs	highly soluble, dependent on Fe content of the melt; depends on oxygen fugacity	Electron microprobe, SIMS, wet chemistry bulk extraction for isotopes

N	Vesicles	low solubility; prone to atmospheric contamination	static mass spectrometry
F	Glass	highly soluble	Electron microprobe, SIMS
Cl, (Br, I)	Glass	highly soluble; prone to brine contamination	Electron microprobe, SIMS, irradiation/gamma counting/noble gas MS, pyrohydrolysis

1.1.5. Carbon, water, sulfur, nitrogen, halogens inventories of the Earth's oceanic mantle (MORB and OIB sources)

1.1.5.1. Carbon

The carbon concentration dissolved in MORB and hotspot submarine glasses is presented against the dissolved water content in Figure 1. For MORB, the dissolved CO_2 content vary from a few ppm up to 600 ppm (Fig. 1a). For hotspot glasses, the dissolved CO_2 content vary from a few ppm up to 800 ppm (Figures 1B and 1C). In both cases, the range of CO_2 concentration is similar, a feature that cannot be reconciled with the larger incompatible element contents measured in hotspot samples compared to MORB samples (acknowledging that carbon is classified as an incompatible element as well). A factor other than the enrichment of C in the source of the magma must control the CO_2 content in the melt.

Because of its low solubility in basaltic magmas (Dixon et al., 1995), carbon is extensively degassed in submarine basaltic glasses, independently of their magmatic source. Therefore, at first order, the similar range of CO_2 content in MORB and hotspot melts reflects a similar range of depth of eruption. As a result, obtaining the CO_2 of primary magmas before degassing is a challenge. Only in rare occasions, the bulk C can be measured or reconstructed with less ambiguity. Following are the type of samples and approaches that have been utilized by the scientific community to constrain carbon budget of the MORB or OIB sources.

1) Rare submarine MORB and OIB glasses are CO_2-vapor undersaturated (Hauri et al., 2017, Michael and Graham, 2015, Saal et al., 2002). Direct measurement of these samples can, therefore, be used to determine C content in the mantle (after correction from partial melting and normalization to an incompatible metallic trace element).

2) Gas-rich samples such as 14 °N and 34 °N mid-Atlantic ridge popping rocks (Cartigny et al., 2008, Javoy and Pineau, 1991) and some high-vesicularity mafic glasses from Society and Pitcairn (Aubaud et al., 2005, 2006). The identification of the mantle isotopic signature in vesicle of some gas-rich samples leads to the assumption that they have degassed under a closed system.

Therefore, the calculated CO_2 content obtained with the vesicularity is taken as representative of the initial CO_2 content of the melt. This is valid only if the calculation procedure does not induce a bias (e.g. Jones et al., 2020) or if the sample did not suffer from gas phase accumulation or dilution effects.

Apart from these two specific sample types, all other submarine samples are degassed, in the sense that part of the vapor phase is lost. Initial C content can only be inferred by reconstructions that are often too inaccurate to provide a reliable answer. Several approaches have been undertaken to address this problem:

1.1.5.1.1. Measurement of the carbon concentration dissolved in basaltic glasses

With accumulation of data on natural samples, it has been recognized, however, that the carbon concentration is controlled by the depth of eruption. When comparing the saturation pressure for MORBs (Figure 2a) and for OIBs (Figure 2b) submarine glasses against the collection pressure, one can observe that most MORB glasses are supersaturated and most OIB glasses are saturated with respect to a CO_2+H_2O gas phase. For MORBs, this supersaturation originates from CO_2 due to slow degassing kinetics combined with relatively fast magma ascent while OIB samples are in full gas-magma equilibrium (Simons et al., 2002; Aubaud, 2022). This difference is further illustrated in Figure 3, where the CO_2+H_2O supersaturation is plotted against the water content in the glass. Volatile supersaturation is common in glasses with low vesicularity and low water content while vesicle and water-rich glasses are mostly closed to volatile equilibrium. High vesicularity means larger gas-melt surface area of contact promoting equilibrium. Similarly, high water content enhances CO_2 diffusion in basaltic melts (Watson, 1991). These two factors explain the difference in MORB and hotspot glass equilibrium state. In both cases, CO_2 concentrations are only minimum estimates of the initial carbon content of magmas.

1.1.5.1.2. Simultaneous measurement of the carbon content and carbon stable isotope coupled with a mass balanced degassing model

Pineau and Javoy (1983, 1994) have proposed that carbon stable isotope ratios and dissolved CO_2 contents could be used with a mass balance degassing model to constrain initial CO_2 contents of the melt. In theory, such an approach is correct; in practice, however, this approach is problematic for several reasons and only leads to inaccurate results. The main caveats are: (a) The poor knowledge of isotopic fractionation between CO_2 in vesicle and carbon dissolved in the melt. Experimental determinations are sparse and gave conflicting results. Javoy et al. (1978) found fractionation between 4 and 4.5‰ while Mattey et al. (1991) obtained lower values (around 2‰). In a closed system, this fractionation represents the slope of the isotopic evolution of the vesicle and melt (at most 4.5‰ which is small) and even a small uncertainty in the fractionation value implies a large uncertainty in the reconstructed CO_2 content. (b) given the fact that MORB melt can undergo various degassing processes at shallow levels (closed system at equilibrium or out of equilibrium, open system at isotopic equilibrium or with partial kinetic

fractionation), there is a large range of degassing models that are possible and thus reconstructed initial carbon content leads to solutions that are not unique, and thus too speculative.

1.1.5.1.3. Carbon scaled to He

Initial work proposed two advantages to this approach. The first is that He flux is relatively well-constrained (Farley, 1995, Lupton and Craig, 1975) and the second is that He and CO_2 are minimally fractionated by shallow degassing processes. By measuring CO_2/He in a single MORB sample, Jambon and Zimmerman (1987) and Marty and Jambon (1987) observed that the CO_2/He ratio is similar in vesicle and melt. They proposed that CO_2 and He are not fractionated by degassing and that measured CO_2/He in vesicle is representative of the source. We know now that this hypothesis is incorrect because solubility determinations showed that He is at least two time more soluble than CO_2 in tholeiitic melts (Dixon et al., 1995, Jambon et al., 1986, Lux, 1987). Also, MORBs are generally not in gas-melt equilibrium so similar ratio in a natural sample is not a proof of similar behavior but, in the light of known solubilities, a clue of non-equilibrium state. The canonical $CO_2/^3He$ value of 2×10^9 of Marty and Jambon (1987) is often kept as a reference value for the upper mantle. However, popping rocks point to a mantle value of 3×10^9 (Javoy and Pineau, 1991, Jones et al., 2019). Lower values are an indication of degassing (CO_2/He decreases as degassing proceeds). Non-equilibrium degassing can also lead to large variations of CO_2/He ratios in comagmatic melts (Aubaud et al., 2004b).

1.1.5.1.4. Carbon scaled to a trace element (Nb or Ba)

The discovery of MORB that are CO_2-undersaturated (Saal et al., 2002) allowed to treat carbon as an incompatible element (a behavior that was controversial in earlier publications) (e.g., Marty and Jambon, 1987). Normalizing CO_2 to Nb or Ba, allowed to constrain this ratio in MORB and OIB sources and to calculate the CO_2 content of mantle sources. Although it was first assumed that this ratio vary little in the mantle, there is more and more evidence to suggest that they do vary from depleted to enriched sources (Cartigny et al., 2008, Miller et al., 2019, Sun and Dasgupta, 2023, Tucker et al., 2019). A comparison of MORB and OIB glasses is shown in Figure 4 in the diagram CO_2 concentration (ppm) against Ba concentration (ppm) for submarine glasses and melt inclusions. While degassing can explain the large range of CO_2 content at a given Ba content, the maximum CO_2 is likely to be representative of the magma before degassing.

Inversely, the absence of CO_2 data for some samples can be overcome by using Nb or Ba as a proxy for CO_2 content assuming a CO_2 to Ba or Nb ratio in the source (Hauri et al., 2019). This approach leads to an indirect estimation of global ridge CO_2 flux.

1.1.5.1.5. Carbon estimated from major element systematics

Building on previous observations (Dasgupta et al., 2007a, Ghosh et al., 2014, Mallik and Dasgupta, 2013), Sun and Dasgupta (2020) re-established a linear relationship between CO_2 and SiO_2 (on an H_2O-free basis) in experimental melts. Given the fact that most OIB melts are low in

silica, this calibration allowed Sun and Dasgupta (2023) to obtain the CO_2 content of OIB parental melts at a global scale, i.e., for all ocean island groups. With the parental melt CO_2 estimated from fractionation corrected, primitive melt SiO_2 contents, Sun and Dasgupta (2023) utilized the reported Nb and Ba contents of the OIBs to discover that on an island average-scale, CO_2 correlates to Ba and Nb. Using the observed correlation, Sun and Dasgupta (2023) derived global average CO_2/Ba and CO_2/Nb for OIB sources.

1.1.5.1.6. Summary of elemental and isotopic composition of MORB and OIB source carbon

A summary of CO_2 content in primary melt, mantle C content, source CO_2/Nb and CO_2/Ba ratios, and fluxes is presented in Table 2.

Table 2. Carbon contents, carbon/trace element canonical ratios, and $\delta^{13}C$ values of MORBs and OIBs and their mantle sources.

Source	Primary melt CO_2 (ppm)	C mantle (ppm)	$\delta^{13}C$ source (‰)	CO_2/Nb (ppm/ppm)	CO_2/Ba (ppm/ppm)	Flux (molC/yr)	Method	Reference
MORB								
MORB						2×10^{13}	C isotopes	Javoy et al. (1982)
MORB						8.3×10^{11}	C isotopes	Des Marais and Moore (1984)
MORB						$1\text{-}8 \times 10^{12}$	$C/^3He$	Des Marais (1985)
MORB						2×10^{12}	$C/^3He$	Marty and Jambon (1987)
14°N MAR	14670	300	–4			15×10^{12}	vesicular, closed system	Javoy and Pineau (1991)
MORB						$(2.3\pm0.6) \times 10^{12}$		Zhang and Zindler (1993)
MORB		40-80				$2.9\text{-}5.8 \times 10^{12}$	model	Holloway (1998)
MORB		36-54				2.2×10^{12}	$C/^3He$	Marty and Tolstikhin (1998)
SWIR						$4\text{-}18 \times 10^{12}$	C isotopes	Cartigny et al. (2001)
DMM	44-244	20±5		239±46	75±25	0.93×10^{12}	undegassed	Saal et al. (2002)
23°S EPR						$10\text{-}18 \times 10^{12}$	C isotopes	Aubaud et al. (2004c)
34°N MAR	1260-57500		–4				vesicular, closed system	Pineau et al. (2004)
MORB						$2.7\text{-}77 \times 10^{12}$	experimental	Dasgupta and Hirschmann (2006)
14°N MAR				570	120±50	2.3×10^{12}	C isotopes	Cartigny et al. (2008)
34°N MAR				730	120±50	2.3×10^{12}	C isotopes	Cartigny et al. (2008)
MORB						$1\text{-}5 \times 10^{12}$	experimental	Dasgupta and Hirschmann (2010)
Axial Smt	9159	330		4000		$19\pm10 \times 10^{12}$	MI	Helo et al. (2011)
JdF EPR				580±50	100±10		MI	Wanless and Shaw (2012)
SEIR		12-24		730±370				Burnard et al. (2014)
MORB		18-21				$(8.7\pm2.8) \times 10^{11}$		Chavrit et al. (2014)
Gakkel				420	90±10		MI	Wanless et al. (2014)
UDM		50		283±32	98±10	$7.8\text{-}13 \times 10^{12}$	undegassed	Michael and Graham (2015)
MORB		75±25		505±168	133±44	$6\text{-}24.2 \times 10^{12}$	experimental	Rosenthal et al. (2015)
Lucky Strike				550±50	90±10		MI	Wanless et al. (2015)
DMM		6±1		258±40	105±61			Shimizu et al. (2016)
DMM		37±15		607±327	105±9		undegassed	Le Voyer et al. (2017)
DMM					140			Matthews et al. (2017)
MORB					100±20	$(4.9\pm0.8) \times 10^{12}$		Tucker et al. (2018)
MORB		110±40		810±220	100±20		compilation	Hirschmann (2018)
E-MORB		107(-49/124)			177(-52/71)			Shimizu et al. (2023)
SWIR 49°E	100-1400	19±5		1134±415	123±32		undersat. inclusions	Moussallam et al. (2023)
OIB								
All hotspots						3×10^{12}	$C/^3He$	Marty and Tolstikhin (1998)
All hotspots	40000	330-410		1850±196	226±22	5.5×10^{12}		Sun and Dasgupta (2023)
Kilauea			–4					Gerlach and Taylor (1990)
North Arc VF	20000-54000	350		1250±50	110±5			Dixon et al. (1997, 2002)
PdF, Réunion	4660-10160					7.3×10^{9}		Bureau et al. (1998)
Society	13970	190	–4			2.1×10^{9}	vesicular, closed-system	Aubaud et al. (2005)
Pitcairn	2970-34650	70-140	–6			1.9×10^{9}	vesicular, closed-system	Aubaud et al. (2006)
Galapagos				350				Koleszar et al. (2009)
Petit spot B				1300±450	130±60			Machida et al. (2009)
Petit spot A				1200±400	38±30			Okumura & Hirano (2013)
Iceland						$0.2\text{-}23 \times 10^{10}$	C isotopes	Barry et al. (2014)
Iceland				420	80±1		MI	Hartley et al. (2014); Neave et al. (2014)
N. Iceland				391	48		undegassed	Hauri et al. (2017)
Hawaii	9700±2500	263±82		758±238	86±23			Anderson and Poland (2017)
Canary	25000-50000							Longpré et al (2017)
PdF, Réunion	35000±14000	716±525						Boudoire et al. (2018)
Iceland				1832±316	396±48			Miller et al. (2019)
Loihi	10330±2300	480±110		631±169	79±18			Tucker et al. (2019)
Kilauea	6890±1210	440±80		594±123	80±17			Tucker et al. (2019)
Mauna Loa	3860±1250	380±120		329±80	34±6			Tucker et al. (2019)
Hualalai	4320±1320	360±110		627±191	84±25			Tucker et al. (2019)
Koolau	6040-2450	520±210		394±166	37±15			Tucker et al. (2019)
Canary	42000	55-185						Taraczak et al. (2019)
Canary	45000±15000							Buron et al. (2023)
Loihi, Hawaii	6535-18960				108		C isotopes	Graham et al. (2023)

MAR: Mid-Atlantic Ridge; SWIR: Southwest Indian Ridge; DMM: Depleted MORB Mantle; EPR: East Pacific Rise; Smt: seamount; JdF: Juan de Fuca; SEIR: Southeast Indian Ridge; UDM: Ultradepleted mantle; E-MORB: enriched Mid-Ocean Ridge Basalt; VF: volcanic field; PdF: Piton de la Fournaise;

The primary melt CO_2 content vary between 44 and 57,500 ppm in MORBs. In OIBs, the primary melt CO_2 content vary from 3,860 to 54,000 ppm. Apart from the large estimate of 57,500 ppm for 34°N alkalic basalts that are likely enriched in CO_2 due to small extent of melting and possible OIB source affinity, the CO_2 content in OIB primary magmas is larger than in MORB primary magmas. Such a difference is also reflected in C content of mantle sources: the values estimated for the MORB source (6 to 330 ppm C) are smaller than those derived for OIB sources (70-716 ppm C).

CO_2/Nb in MORB range from 239 to 4000 while in OIB they range from 329 to 1850. Such difference in CO_2/Nb ratios reflects difference in source enrichment because CO_2 and Nb do not have the same degree of incompatibility (Rosenthal et al., 2015). On the contrary, the range of CO_2/Ba in MORB (75-177) is similar to, although more restricted than the range of CO_2/Ba in OIB (34-396) because of similar degree of incompatibility.

The fluxes of CO_2 from ridges vary other several orders of magnitude 0.8-77 $\times 10^{12}$ mol C/y reflecting the large diversity of approaches used to calculate this value. An average value of 10×10^{12} mol C/y is similar in magnitude to the flux estimated for all OIBs. This implies that OIB CO_2 emissions are similar to MORB CO_2 emissions in recent geological times. It is probably only during emplacement of large volumes of magma during LIPs (large igneous provinces) episodes that OIB likely surpasses ridges in terms of CO_2 emissions.

1.1.5.2. Water

A summary of water content in melts, water content in mantle sources and water fluxes is presented in Table 3.

Table 3. Water contents and δD values in MORBs and OIBs and their mantle sources.

Source	Melt H_2O (wt%)	H_2O mantle (ppm)	H_2O/Ce (ppm/ppm)	δD (‰)	Flux (molH_2O/yr)	Reference
MORB						
MORB					(6.1±1.7) × 10^{12}	Ito et al. (1983)
MORB	0.15-0.35			–80±5		Kyser and O'Neil (1984)
MORB	0.2			–77		Poreda et al. (1986)
MORB	0.17-0.6	70-550 (**150**)				Jambon & Zimmermann (1990)
14°N MAR	0.42-0.53			–64±2		Pineau and Javoy (1994)
MORB			155-213(±40)			Michael (1995)
22°N MAR			240-280(±50)			Michael (1995)
MORB		250		–70		Javoy (1997)
					1.1×10^{13}	Javoy (1998)
MORB Atlantic	0.3		250			Dixon et al. (2002)
MORB Pacific	0.2		150			Dixon et al. (2002)
DMM	0.01		200			Dixon et al. (2002)
MORB Pacific 23°S		120±27	150±10			Simons et al. (2002)
MORB Pacific 23°S	0.07			–63		Kingsley et al. (2002)

DMM		142	168±95			Saal et al. (2002)
EPR	0.06-0.7	128±5	134-277			Le Roux et al. (2006)
14°N & 34°N MAR	0.13-0.77		154-345			Cartigny et al. (2008)
Macquarie MORB				–75		Bindeman et al. (2012)
MORB			180	–60		Clog et al. (2013)
N Atl. DM			200	–100		Dixon et al. (2017)
Pacific DM			150	–75		Dixon et al. (2017)
South Atl. DM			150	–70		Dixon et al. (2017)
N EPR DM			170	–70		Dixon et al. (2017)
SWIR (background)			232±92			Wang et al. (2021)
SWIR 48-51°E			459±15			Wang et al. (2021)
SWIR 5°E			322±13			Wang et al. (2021)
OIB						
All hotspots					$(0.70.4) \times 10^{12}$	Ito et al. (1983)
Loihi						Rison and Craig (1983)
Hawaii	0.25-1.1			–52 to –73		Kyser and O'Neil (1984)
Reykjanes	0.4			–50		Poreda et al. (1986)
Mohns Ridge	0.4-1.2			–60 to –44		Poreda et al. (1986)
Hawaii				–80		Garcia et al. (1989)
North Arch, Hawaii	1.3-1.9	525±75				Dixon et al. (1997)
Réunion	0.7-1.1	350-1100			3.4×10^9	Bureau et al. (1998)
Kilauea		450±190				Wallace (1998)
Loihi	0.4-1.0	400	167±13			Dixon and Clague (2001)
Atlantic FOZO	0.075		250			Dixon et al. (2002)
Pacific FOZO	0.075		200			Dixon et al. (2002)
EM	<0.04		<100			Dixon et al. (2002)
Easter/Salas y Gomez		750±210	210±20			Simons et al. (2002)
Easter/Salas y Gomez	1.54			–35		Kingsley et al. (2002)
Loihi (alk)	0.60			–77		Hauri (2002)
Loihi (thol)	0.48			–77		Hauri (2002)
Kilauea	0.40			–48		Hauri (2002)
Mauna Loa	0.36			–82		Hauri (2002)
Mauna Kea	0.36			–65		Hauri (2002)
Koolau	0.40			–120		Hauri (2002)
Society	1.43	720			5.4×10^9	Aubaud et al. (2005)
Pitcairn	0.63-1.04	410-820			7.3×10^9	Aubaud et al. (2006)
Samoa (**EM2**)	0.63-1.50	385	**58**-157			Workman et al. (2006)
Pitcairn (**EM1**)	0.7-1.7		**75**-150			Kendrick et al. (2014)
Society (**EM2**)	0.9-1.5		**50**-120			Kendrick et al. (2014)
Mangaia (**HIMU**)	1.2-1.7	440	119-**245**			Cabral et al. (2014)
Baffin (Iceland)	0.2			–218		Hallis et al. (2015)
Pacific PREMA			215±30	–45±5		Dixon et al. (2017)
North Atl. PREMA			220±30	–30 to –40		Dixon et al. (2017)
North Atl. EM			330±30	–57		Dixon et al. (2017)
South Atl. EM			120±10	–68		Dixon et al. (2017)
North Pacific EM			110±20	–94		Dixon et al. (2017)

In bold are mantle endmembers identified among the lavas from a given island and the corresponding H_2O/Ce ratio is also in bold.
PREMA: Prevalent mantle; FOZO: Focus Zone; EM: enriched mantle endmember; HIMU: high-μ endmember.

The concentration of dissolved water in MORB and hotspot glasses is shown in Figure 1. Concentrations of water in MORB is generally in the range 0.05 to 0.5 wt% with a mode at 0.2 wt% (Aubaud, 2022; Fig. 1a and Table 3), higher values being encountered close to ridge-centered hotspots. In hotspot glasses, water concentrations are mostly in the range between 0.5 and 1.5 wt% (Table 3; Figures 1b and 1c). Contrary to CO_2, there is a significant difference in water content between MORB and hotspot magmas. As water is an incompatible species (e.g., Aubaud et al., 2004a, O'Leary et al., 2010), this observation essentially reflects that hotspot

sources are enriched in water compared to the MORB source. Due to its high solubility in basaltic melts (Hamilton et al., 1964; Dixon et al., 1995), water is less prone to degassing at the common eruption pressure range of MORB and OIB. As a result, more information can be extracted from its direct analysis in submarine glasses.

Since the earliest measurements, it was quickly understood that water behaves as an incompatible element like K and Ce (Danyushevsky et al., 1993, Dixon et al., 1988, Jambon and Zimmerman, 1990). Comparison of H_2O with K_2O have helped to understand its recycling and behavior in the upper mantle. Jambon and Zimmermann (1990) have found that recycled oceanic crust must be strongly dehydrated upon its passage through subduction zone to explain the observed enriched endmember in the MORB samples. Water behavior was deemed closed to that of Ce (Michael, 1995) and the H_2O/Ce was then adopted to discuss source variability. This ratio vary significantly in MORB and is significantly different between MORB and OIBs (Dixon et al., 2017, Dixon et al., 2002). Notably, Dixon et al. (2002) have noted lower H_2O/Ce in some OIB end members that they interpret as extensive dehydration at subduction zones during recycling of oceanic crust (a component in OIB sources). Recently, Wang et al. (2021) has identified a high H_2O/Ce component in the Southwest Indian ridge basalts that they interpret as a remnant of subduction material during ocean opening in this area.

Typical water concentration in the MORB mantle is in the range 120-250 ppm. In OIB sources, water content is larger: 350-1100 ppm (Table 3). The flux of water at ridges is about 1×10^{12} mol H_2O/y (Javoy, 1998), almost in the same order of magnitude as that estimated for intraplate ocean islands (0.7×10^{12} mol H_2O/y; Ito et al., 1983).

1.1.5.3. Sulfur

A summary of S content in melts and mantle sources as well as S fluxes is presented in Table 4.

Table 4. Sulfur contents and $\delta^{34}S$ values in MORBs and OIBs and their mantle sources

Source	Melt S (ppm)	Mantle S (ppm)	$\delta^{34}S$ (‰/CDT)	S/Dy	Flux molS/yr	Method	Reference
MORB							
DMM		146±35		225		S/Dy	Saal et al. (2002)
EPR MORB		129±6				S/Dy	Le Roux et al. (2006)
MORB	711-1086		–0.91±0.50				Labidi et al. (2012)
DM		200±40					Lorand et al. (2013)
MORB (**DM**)	642-1388		**–1.28±0.33**				Labidi et al. (2013)
MORB		195±45				Ce/Tl	Nielsen et al. (2014)
MORB (PacAnt)	900-1800		–1.57 to +0.60 **–0.89±0.11**				Labidi et al. (2014)
MORB					100×10^9		Kagoshima et al. (2015)
MORB		100-165				S/Dy	Shimizu et al. (2016)
Garrett DMORB		100±40	–0.68±0.08				Labidi et al. (2016)
MORB	900-1900	100-200				S-Cu syst	Ding and Dasgupta (2017)
MORB		206±25				S-Cu exp	Sun et al. (2020)

OIB							
Primordial M		>1000					Labidi et al. (2016)
LOMU			0.00				Labidi et al. (2013)
Discovery			+1.05				Labidi et al. (2013)
Shona			–0.59				Labidi et al. (2013)
HIMU		175-300					Labidi et al. (2014)
EM endm.		5000					Labidi et al. (2014)
Samoa (**EM2**)	835-2279		+0.11 to +**2.79**				Labidi et al. (2015)
Canary	4290	265-450					Taraczak et al. (2019)
Samoa (**EM2**)	809		+1.08 to +**4.23**				Dottin et al. (2020)
Mangaia (**HIMU**)			–**5.13** to +0.21				Dottin et al. (2020)
Samoa (**EM2**)	1000		–0.29 to +**4.84**				Dottin et al. (2021)
Pitcairn	1300		–0.9 to +0.6				Labidi et al. (2022)

In bold are preferred values of endmembers quoted in the original publications.
PacAnt: Pacific Antarctic ridge; M: Mantle

Sulfur is a moderately incompatible element during mantle partial melting (Ding and Dasgupta, 2017, Ding and Dasgupta, 2018). In MORB, it is assumed to behave in a manner similar to Dy (Saal et al., 2002). S concentrations in MORBs vary from ~750 ppm to ~1750 ppm (Table 4 and Fig. 5), with S contents largely increasing with decreasing Mg# and increasing FeO* contents of basalts.

Sulfur solubility in basaltic melts is sufficient to keep sulfur dissolved in the melt at the eruption pressures of submarine MORBs and OIBs. However, sulfur is very sensitive to oxidation state conditions and generally partly precipitates as sulfides droplets that are sometimes observed submarine glass thin sections (e.g., Mathez, 1976, Patten et al., 2012). It has been recognized that S content in MORB glasses is dependent on FeO content, i.e., the maximum S is controlled by total Fe of the melt (Fig. 5). S content in the MORB mantle has been inferred to be in the range 100-206 ppm, estimates that are essentially consistent considering that different approaches have been used (Table 4). A MORB sulfur flux of 100×10^9 molS/yr has been calculated by Kagoshima et al. (2015).

In OIBs, S is controlled by the same processes as in MORBs except that degassing might be an additional factor (Spilliaert et al., 2006). Therefore, disentangling the effect of sulfide precipitation and degassing can be difficult (Labidi et al., 2022). The concentration of Cu can be used to track sulfide precipitation (Lee et al., 2012) while modelling of experimental data might give constraints on degassing effects (Witham et al., 2012). It is still under scrutiny to establish whether OIBs are more oxidized than MORBs and if dissolved sulfate is significant in these melts (e.g., O'Neill, 2021). The HIMU mantle endmember has a S content of 175-300 ppm (Labidi et al., 2014). EM mantle endmembers are assumed to be S-rich up to 5000 ppm due to sedimentary S contribution (Labidi et al., 2014). The modelled primordial mantle has S content larger than 1000 ppm (Labidi and Cartigny, 2016). No OIB S flux has ever been estimated.

1.1.5.4. Halogens

1.1.5.4.1. Chlorine

A summary of Cl content in MORB and OIB melts, Cl content in the mantle and Cl fluxes is presented in Table 5.

Table 5. Chlorine contents and $\delta^{37}Cl$ values of MORBs and OIBs and their mantle sources.

Source	Melt (ppm Cl)	Mantle (ppm Cl)	$\delta^{37}Cl$ (‰/SMOC)	Flux (molCl/yr)	Reference
MORB					
MORB				$(5.4\text{-}9.0) \times 10^{10}$	Schilling et al. (1978)
MORB				$(4\text{-}15) \times 10^{10}$	Ito et al. (1983)
MORB uncontam.	20-50				Michael & Schilling (1989)
MAR	49-153				Jambon et al. (1995)
EPR	280-320				Jambon et al. (1995)
GSC	53-2066				Jambon et al. (1995)
MORB uncontam.	55			9.3×10^{10}	Jambon et al. (1995)
MORB uncontam.	2-80				Michael and Cornell (1998)
DMM		1±0.5			Saal et al. (2002)
EPR		5.38±1.1			Le Roux et al. (2006)
MORB			–1.0 to +0.4 **(–0.1±0.4)**		Sharp et al. (2007)
MORB	42-701 (**80**)	4±3	0 to –1.6 (**<–1.6**)		Bonifacie et al. (2008)
OIB					
OIB				$(0.3\text{-}7.3) \times 10^{10}$	Ito et al. (1983)
Primitive mantle		35±5			Jambon et al. (1995)
North Arch VF	400-1360	30			Dixon et al. (1997)
PdF, Réunion	150-370			7.3×10^{6}	Bureau et al. (1998)
Loihi thol.	130				Kent et al. (1999a, 1999b)
Loihi (uncontam.)	240-600				Dixon and Clague (2001)
HIMU	418-755				Stroncik and Haase (2004)
EM1	250-783				Stroncik and Haase (2004)
EMII	566-845				Stroncik and Haase (2004)
OIB (HIMU) St Hel	58-**749**		**–1.6** to +1.1		John et al. (2010)
OIB (EM1) Pitcairn	262-285		–0.4 to +1.0		John et al. (2010)
OIB (EM2) Society	**468**-690		+1.5 to **+2.9**		John et al. (2010)
OIB Réunion	383-492		+0.2 to +1.2		John et al. (2010)
Mangaia	225-906				Cabral et al. (2014)
Pitcairn	280-680				Kendrick et al. (2014)
Society	610-1180				Kendrick et al. (2014)
Samoa uncontam	490				Kendrick et al. (2015)

In bold are preferred (generally uncontaminated) values of pure endmember in the original publications. When brine assimilation have been identified, we have retained only the lowest Cl content as representative of the melts.
Uncontam: uncontaminated melts (free of brine interaction); St Hel: St Helena

First studies recognized that the extent of contamination was larger in samples from fast spreading ridges (EPR) than for slow spreading ridges (MAR) (Jambon et al., 1995, Michael and Cornell, 1998, Michael and Schilling, 1989). The excess chlorine has been proposed to be due to incorporation of brine derived from seawater unmixing at high temperature at ridges (Jambon et

al., 1995, le Roux et al., 2006). Brines have also been identified in various OIBs (Stroncik and Haase, 2004) including Samoan samples (Kendrick et al., 2015) and Hawaiian lavas (Dixon and Clague, 2001, Kent et al., 1999a, Kent et al., 1999b).

Uncontaminated Cl concentration in MORB is in the range 2-80 ppm (Jambon et al., 1995, Michael and Cornell, 1998, Michael and Schilling, 1989). Chlorine is incompatible during crystal fractionation and correlated with strongly incompatible elements (Jambon et al., 1995). Inferred Cl content of the MORB source mantle in the range 1-6 ppm (Bonifacie et al., 2008, le Roux et al., 2006, Saal et al., 2002). The flux of chlorine at ridges is estimated to be in the range 4-15 $\times 10^{10}$ mol Cl/y (Ito et al., 1983, Jambon et al., 1995, Schilling et al., 1978).

Cl/K was used to characterize the source (when not contaminated) and sometimes found to be correlated with $^{3}He/^{4}He$ (Jambon et al., 1995) and radiogenic isotopic ratios (Stroncik and Haase, 2004). Notably, Cl is enriched in Azores and Iceland hotspots (both in concentration and in Cl/K ratios). K/Cl in MORB is 13±4 (Kendrick et al., 2012). K/Cl are up to 40 in Society and Pitcairn OIBs and are correlated with $^{87}Sr/^{86}Sr$ (Kendrick et al., 2014, Kendrick et al., 2012b). The uncontaminated chlorine concentrations in hotspot lavas are higher than those measured for MORB, generally by an order of magnitude (Table 5). Primitive mantle Cl concentration is estimated to be 35±5 ppm (Jambon et al., 1995) that is one order of magnitude higher than the depleted MORB mantle concentration. The chlorine flux for OIB is estimated to be in the range 0.3-7.3 $\times 10^{10}$ mol Cl/yr similar in magnitude to the MORB flux.

1.1.5.4.2. Fluorine

Fluorine is incompatible during crystal fractionation and partial melting (Beyer et al., 2012). F is not affected by degassing. F/Nd in MORB is 22 ±2 (Saal et al., 2002). F/Cl in MORB (1±0.5) is lower than in EMI and EMII hotspots (up to 3) and well correlated to K/Cl for Pitcairn samples. F well correlated to H_2O (Shimizu et al., 2019).

1.1.5.4.3. Bromine

Bromine has a similar behavior as chlorine. In basalt glasses, they are highly correlated with a Cl/Br ratio of 430 and concentration of 60-1300 ppb. All processes that apply to chlorine can be extrapolated to Br (Jambon et al., 1995). Br/Cl in the MORB source is $(3.7 \pm 0.5) \times 10^{-3}$ (Kendrick et al., 2012a). Br is not fractionated during partial melting and crystal fractionation.

1.1.5.4.4. Iodine

Concentrations are low 2.5-13 ppb. Higher concentrations have been measured in plume type samples (up to 363 ppb) an indication of a recycled component that includes organic matter of sedimentary origin (this reservoir is 80% of the terrestrial iodine). Iodine is a highly incompatible element and correlates with K. Iodine's mantle abundance is estimated to be 10 ppb (Déruelle et al., 1992). I/Cl in the MORB source is $(130 \pm 100) \times 10^{-6}$ (Kendrick et al., 2012a).

Br/Cl and I/Cl for samples least affected by brines indicates that MORB and OIB samples (Samoa, Pitcairn, Society, high $^{3}He/^{4}He$ Baffin island samples) share the same source characteristics (Kendrick et al., 2015).

1.1.5.5. Nitrogen

Study of nitrogen in the mantle with submarine glasses has been a challenging analytical task. There are two main reasons for this: (1) nitrogen abundance is very low and (2) nitrogen is prone to atmospheric contamination. It is only by the use of a gas-rich sample (Javoy and Pineau, 1991) and of static mass spectrometry on more common gas-poor samples that nitrogen concentrations and isotopic ratios could be measured accurately (Marty, 1995, Marty and Zimmermann, 1999)(Cartigny et al., 2001).

A summary of N content in melt and mantle sources, and nitrogen fluxes is presented in Table 6.

Table 6. Nitrogen contents and $\delta^{15}N$ values of MORBs and OIBs and their mantle sources.

Source	Melt N (ppm)	Mantle N (ppm)	$\delta^{15}N$ (‰)	Flux (mol N/y)	Reference
MORB					
14°N MAR	12	1	–3.5		Javoy and Pineau (1991)
MORB		0.24		3.2×10^{9}	Zhang and Zindler (1993)
MORB				$(2.2\pm1.0) \times 10^{9}$	Marty (1995)
MORB			–3.3±1.0	$(3.8\pm1.5) \times 10^{9}$	Marty and Zimmermann (1999)
SWIR			–6	$(31\text{-}138) \times 10^{9}$	Cartigny et al. (2001)
MORB		0.27±0.16	–3 to **–5**		Marty and Dauphas (2003)
MORB				5×10^{9}	Busigny et al. (2011)
MORB		1.3±0.6			Marty (2012)
MORB		1.1±0.55		$(5.7\text{-}36) \times 10^{9}$	Hirschmann (2018)
OIB					
OIB				4.1×10^{6}	Sano et al. (2001)
OIB		2.7±1.4	–1.5 to +7.9 **+3**		Marty and Dauphas (2003)

In bold are preferred values of the original references among the measured range of values.

In undegassed MORB samples, the nitrogen abundance is 12 ppm (Javoy and Pineau, 1991). Assuming 10% mantle partial melting for MORB genesis and an incompatible behavior for N during melting returns a MORB mantle abundance of 1 ppm, a value consistent with later estimates (from 0.24 to 1.3 ppm, Table 6). N_2 in MORB has been found to be well correlated to ^{40}Ar (Marty, 1995). Argon is incompatible during partial melting; therefore it might be inferred that N is incompatible as well. Also, nitrogen has a low solubility in basaltic melts at relevant oxidation conditions of the MORB mantle (Bernadou et al., 2021, Dasgupta et al., 2022b, Libourel et al., 2003) so that it is preferentially partitioned into the gas phase during degassing.

Flux of N from the MORB mantle has been estimated to range from 2.2 to 138×10^{9} mol N/y (Table 6) much larger than that of OIB (4.1×10^{6}; (Sano et al., 2001)).

1.1.6. Isotopes of C, H, S, N and halogens in the oceanic mantle

1.1.6.1 Carbon isotopes

Carbon has two stable isotopes: ^{12}C and ^{13}C, with respective abundances of 98.89% and 1.11%. The largest reservoir of carbon at the Earth's surface is marine sedimentary carbonates that are used to define the isotopic standard (PDB for Pee Dee Belemnite) (Craig, 1953). In MORBs, the $\delta^{13}C$ in vesicle vary from –14 to –0.5‰ with a majority of values around –6‰ (Aubaud, 2022). Dissolved carbon vary mostly between –4 and –11‰. In OIB, vesicle $\delta^{13}C$ values vary between –4 to –16‰ and dissolved carbon vary between –4 and –28‰ (Aubaud, 2022). Due to strong degassing effects, carbon stable isotopes vary in MORB and OIB essentially due to degassing. Experimental determinations of carbon isotope fractionation between CO_2 in vesicle and C dissolved in magma have established that vesicles are enriched in ^{13}C compared to the melt. The magnitude of this fractionation is however, debated between relatively high values +4 to +4.5‰ (Javoy et al., 1978) and relatively low values +2‰ (Mattey, David P., 1991). This explains why most MORB values are depleted compared to the mantle value (–4‰).

Schematically, three processes occur to explain all isotopic variation in submarine glasses: (1) degassing under a closed system at isotopic equilibrium, which mainly explains values between –4 and –8‰, (2) degassing under an open-system at isotopic equilibrium (Rayleigh distillation), which explains all values lower than –8‰, and (3) kinetic isotopic fractionation superimposed to the two previous processes, which can explain values higher than -4‰ in vesicles.

If one undertakes tracking mantle heterogeneity with carbon isotopes, this can only be accomplished by considering samples that have degassed under a closed system. Since CO_2 has low solubility, most of the carbon is present in the vesicles and its stable isotope ratio approaches that of the initial magma. Few samples meet the criteria (Table 2): samples 2πD43 and OT03-09 in MORB (Javoy and Pineau, 1994; Pineau et al., 2004) and a few alkalic basalts from Pitcairn and Society (Aubaud et al., 2005, 2006). For MORB, a source of –4‰ might be inferred. For Society, a signature around –4‰ can also be deduced (Aubaud et al., 2005). For Pitcairn, however, the source of carbon seems to be around –6‰, that is 2‰ lower than the MORB source (Aubaud et al., 2006). Although the isotopic signature around –4‰ seems frequent (it is also encountered in Hawaii as seen with volcanic gases, (Gerlach and Thomas, 1986)), it is possible that carbon isotopes are heterogeneous in the mantle. Whether this is due to recycling or primordial inheritance remains to be elucidated. Indeed, some studies argued that a relatively lighter carbon isotope signature of less degassed OIBs (Exley et al., 1986, Hauri, 2002) may be true mantle source signature and may indicate greater proportions of subducted organic C in the OIB source compared to MORB source (e.g., Eguchi et al., 2020).

1.1.6.2. Hydrogen isotopes

Hydrogen has two stable isotopes: ^{1}H and ^{2}H (also called deuterium and denoted by D) with respective abundances of 99.9855% and 0.0145%. The largest reservoir of hydrogen at the surface is the ocean (standard mean oceanic water, SMOW, 0‰ by definition; Craig, 1963). Because dissolved magmatic water is little affected by degassing, hydrogen isotopes of silicate glasses have been used to discuss mantle source heterogeneity. Data in the literature are scarce, however, because hydrogen isotopes determination by conventional techniques (extraction by heating, water reduction to H_2 and MS) are not easy.

A summary of δD-values obtained for MORB and OIB is presented in Table 3. Earlier studies have recognized that mantle sources are depleted in deuterium (–80‰ for the upper mantle) (Kyser and O'Neil, 1984). This is in strong contrast with the surface water, which is a few per mil below the SMOW (Lécuyer et al., 1998). Various authors have speculated whether this difference is due to recycling or the inheritance from a primordial accretion. More recent studies are debating the isotopic signature of the MORB source (–75‰, (Bindeman et al., 2012); –60‰, (Clog et al., 2013); or even larger potential range with regional variations, (–70 to –100‰; (Dixon et al., 2017)). There might also be an issue with earlier studies due to analytical problems with platinum crucible (Clog et al., 2012). This requires confirmation, however, because the experiments conducted by Clog et al. (2012) were conducted in analytical conditions (allowing the water vapor to remain statically in contact with the crucible at high temperature) that are different from those used to extract water from the glass samples (where the released water is dynamically trapped in a liquid nitrogen trap).

OIB glasses are notably enriched in water and deuterium (Table 3). Poreda et al. (1986) showed that Iceland source is –45‰ significantly higher than the ambient mantle in this region (–80‰). Kingsley et al. (2002) also obtained similar results for the Salas y Gomes (Easter) hotspot, with values up to –35‰. Other studies seem to have identified a dry and low deuterium source corresponding to the deep, primordial mantle (–165‰ in Hawaiian samples: (Hauri, 2002); –218‰ for Baffin island picrites: (Hallis et al., 2015)). However, such values are always obtained using SIMS and it remains to be verified that these results are not analytical artefacts. Dixon et al. (2017) clearly established, however, that the common tendency of OIBs is to be enriched in D with a large variability in isotopic signatures sometimes down to low values (–30 to –94‰ in PREMA and EM mantle endmembers).

1.1.6.3. Sulfur isotopes

Sulfur has four stable isotopes: ^{32}S, ^{33}S, ^{34}S, ^{36}S with respective abundances of 94.8%, 0.76%, 4.37%, and 0.02%. The international standard is the sulfur of the Canyon Diablo Troilite (CDT) meteorite.

Early studies on sulfur isotopes have concentrated on $\delta^{34}S$-values only. Chaussidon et al. (1989) have inferred a mantle $\delta^{34}S$ of +0.5‰, not far from meteorite international standard.

Progress in mass spectrometry has allowed refinement of mantle S isotope geochemistry and the study of minor sulfur isotopes $\Delta^{33}S$ and $\Delta^{36}S$ (Labidi et al., 2012). These low abundance sulfur isotopes are interesting because before the great oxygenation event, large anomalies due to mass-independent fractionations are present in Earth's sediments (Farquhar et al., 2000). The

873 SIMS technique has also been used to measure both $\delta^{34}S$ and low abundance isotope ratios (e.g.
874 Delavault et al., 2016).
875 Partial melting of mantle rocks has no effect on sulfur isotope fractionation (Labidi and
876 Cartigny, 2016). Sulfur isotopes in melts can thus be interpreted in terms of source processes
877 provided that secondary effects such as degassing, for example, did not occur.
878 A summary of recent determinations of $\delta^{34}S$-values in MORB and OIB sources is
879 presented in Table 4.
880 The MORB mantle has been re-evaluated at –1‰ (Labidi and Cartigny, 2016, Labidi et
881 al., 2012, Labidi et al., 2014, Labidi et al., 2013). The $\Delta^{33}S$ and $\Delta^{36}S$ for the MORB mantle are –
882 0.019±0.005‰ and –0.193±0.093‰ relative to the IPGP working gas standard, identical to CDT
883 measurement in the IPGP laboratory. The analyses of OIB have shown enrichment in $\delta^{34}S$ up to
884 +1‰ in Shona and Discovery hotspots, well correlated with Sr and Nd radiogenic isotope ratios
885 (Labidi et al., 2013) and up to a value of +2.79‰ (Labidi et al., 2015) and +4.84‰ in Samoan
886 basalts (Dottin III et al., 2021). Mangaia island is found to be strongly heterogeneous in $\delta^{34}S$
887 values from –5.13 to +0.21‰, but is mostly negative suggesting a source of crustal sulfur
888 (Dottin, J. W. I. et al., 2020). Although Pitcairn basalts seem to have partly degassed, their
889 source $\delta^{34}S$-values are proposed to be higher than that of MORB (Labidi et al., 2022).
890 The presence of $\Delta^{33}S$ and $\Delta^{36}S$ anomalies in OIB sources is debated. Some studies have
891 shown anomalies in $\Delta^{33}S$ and $\Delta^{36}S$. Cabral et al. (2013) measured mostly negative $\Delta^{33}S$ in
892 Mangaia samples while Dottin et al. (2020) found values around 0 or slightly positive. Delavault
893 et al. (2016) found mostly negative $\Delta^{33}S$ in Pitcairn samples while Labidi et al. (2022) found no
894 significant anomaly. It is not known if such conflicting results originate from different
895 performances of analytical techniques (SIMS vs bulk extraction and mass spectrometry) or due
896 to intra-sample fractionation (bulk rock vs sulfide analysis).
897
898 1.1.6.4. Halogen (chlorine) isotopes
899
900 Chlorine has two stable isotopes ^{35}Cl and ^{37}Cl with respective abundances 75.76% and
901 24.24%. The international standard is the Standard Mean Oceanic Chlorine (SMOC, e.g., Godon
902 et al., 2004). It has been chosen because the largest reservoir of chlorine at the Earth's surface is
903 the ocean.
904 Measurement of Cl isotopes in rocks has been a challenging task. Older TIMS data
905 (Mangenheim et al., 1995) are not reliable and should be discarded. It is only with the progress in
906 gas source mass spectrometry on CH_3Cl that this kind of measurement has been possible (Sharp
907 et al., 2007; Bonifacie et al., 2008).
908 A summary of $\delta^{37}Cl$ values in MORB and OIB glasses is presented in Table 5. In
909 MORBs, studies have yielded conflicting results and interpretations. Sharp et al. (2007) has
910 found a range between –1 and +0.4‰. These authors consider the average (around –0.1±0.4‰)
911 to suggest no fractionation between the ocean and the mantle. By contrast, Bonifacie et al. (2008)
912 found a range between 0 and –1.6‰ with isotopic values correlated with chlorine content.
913 Bonifacie et al. (2008) propose that samples with higher chlorine content with $\delta^{37}Cl$ of 0‰ are a
914 sign of contamination by seawtaer derived brines whereas a signature of depleted $\delta^{37}Cl$ and low

content points to the mantle value, significantly (–1.6‰) depleted than the surface reservoir. By using SIMS, John et al. (2010) showed a range in OIBs between –1.6 and +1.1‰ for HIMU, between –0.4 and +1.0 for EMI Pitcairn, and between +1.5 to +2.9‰ for EM2 Society mantle sources. These authors interpret their data as reflecting heterogeneities in the mantle with DMM-HIMU sources depleted in $\delta^{37}Cl$ (potentially down to –3‰) and EM sources enriched in $\delta^{37}Cl$ (potentially up to +4‰ due to hypothetical subducted marine sediment reservoir).

1.1.6.5. Nitrogen isotopes

Nitrogen has two stable isotopes: ^{14}N and ^{15}N, with respective abundance of 99.636% and 0.364%. The international reference standard value is that of modern atmospheric nitrogen (ATM).

A summary of $\delta^{15}N$ values measured in MORBs and OIBs is presented in Table 6. The $\delta^{15}N$ values of MORB glasses are variable but generally point to a mantle value around –5‰ (Cartigny et al., 2001, Javoy and Pineau, 1991, Marty and Zimmermann, 1999) a value also seen in peridotitic diamonds (Cartigny et al., 1997, 1998). By contrast, OIBs show significantly positive $\delta^{15}N$ values from –1.5 to +7.9‰ with an average at +3‰ (Marty and Dauphas, 2003). Since sediments are generally positive in $\delta^{15}N$ (Ader et al., 2016), this can be in support of recycled nitrogen since the Archean.

1.1.7. Summary of global concentration and stable isotope distribution in MORB and OIB source

A simplified view of the distribution of volatile (H-C-N-S-Cl) concentration and stable isotope ratios in MORB and OIB sources is presented in Figure 6. These values represent a summary of what is estimated based on the analyses of submarine glasses and melt inclusions. In all cases, the OIB sources are systematically enriched in volatile compared to the MORB source. Similarly, current knowledge highlights the fact that MORB and OIB sources are generally isotopically distinct for all elements. Whether these differences were generated by the predominance of primordial or recycled material (or both) is a classic debate in the geochemical community. In any case, the geochemical approach to characterize MORB and OIB sources has been successful to make a clear distinction between them.

1.1.8. Storage mechanisms of volatiles in the MORB and OIB source mantles

In order to present our current understanding of how different volatile elements are stored in the mantle, it is important to clarify what one means by ‘source regions’. For the purpose of this presentation, we define the ‘source mantle’ of MORBs and OIBs as the subsolidus mantle rocks at the onset of partial melting. Such rocks may derive from deeper portions of the Earth’s mantle where the storage mechanisms of volatiles are different. However, for exchanges with the near-surface reservoirs that is the crust-ocean-atmosphere system, the storage mechanism of relevance is the near-solidus storage.

955

956 1.1.8.1. Water storage in the MORB and OIB source mantle

957 As outlined in the previous section, geochemistry of ocean-floor basalts erupted along
958 MOR and in intraplate settings suggest their parental melts contain minor to trace quantities of
959 water (70-1100 ppm; Table 3). Given that and the calculated extent of mantle partial melting, the
960 entire inventory of water is thought to be stored in nominally anhydrous minerals or NAMs
961 (Aubaud et al., 2004a, Bolfan-Casanova, 2005, Hauri et al., 2006, Hirschmann et al., 2009,
962 Kohlstedt et al., 1996, O'Leary et al., 2010) at the onset of melting. Several incorporation
963 mechanisms such as proton substitution or as point defects have been suggested for the major
964 mantle minerals.

965 In olivine, several mechanisms have been proposed. All studies highlight the complexity
966 of H incorporation in olivine. For natural olivines, the reader must refer to the studies of Miller et
967 al. (1987) and Matsyuk and Langer (2004). In experimental olivines, hydrogen incorporation is
968 related to octahedral site defects (Bai and Kohlstedt, 1993) with the tetrahedral (Si) site related
969 defects being unfavorable. This has been apparently experimentally confirmed by the study of
970 Matveev et al. (2004) who showed that H might be incorporated in Si-related defect only when
971 olivine is present in low Si activity environment. Effect of trivalent cations has been investigated
972 by Berry et al. (2007) who showed H can be stored in the Mg^{2+} site when Fe^{3+} in present in
973 natural peridotites.. Whatever the mechanism, H solubility in olivine is large so that there is no
974 limitation to incorporate H in the mantle at reasonable water content in MORB and OIB sources
975 (Kohlstedt et al., 1996, Mosenfelder et al., 2006).

976 For pyroxenes, some H can be stored in pure diopside (Bromiley et al., 2004) and
977 enstatite (Stalder, 2008) end-members, mostly in octahedral sites. Numerous studies, however,
978 have recognized that incorporation of Al^{3+} in pyroxene enhances H incorporation due to coupled
979 substitutions (Aubaud et al., 2004a, Hauri et al., 2006, O'Leary et al., 2010, Rauch and Keppler,
980 2002, Stalder, 2004, Stalder and Skogby, 2002). Variation in Fe^{2+}/Fe^{3+} ratio has also been
981 recognized as an important control for H incorporation in pyroxenes (Stalder, 2004).

982 In garnet, H may get incorporated via the hydrogarnet substitution (where $4H^{+}$ replace
983 Si^{4+}, e.g., Withers et al., 1998). However, not all studies found evidence of hydrogarnet
984 substitution for H incorporation in garnet; instead, Mookherjee and Karato (2010) found the H
985 substitution mechanism to be similar to those in pyroxenes, where H^{+} and Al^{3+} together
986 substitute for Si^{4+} (e.g., Hauri et al., 2006, Rauch and Keppler, 2002). The presence of Ti is
987 responsible for additional storage of H in garnet (e.g., Aubaud et al., 2008, Bell et al., 2004).
988 Compositional effects have been reviewed and showed that H incorporation is enhanced with
989 increasing grossular component, and very low in the almandine component (Geiger and
990 Rossman, 2018).

991

992 1.1.8.2. Carbon storage in the MORB and OIB source mantles

Carbon can be present in the Earth's mantle either in oxidized form, i.e., C^{4+}-bearing components or phases (CO_2-rich fluid, mineral carbonates) or in reduced forms such as C^0 (graphite and/ or diamond) or C^{4-} (methane-rich fluid) (Dasgupta, 2018, Dasgupta et al., 2022a, Dasgupta and Hirschmann, 2010, Dasgupta et al., 2013, Luth, 1999, Stagno et al., 2013) (Fig. 7). On the one hand, the form of storage of carbon is heavily dependent on the oxygen fugacity of the mantle and on the other hand, depending on its valence state, carbon may oxidize or reduce other multi-valent elements (e.g., Fe, S) in the mantle (e.g., Luth, 1999). For the OIB and MORB source mantle, however, it is argued that carbon's stable form is reflective of the oxygen fugacity set dominantly by iron redox. One key difference in the storage of carbon as opposed to water, is that the former is stored chiefly in trace accessory phases rather than being incorporated in major silicate minerals. Carbon solubility in the silicate mantle minerals is no more than few ppm (Keppler et al., 2003, Shcheka et al., 2006). For the shallow upper mantle beneath MOR and intraplate OIs, or specifically at depths where major melting and basalt generation take place, fO_2 is high enough that C is expected to be present as mineral carbonates (dolomitic or magnesite-rich solid solution) or CO_2-rich melts, depending on the depth. The following end-member reactions explain how C storage in the form of carbonates (as minerals or components in melts) are rationalized for the Earth's shallow mantle (Brey et al., 1983, Falloon and Green, 1989, Newton and Sharp, 1975, Yaxley et al., 2019).

$$2Mg_2SiO_4 + CaMgSi_2O_6 + 2CO_2 = 4MgSiO_3 + CaMg(CO_3)_2 \quad (2)$$

(olivine) (clinopyroxene) (fluid) (orthopyroxene) (dolomite/melt)

$$Mg_2SiO_4 + CO_2 = MgCO_3 + MgSiO_3 \quad (3)$$

(olivine) (fluid) (magnesite/melt) (orthopyroxene)

$$2MgSiO_3 + CaMg(CO_3)_2 = CaMgSi_2O_6 + 2MgCO_3 \quad (4)$$

(orthopyroxene) (dolomite/melt) (clinopyroxene) (magnesite/melt)

The above set of reactions (Eqns. 2-3) apply generally for the Earth's shallow upper mantle. But specifically for the MORB and OIB source upper mantle, the temperature is too hot for the mineral carbonate to be stable at shallow (~70-150 km) melting regime. If the oceanic mantle remains oxidized with depth, then C storage as solid mineral carbonate should be restricted to depths deeper than 300 km for the MORB source and even deeper for the hotter OIB source. Debate remains, however, whether the oceanic mantle undergoes carbonated versus C-redox melting at the solidus. In other words, whether the stability of C^{4+} species is only restricted to carbonated melt phase after the onset of melting. We will return to this debate on the section of volatile-present mantle melting.

If the fO_2 profile, as determined using the continental mantle xenoliths is applied to the oceanic mantle (e.g., Frost and McCammon, 2008; Stagno et al., 2013), then the mid- to deep-upper mantle beneath MORs and OIs may have carbon stored in the form of diamond (rather than carbonate minerals; Rohrbach and Schmidt, 2011) and/or dissolved in Fe-Ni alloy or Fe-Ni-S sulfide-rich phases (e.g., Dasgupta and Hirschmann, 2010; Dasgupta, 2013; Rohrbach et al., 2014; Tsuno and Dasgupta, 2015). For example, Rohrbach and Schmidt (2011) showed that reaction such as the following, can take place at deep upper mantle conditions:

$$MgCO_3 + 2(Fe,Ni)^0 = (Fe,Ni,Mg)O + C \quad (5)$$

(mineral/melt) (alloy) (silicate) (diamond)

Where, $MgCO_3$ is either a mineral carbonate phase or a component in molten carbonate, $(Fe,Ni)^0$ is an alloy phase, and C is diamond. The reaction above shows that as the mantle gets reduced enough at depths to start precipitating Fe-Ni alloy phase, carbon should get reduced to C^0. Frost and McCammon (2008) argued that with increasing depth, metal precipitation can commence as shallow as 8 GPa where the metal composition is extremely Ni-rich but which gradually becomes more and more Fe-rich with depth. An interesting consequence of the metal precipitation, however, is that diamond can chemically react with the alloy phase, being partially or completely dissolved in the accessory alloy phase. Several studies have considered and investigated this possibility of carbon sequestration in the accessory alloy phase at deep upper mantle conditions (Dasgupta, 2013, Dasgupta and Hirschmann, 2010, Rohrbach et al., 2014, Tsuno and Dasgupta, 2015, Zhang et al., 2018, Zhang et al., 2019). Rohrbach et al. (2014) and Tsuno and Dasgupta (2015) investigated phase relations in Fe-Ni-C and Fe-Ni-Cu-S systems, respectively. These authors argued that for the typical range of C content of the MORB source mantle, deep upper mantle assemblage that stores C is likely to be diamond and Fe-Ni-C±S alloy melt. For OIB source mantle, richer in C, the assemblage may include $(Fe,Ni)_7C_3$ carbide and diamond. Zhang and Hirschmann (2015), on the other hand, argued that with increasing depth, if and as the mantle gets reduced, the following reactions should proceed to the right –

$$NiO + 2FeO = Fe_2O_3 + Ni \quad (6)$$

(olivine) (olivine) (garnet) (sulfide melt)

$$3\,FeO = Fe_2O_3 + Fe \quad (7)$$

(olivine) (garnet) (sulfide melt)

Where NiO and FeO are the components in olivine, Fe_2O_3 in garnet, and Fe and Ni are components in sulfide or sulfide-bearing alloy melt. Given the carbon solubility in alloy or sulfide melt, irrespective of pressures, diminishes strongly with increasing sulfur content (e.g., Dasgupta et al., 2009, Tsuno and Dasgupta, 2015, Tsuno et al., 2018, Wang et al., 1991, Zhang et al., 2019), Zhang and Hirschmann (2015) argued that higher metal/sulfur ratio of deep mantle sulfides should lead to much greater solubility of carbon in such alloy melts. The consequent argument of these authors was that the entire MORB source C budget, both for the enriched or depleted MORB source regions should be dissolved in metal-rich sulfide melt at mid- to deep-upper mantle conditions. Although, an important point to note is that an increase in metal/sulfur

ratio of mantle sulfide owing to iron disproportionation has not been demonstrated experimentally. Furthermore, if the argument of Zhang et al. (2015) was indeed correct, the deep mantle diamonds and their sulfidic inclusions will be difficult to explain and may only be coming from carbon-rich domain, with C content much higher than the MORB source mantle (~20-50 ppm C). In a latter study, these same authors refined their claim, however (Zhang et al., 2019). Using the depth-fO_2 profile of Stagno et al. (2013), Zhang et al. (2019) showed that even for a C-depleted MORB source mantle (e.g., ~20 ppm C), both diamond and Fe-Ni-S-C liquid are expected down to 350 km depth. Only at deeper depths and C-poor domains, diamond may be destabilized, with all C being stored in Fe-Ni-S-C liquid or solid and liquid alloys. For OIB source mantle, expected to be richer in C (as much as ~330-400 ppm globally and maybe even more locally) (Miller et al., 2019, Sun and Dasgupta, 2023), C storage in both diamonds and in Fe-Ni-S liquid is expected to be the norm.

However, it is not agreed upon whether the convective, oceanic mantle fO_2 with depth is as reduced as the continental lithospheric mantle. Suggestions of more oxidized oceanic mantle, at depths down to several hundred kilometers do exist in literature (Eguchi and Dasgupta, 2018b, Gaillard et al., 2015).

1.1.8.3. Sulfur storage in the MORB and OIB source mantles

Sulfur is yet another element that can exist in multiple valence states, from S^{2-} (sulfide) to S^{6+} (sulfate). Both of these end member valences are documented as dissolved sulfur species in natural silicate glasses (Jugo et al., 2005, Jugo et al., 2010). Needless to say that the stability of S^{2-} versus S^{6+} depends on oxygen fugacity of the system. For MORB and OIB source mantle, the fO_2 is thought to be reduced enough (e.g., Bezos and Humler, 2005, Christie et al., 1986, Cottrell and Kelley, 2011) that sulfur should be chiefly present in the reduced form, i.e., as S^2. Indeed, sulfide globules have been observed in MORB glasses (Mathez, 1976) and S^{2-} sulfur species have been documented as the main species in MORB glasses (Métrich et al., 2009, Wallace and Carmichael, 1994). Furthermore, geochemistry of chalcophile elements in MORBs and OIBs is understood via partial melting of the Earth's upper mantle in the presence of residual sulfides (e.g., Ding and Dasgupta, 2017, Ding and Dasgupta, 2018, Lorand and Luguet, 2016, Sun et al., 2020).

Similar to carbon, sulfur is also known to be stored in the oceanic mantle chiefly in trace, accessory sulfide phases. This is supported by the recent analyses that show S storage in the nominally sulfur-free mantle minerals is no more than ~10 ppm (Callegaro et al., 2020, Johnson et al., submitted). The accessory sulfide in the oceanic mantle is a monosulfide solid or liquid solution depending on depth (Ballhaus et al., 2006, Beyer et al., 2022, Bockrath et al., 2004, Zhang and Hirschmann, 2016) (Fig. 8). Both Ni-poor sulfide solid solution (MSS, <10 wt.% Ni) (e.g., Alard et al., 2000, Luguet et al., 2003, Shaw, 1997) and Ni-rich (10–30 wt.%), Fe (~40 wt.%), and Cu (<10 wt.%)-poor MSS (e.g., Bulanova et al., 1996, e.g., Guo et al., 1999, Liu et al., 2010) have been reported as lherzolite-hosted sulfides. If eclogite-associated sulfides are considered, Ni contents are generally even lower (<12 wt.%; (Bulanova et al., 1996). Given

limited miscibility of sulfides and silicates, constraining the phase relations of the sulfide subsystem is sufficient to understand the stability of the sulfide phases in the mantle. Experimental melting phase relations of mantle-relevant sulfide compositions suggest that trace sulfide phases in the shallow MORB and OIB source mantle should be entirely molten down 250-300 km depth and only at conditions deeper than such, the sulfide phases may be partially molten or solid (Fig. 8) (Beyer et al., 2022, Zhang and Hirschmann, 2016, Zhang et al., 2015). While Zhang et al. (2015)and Zhang and Hirschmann (2016) studied melting curves for a fixed, average sulfide composition of the mantle, Beyer et al. (2022) performed experiments and developed a model to calculate solidi and liquidi of sulfides as a function of composition and over a larger pressure range, to 14 GPa (Fig. 8). Greater abundance of Ni leads to lower melting temperatures (Beyer et al., 2022). The presence of reduced carbon, i.e., graphite or diamond, further suppresses the melting curves of sulfides (Zhang and Hirschmann, 2015). Figure 8 compares the estimated melting curves of sulfides with the thermal regime beneath MORs and ocean islands (OIs). It can be seen that irrespective of the exact composition, in terms of Ni content or metal/sulfur ratio, sulfides should be molten throughout the entire upper mantle down to the top of the transition zone, especially those hosted in peridotite. Only for very Ni-poor sulfides, similar to those hosted in eclogitic diamonds, the liquidus is high enough that the sulfides are expected to be partially molten.

Although molten, sulfide melts are not thought to be efficiently extracted from the mantle. Connectivity of sulfide melt in the mantle is known to depend on oxygen content of sulfide melt (Ballhaus and Ellis, 1996, Gaetani and Grove, 1999, Minarik et al., 1996, Shannon and Agee, 1996, Shi et al., 2013). At relatively oxidizing conditions, i.e., $\log fO_2 \geq$ FMQ, sulfide melts was suggested to dissolve as much as 9 wt.% oxygen, which was observed to correlate with relatively low dihedral angle (<60°) in olivine-dominated mantle matrix. The required fO_2 conditions for sulfide melt mobility, is thought to be most relevant for MORB and OIB source regions at 30-60 km depths, conditions where mantle is partially molten. Sulfide melt mobility at such conditions, however, does not need to depend on lowered dihedral angle of sulfide in solid silicate mineral matrix. Instead, such sulfide melt mobility can be achieved via more-wetting, basaltic melt carrier (Ballhaus et al., 2006). However, if and as the deeper mantle domains are more reduced, dihedral angle increases above 60° and even ≥90° (Shannon and Agee, 1998; Shi et al., 2013), which inhibit percolation of sulfide melt. Hence for most conditions in the MORB and OIB source subsolidus mantle, sulfide melt is still thought to act as a residual phase during silicate partial melting and generation of mobile silicate or volatile-rich melts. More on this topic in one of the following sections.

1.1.8.4. Nitrogen storage in the MORB and OIB source mantle

Given the low concentration of mantle nitrogen, almost the entire inventory of mantle N is expected to be hosted in nominally N-free, major mantle minerals. K-bearing hydrous phases such as mica and clay minerals provide important hosts for nitrogen, where NH_4^+ can replace K^+. However, those hydrous phases are not expected to be present in the high temperatures prevalent in the MORB and OIB source regions (e.g., Dasgupta, 2018). Based on the solubility data of

nitrogen in major mantle minerals, upper mantle likely hosts N mostly in clinopyroxenes, orthopyroxenes, and garnet and much less in olivine (Li et al., 2013). However, the absolute solubility at relatively oxidized upper mantle conditions are known to be low, i.e., ≤10 ppm. It remains uncertain how N gets incorporated in nominally N-free, major mantle minerals, but incorporation as ammonium cation, NH_4^+ replacing K^+ in phases such as clinopyroxene has been suggested (Watenphul et al., 2010). If N incorporation as ammonium ion is the dominant mechanism, it is expected that N solubility to correlate positively with non-quadrilateral components in pyroxenes.

If OIB sources are deeper and originate from somewhere in the lower mantle, then nitrogen storage in the distal mantle sources at depth may take place involving other phases too. For example, N solubility in deeper mantle phases such as wadsleyite, ringwoodite, has been shown to be higher through laboratory experiments (Yoshioka et al., 2018). Similarly, given the siderophile character of N over silicate minerals and melts for a wide range of fO_2 conditions relevant for the Earth's mantle (e.g., Dasgupta et al., 2022b, Grewal et al., 2019a, Grewal et al., 2021, Jackson et al., 2021, Shi et al., 2022), accessory Fe-rich metallic phases such as Fe-Ni-C alloy, precipitated via iron disproportionation, may also serve as hosts of nitrogen in the deep MORB and OIB sources. Storage of N in small quantities of Fe-Ni alloy phase in the mantle is expected to depend on its composition. Ni-rich alloy, which is expected at deep upper mantle conditions, should provide a lower storage of N compared to alloys in the deeper mantle that are richer in Fe (e.g., Grewal et al., 2019a). Similarly, sulfide phases are also expected to host finite proportion of N with greater storage in sulfides with higher metal-to-sulfur ratio (e.g., Grewal et al., 2019b).

1.1.9. The fate of volatiles during MORB and OIB source melting

Supplying the mantle volatiles to the crust and ocean-atmosphere system takes place via mantle melting. The process of partial melting for the MORB and OIB sources is chiefly via adiabatic decompression (Langmuir et al., 1992, Stolper and Asimow, 2007). The volatiles, being incompatible elements in silicate minerals, partition to the partial melt as opposed to get preferentially sequestered in the solid melting residue. One of the most important aspects of trace volatile elements such as carbon and hydrogen, however, is that unlike other trace elements, they do not behave passively during mantle melting. Instead, they affect the melting temperatures, melting phase relations, and near-solidus melt compositions in terms of major and trace elements (Aubaud et al., 2004a, Dasgupta, 2018, Falloon and Green, 1989). However, not all volatile elements or species behave the same in the mantle and their fate and influence during mantle melting are not similar. For example, sulfur, although present in 100-300 ppm range, does not impart any significant control on melting phase relations at Earth's upper mantle conditions. Nitrogen, being present in ultra-trace quantity also does not appreciably affect melting at the Earth's mantle. Hence, in this section we will discuss the role of carbon and water on MORB and OIB source mantle melting. For sulfur and nitrogen, the discussion will be on their fate during partial melting.

Notably, MORB source is estimated to be relatively cooler with mantle potential temperatures of ~1315-1400 °C, whereas OIB sources are hotter with mantle potential temperatures of ~1400-1600 °C (Herzberg and Asimow, 2008, Lee et al., 2009, McKenzie et al., 2005). Furthermore, mantle melting by decompression continues to shallower depths beneath MOR compared to those beneath intraplate ocean islands. For the latter, the increased lithospheric thickness prevents shallower melting. These differences also impart differences in terms of the effects and fate of volatiles during mantle melting in two settings.

1.1.9.1. The roles and fates of water during MORB and OIB source melting

It is known for a long time that water has a significant effect on melting processes of silicate rocks in the mantle mainly by solidus depression and change in phase relations (Ulmer, (Ulmer, 2001;Bowen, 1928). Because magmas are the wettest in subduction zone environment, the effects of water on magma genesis have mainly been studied in the context of arc magma generation (Grove et al., 2012, Kushiro et al., 1968, Till et al., 2012, Ulmer, 2001). In comparison, MORBs and OIBs and therefore, their sources are essentially "dry". In the sections above, we described how dry these sources are: the MORB source is considered to have up to 200 ppm H_2O while OIB sources are wetter and more diverse (from 350 to 1100 ppm H_2O depending on the type of OIB). Hence, experiments under water-rich conditions and in particular purpose of our presentation, the key question is what is the fate and roles of tens to hundreds of ppm by weight of water in the oceanic mantle-melting environment.

Studying hydrous melting of mantle rocks for MORB and OIB generation would require conducting experiments with a fertile peridotite having 100-1000 ppm water concentrations. The effect of water could then be appreciated by comparison with experiments that are perfectly dry. In reality, perfectly dry experiments are impractical because it is not possible to control such low amount of water in experiments. Furthermore, perfectly dry experiments are virtually impossible to conduct because water is a common contaminant in terrestrial environment and during high pressure experiments (Hirschmann, 2000, Laporte et al., 2004, Sarafian et al., 2017). As a result, our understanding of the effect of trace water on melting in the MORB and OIB source comes from two approaches: (1) interpolation between hydrous fluid-present or wet solidus and dry solidus of peridotite (2) the study of hydrogen partitioning between melt and nominaly anhydrous minerals and the application of the freezing point depression approximation (Aubaud et al., 2004a, Dasgupta, 2018, Dasgupta et al., 2007b, Dasgupta et al., 2013, Hirschmann et al., 2009, O'Leary et al., 2010).

Katz et al. (2003) surmised that the solidus depression caused by water, relative to the dry peridotite solidus, is directly proportional to the partial melt water content. Using the quantitative effects of water on liquidus depression of basaltic melt, these authors came up with an empirical formalism to compute solidus depression such as –

$$\Delta T\,(X_{H2O}) = K X H2O \gamma \qquad (8)$$

Where, the γ is between 0 and 1 and melt water content came from the use of a fixed bulk partition coefficient for H_2O between peridotite and melt of 0.01. Katz et al. (2003) parameterization also allows calculating extent of melting as a function of temperature for different bulk H_2O contents. A key aspect of Katz et al. (2003) approach is calculating melt water content using a fixed bulk partition coefficient of H_2O between peridotite and basalts. Indeed, with all water being stored in nominally anhydrous minerals, the influence of 'water' in lowering the MORB or OIB source peridotite solidus comes from partitioning of hydrogen from the mantle silicate minerals to the near solidus partial melts. In this framework, the depression of solidus below the 'dry' peridotite solidus is proportional to the water content of the low-degree partial melt at the solidus as the melt fraction approaches zero.

Another approximation of quantitative estimate of nominally anhydrous solidi comes from the application of the cryoscopic equation with respect to the experimentally determined 'dry' solidus, following the equation –

$$T = 1(1T\text{peridotitefusion} - R\Delta H\text{peridotitefusion}\ln 1 - X\text{OH} - \text{melt}) \quad (9)$$

Where T is the temperature of hydrous solidus with respect to the dry peridotite solidus. Dissolved water in silicate partial melt is assumed to be completely dissociated to hydroxyl, $X\text{OH} - \text{melt}$ and silicate components of the melt are assumed to have molar units and can be assumed to have either oxide molar units or those expected on the basis of 8-oxygen mole or something in between (e.g., Dasgupta, 2018). Following this approach, many authors have computed the possible loci of hydrous peridotite solidi with trace H_2O content (Aubaud et al., 2004a, Hirschmann, 2006, Hirschmann et al., 2009, O'Leary et al., 2010). Most recent efforts took into account more accurate models of variation of mineral-melt D_{H2O} values as a function of depth and change in modal mineralogy with depth. Importantly, water is less incompatible in pyroxenes for shallower mantle domains in the spinel peridotite field. At deeper depths, in the garnet stability field, pyroxenes become less aluminous and consequently water is more incompatible. Greater incompatibility of water in peridotitic minerals in the garnet stability field means higher water content of near-solidus partial melts, which leads to greater depression of the peridotite solidus. Following O'Leary et al. (2010), in Fig. 9, we show the solidi of damp peridotite for 50-200 ppm bulk water. Superimposed on the hydrous solidi in Fig. 9 are the estimated thermal regimes prevailing below the MORs and OIs globally. Given the slopes of the hydrous solidi and those of the mantle adiabats that the effects of solidus depression caused by water is more effective beneath OIs compared to MORs. The deepening of the solidus caused by a given water content is greater for hotter mantle domains similar to those estimated for the ocean islands compared to relatively cooler MORB mantle domains (Fig. 9).

Although the calculations of sort presented above have thus far provided the most realistic ways to constrain the solidi of peridotite with trace concentrations of bulk H_2O, this approach may overestimate the solidus depression effect of trace water. This is because of the

fact that the experimentally determined nominally volatile-free peridotite solidus is not truly a dry solidus as it is impossible to avoid few tens of ppm H_2O in the nominally anhydrous residual minerals in laboratory experiments (Sarafian et al., 2017).

Given the range of water contents in the MORB source of ~50-200 ppm, H_2O contents in the 0.1% partial melt is ~0.75-3 wt.%. The effects of such water contents on major element compositions of partial melts are not expected to be significant and hence are not discussed further. In other words, water content is not estimated to be high enough to affect mantle melt compositions as known to occur in subduction zones (e.g., Ulmer, 2001; Grove et al., 2006). For OIB source mantle, however, H_2O content of 0.1 wt.% partial melt can be as high as ~9 wt.%. Tenner et al. (2012) performed hydrous partial melting of garnet peridotite, similar to those expected for source regions of OIBs. Based on the partial melt compositions of Tenner et al. (2012), it can be surmised that the effects of such water contents on major element compositions of melts are also not major; although hydrous melts of OIB source garnet peridotite appear to be silica undersaturated (Tenner et al., 2012).

1.1.9.2. The roles and fates of carbon during mantle melting

Because of the difference in the mantle storage of CO_2 versus H_2O at hundreds of ppm level, the effects and fates of CO_2 are distinctly different from that of water. Dasgupta (2018) has recently synthesized these differences. The main essence from that study is summarized here in the context of MORB and OIB sources. At depths deeper than the corresponding pressure of ~2 GPa, peridotite cannot be saturated in a CO_2-rich fluid at mantle temperatures (Brey et al., 1983, Eggler, 1978, Falloon and Green, 1989, Newton and Sharp, 1975, Wyllie, 1978). Instead, at depths deeper than 60-70 km, a series of reactions between CO_2-rich vapor and mantle silicates stabilize mineral carbonate phases and hence the solidus of relevance becomes that of carbonated peridotite. The subsolidus peridotite is a dolomite-bearing peridotite at shallow depths (~70–100 km) and magnesite-bearing peridotite at deeper depths (>100 km; (Dasgupta and Hirschmann, 2006, Falloon and Green, 1989)). The carbonated peridotite solidus does not vary as a function of bulk CO_2 content of peridotite (Dasgupta and Hirschmann, 2007a), that is, the solidus temperature at a given pressure is unchanged for any bulk CO_2 content above few tens of ppm, which is the solubility limit of CO_2 in nominally carbon-free mantle silicates (Keppler et al., 2003, Shcheka et al., 2006). This is because that the near solidus melt of natural carbonated peridotite is carbonatitic (~40 wt.% CO_2) at all depths greater than 70 km (e.g., Dasgupta, 2013, Dasgupta and Hirschmann, 2006, 2007b, Falloon and Green, 1989, 1990, Wallace and Green, 1988). Therefore, the natural carbonated mantle solidus is chiefly controlled by melting of the carbonate phase aided by freezing point depression effect of alkalis. The invariance of mantle solidus in the carbonate stability field, as a function of bulk carbon content is distinctly different from the variable solidus location of peridotite with variable water content as discussed previously. The key point is that at depths deeper than the stabilization of carbonate minerals, the mantle solidus is a carbonated peridotite solidus and is 500-600 °C lower than the solidus of volatile-free peridotite.

The consequence of the possible existence of a carbonated MORB and OIB source mantle is that the onset of melting of upwelling mantle could be 300-350 km deep for the MORB source and even deeper for the OIB source (Fig. 10). Upwelling MORB or OIB source mantle,

therefore, generates incipient carbonatitic melt first. Such carbonatitic melt gradually evolves to carbonated silicate melts or CO_2-rich silicate melts as mantle continues to melt further upon decompression or as the deep carbonatitic melt percolates upward and reacts with the peridotitic assemblage above. Dasgupta et al. (2013) experimentally investigated the transition from carbonatitic melt to CO_2-rich silicate melt in the melting interval of peridotite. These authors found that carbonatitic melt with ~40 wt.% dissolved CO_2 evolves to a strongly silica-undersaturated melt with ~25 wt.% CO_2 as deep as 200 km beneath MOR (Fig. 10). In other words, in the presence of oxidized carbon, silicate melting also commences deep in the mantle. In hotter OIB source mantle, this generation of CO_2-rich silicate melt is expected to occur much deeper but the exact depth remains uncertain as higher pressure data on carbonated mantle melting (e.g., Ghosh et al., 2014) have not been parameterized to extract quantitative information on low-degree carbonated melting.

As mentioned in the section on volatile storage, carbon exists in the Earth's mantle as diamond or graphite as well. Or perhaps partly in Fe-Ni±S melt or (Fe,Ni) carbide. In the context of mantle melting, it matters immensely whether carbon exists as oxidized or reduced species. If the latter that is carbon being present as graphite/diamond or CH_4-rich fluid, deep melting of MORB and OIB source as summarized in the preceding section will not apply. In such a case, the initial release of carbon to the partial melt would be via redox breakdown of diamond/graphite or Fe-Ni±S(±Cu)-C phase or (Fe,Ni)-carbide to formation of carbonated melt. However, such melting relations, especially those involving C-bearing alloy/sulfide phase and carbide have yet to be fully understood. Rohrbach and Schmidt (2011) and Stagno et al. (2013) investigated redox melting/freezing of carbon in peridotite systems. According to these authors, the release of carbon to shallower MORB or OIB sources should take place via redox melting such as the following (e.g., (Dasgupta, 2018, Dasgupta and Hirschmann, 2010); reaction progressing from left to right) –

$$Mg_2SiO_4 + C + O_2 = MgSiO_3 + MgCO_3 \quad (10)$$

(olivine) (diamond/graphite) (source of oxidation) (orthopyroxene) (magnesite)

Of course, there is no molecular oxygen-rich fluid in the mantle to oxidize C^0. Rather this is realized by reducing Fe^{3+} in garnet from deeper depth and oxidizing C^0 to C^{4+} in the process, such as the following reaction.

$$C + 3FeSiO_3 + 2Fe_2O_3 = FeCO_3 + 3Fe_2SiO_4 \quad (11)$$

(diamond/graphite) (orthopyroxene) (in garnet) (melt) (olivine)

Stagno et al. (2013) argued that for the average $Fe^{3+}/\Sigma Fe$ ratio of the upper mantle, reaction such as the one above would drive redox melting of the mantle and release of carbonated melt at depths ~150 km beneath MORs. Again, this conclusion was reached assuming that the Earth's asthenospheric mantle beneath MORs and OIs get reducing with depth following the same trend as those constrained by continental mantle xenoliths. Therefore, if the MORB and OIB source mantle with depth have the same fO_2-depth trend as that for the continental mantle, no carbonatite generation would take place at depths ≥300 km. Moreover, given the transition from carbonatitic to carbonated silicate melt takes place at depths as deep as ~240 km (Dasgupta et al.,

2013), redox melting of C-bearing mantle would generate silica-poor, carbonated basaltic melt at the solidus.

Several studies argued that the OIB source regions are variably more oxidized than the MORB source mantle (Brounce et al., 2017, 2021, Hartley et al., 2017, Moussallam et al., 2019). If this is applicable globally and all plume sources are more oxidized with the depth-fO_2 trend being offset from those beneath ridges, melt generation and CO_2 release would commence deeper for the OIB sources but shallower for more reduced MORB sources (Fig. 10). The exact depth of C-induced melting for the OIB source and the mechanism of such melting would depend on how oxidized the OIB source is. Oxygen fugacity enhancement of ~0.5 log units can push the transition from carbonated melt to graphite/diamond by 30-40 km (Fig. 7). If OIB sources are oxidized by no more than 0.5 log units compared to the MORB sources, then the onset of melting for OIB sources are still expected via redox melting. For the OIB sources to start melting across the carbonated peridotite solidus, the depth-fO_2 dependence for the OIB source needs to be different from what is estimated for the continental mantle (Frost and McCammon, 2008, Stagno et al., 2013). Irrespective of whether the OIB source begins to melt at the redox or carbonated solidus, the deepening of the solidus would allow generation of carbonated melts with higher dissolved CO_2 contents from the OIB sources. Such strongly carbonated primary melts indeed seem to be necessary to explain the many major and trace element geochemistry of alkalic OIBs globally (Dasgupta et al., 2007a, Gerbode and Dasgupta, 2010, Hirose, 1997, Mallik and Dasgupta, 2013, Mallik and Dasgupta, 2014, Sun and Dasgupta, 2023).

1.1.9.3. The combined roles of CO_2 and H_2O during MORB and OIB source melting

In the section on volatile abundance of the oceanic mantle, we established that the MORB and OIB source mantle contains both water and carbon dioxide. Direct experimental constraints on mixed CO_2-H_2O-bearing mantle melting, especially at minor to trace concentrations of those volatiles, are limited and difficult to obtain and interpret (Lara and Dasgupta, 2022, 2023, Pintér et al., 2021, Saha and Dasgupta, 2019). The combined effects of carbon and water on mantle melting are complex and depend on relative concentrations of the two species, as well as on oxygen fugacity of the mantle domain, which can change the carbon storage from CO_2/carbonate to graphite/diamond.

At conditions where both volatiles are present in the fluid phase, the presence of CO_2 lowers the activity of H_2O, a_{H2O} in the fluid and thus the H_2O fluid-present solidus increases and isobaric melt productivity decreases. This was first observed for H_2O-rich fluid-present solidus of metapelites (Mann and Schmidt, 2015, Tsuno and Dasgupta, 2012), and has recently been observed for peridotitic system as well (Lara and Dasgupta, 2023). However, MORB and OIB source mantles are fluid-absent and at such conditions the effect of CO_2 and H_2O on freezing point depression and melt productivity are expected to be additive. The previous sections established that trace CO_2 in the form of accessory carbonates has a greater influence, compared to trace water, in inducing incipient melting of the MORB and OIB sources. Therefore, even for

natural mantle sources with both volatiles, the onset of melting is chiefly controlled by carbonated or C-involved redox melting. However, the conditions of such C-involved melting in the MORB and OIB source mantle are modulated by the presence of trace amount of water. Water partitions from mantle minerals to carbonated melts and thus stabilizes carbonated melt of a given CO_2 content at a lower temperature for a given pressure (Dasgupta et al., 2013; Dasgupta, 2018; Dasgupta et al., 2022). In other words, stability of carbonated silicate melts takes place at even deeper depths beneath MOR and OIs in the presence of trace water. This is because of the effect of water on freezing point depression that leads to melt fraction enhancement. Higher the bulk water, deeper is the stability of carbonated melts of any given CO_2 contents. Given silica and CO_2 shows strong inverse correlation in mantle-equilibrated melts (e.g., Dasgupta et al., 2007; Dasgupta et al., 2022), the effects of water is stabilizing less silica-undersaturated melts at deeper depths. The combined effects of CO_2 and H_2O is, therefore, deeper generation of strongly alkalic to alkalic primitive magmas in MORB and OIB source regions. Sampling of such melts occurs primarily at ocean islands chiefly because of thicker lithospheres in these settings. Thicker lithospheres suppress shallower and more voluminous volatile-poor, basaltic magmatism, thereby, preserving the geochemical signatures of deeper, volatile-rich melts.

1.1.9.4. The fate of sulfur during MORB and OIB source mantle melting

We described in the previous section that shallow to deep upper mantle beneath MORs and OIs contains sulfur chiefly in sulfide melts that are immobile and present disconnected droplets at mineral grain junctions. Hence, the extraction of S from the mantle and concentration in the ocean-floor basalts depend on the dissolution of the sulfide melts in mantle-derived partial melts. Given sulfur's storage in accessory sulfide phases, which even in a molten state is immiscible with respect to silicate or CO_2-H_2O-rich partial melts, S cannot be modeled as an incompatible trace element during the onset of mantle melting. Instead, sulfur extraction from the MORB and OIB source mantle is understood via dissolution capacity of sulfur in mantle partial melts at sulfide saturation. The parameter is called sulfur concentration (of mantle melts) at sulfide saturation (SCSS). Because the low-degree melts from the mantle is sulfide saturated, S enrichment in such melts is limited to what is permitted by SCSS.

A large number of experimental studies from the 1970s studied the control of various intensive and extensive variables on SCSS (e.g., Ding et al., 2014, Ding et al., 2018, Fortin et al., 2015, Holzheid and Grove, 2002, Li and Ripley, 2005, O'Neill and Mavrogenes, 2002, Smythe et al., 2017, Wykes et al., 2015). The key findings are that SCSS increases with increasing temperature and melt FeO* content and with decreasing pressure and melt SiO_2 content for basaltic to andesitic melts. Melt SCSS also decreases if the equilibrium sulfide is not pure FeS melt but rather Ni- and Cu-bearing (Ariskin et al., 2013, Ding et al., 2018, Smythe et al., 2017). Utilizing SCSS models, many authors have attempted to reconcile the S inventory of MORBs and OIBs (Ding and Dasgupta, 2017, Ding and Dasgupta, 2018, Sun et al., 2020). These studies also independently bracketed S inventory of MORB or OIB source mantles (Table 4). Although the SCSS model predictions vary from one another (e.g., Ariskin et al., 2013, Ding et al., 2018,

Fortin et al., 2015, Li and Ripley, 2005, Smythe et al., 2017), all models yield sulfur content of basaltic partial melts at mantle melting conditions that are too high to match the primitive MORB sulfur contents. Such discrepancy is not thought to be caused by degassing of sulfur during MORB emplacement or eruption. Instead, the hot, primitive basalts are thought to be sulfide undersaturated at the magma chamber depths, owing to high SCSS at high-*T* and low-*P*. Upon cooling, the primitive MORB parental melts saturates in sulfide once again as the SCSS drops with decreasing temperature (Ding and Dasgupta, 2017, O'Neill, 2021, Smythe et al., 2017). This is evident from the geochemistry of sulfur and other chalcophile elements in MORBs (Ding and Dasgupta, 2017, Jenner and O'Neill, 2012, Wallace and Carmichael, 1992, Wallace and Edmonds, 2011). However, some MORB glasses also clearly appear to be sulfide undersaturated (Shimizu et al., 2016), despite the claim that nearly all ocean-floor basalts are sulfide-saturated. For sulfide undersaturated MORBs, the observation of sulfide blebs (Patten et al., 2012) may indicate rapid cooling features.

Given the OIB sources are hotter and melting is typically restricted to deeper depths, extraction efficiency of sulfur from sulfide-present mantle beneath ocean islands may be different than that beneath MORs. In addition, OIB sources may also be relatively more oxidized and consequently may dissolve sulfur in basaltic melts not only as S^{2-} but also as S^{6+}. Indeed basaltic glasses in Samoa and Hawaii (Mauna Kea) show the presence of dissolved S^{6+} species (Brounce et al., 2017, Labidi et al., 2015). However, interestingly, S contents of primitive MORBs and OIBs are similar (Ding and Dasgupta, 2018). Ding and Dasgupta (2018) explored ways of explaining the primitive OIB sulfur budget by combining decompression mantle melting model and models for SCSS. These authors concluded that if the S and Cu (a sulfide-loving element) budget of OIBs are consistent with a sulfide-saturated peridotitic source, then one of the following conditions need to be met: (1) Ni content in the sulfide melt is ~25–30 wt % and the parental OIB melts are derived from a relatively cold mantle (T_P ≤1450 °C); (2) partial melts parental to OIB are enriched in S (>1500 ppm), or (3) an extremely low (≤1%) degree of melting is applicable. However, if the T_P if high (e.g., 1450-1650 °C) and Ni content in the equilibrium sulfide in the peridotitic mantle is ≤20–25 wt.%, then the OIB sulfur and Cu budgets are difficult to reconcile with sulfide-present partial melting of fertile peridotite. In such a case, mixing of partial melts, derived from low-degree melting of MORB-eclogite and metapelite, with sulfide-absent peridotite partial melts can explain the measured S and Cu contents in the low-F (<10%, where F is melt fraction) OIBs. The analyses of Ding and Dasgupta (2018) called for heterogeneous distribution of sulfur in the OIB source. Peridotitic matrix in the OIB source was suggested to be depleted in S with bulk contents of 50-100 ppm, whereas veins of eclogite or sediments was suggested to contain much greater proportion of sulfides. Greater proportion of sulfides in the subducted sediments and ocean crust is expected owing to higher bulk abundance of S in the ocean-floor basalts and sediments and relative lack of mobility of sulfides from crustal lithologies during subduction (e.g., Canil and Fellows, 2017, Jégo and Dasgupta, 2013, 2014, Li et al., 2020). Ding and Dasgupta (2018) posited that because of lower SCSS of MORB-eclogite or sediment-derived partial melts with higher silica and lower FeO*, the OIB source eclogite should supply sulfide-saturated melts to to OIB petrogenesis. In other words, sulfur and chalcophile element inventories of OIBs may call for mixing between peridotite-derived partial melts from sulfide-absent source and eclogite-derived partial melts from sulfide-present source.

Extraction of sulfur from MORB and OIB source mantle thus far mostly focused on sulfur dissolution during shallow basalt petrogenesis, i.e., at conditions of partial melting across the volatile-free peridotite solidus. Recently, Chowdhury and Dasgupta (2020) explored the extent of sulfur mobilization by incipient melts prior to the onset of major silicate melting beneath MORs. The experiments on sulfide melt-carbonated melt equilibria showed that unlike in the case of silicate magmas, SCSS of carbonated magmas increase with increasing SiO_2 contents, i.e., it increases as the melt evolves from carbonatite to carbonated silicate melts. More importantly, SCSS of strongly carbonated melts at reducing conditions is distinctly lower compared to those of basalts (Chowdhury and Dasgupta, 2020, Woodland et al., 2019). Therefore, deep incipient carbonated melt generation is unable to exhaust sulfide from the peridotite residue for the MORB and OIB source mantles.

1.1.9.5. The fate of nitrogen during mantle melting

Much less is known about the fate of nitrogen during mantle melting. Under the conditions of the Earth's present-day upper mantle, N is thought to be highly incompatible (e.g., Keppler et al., 2022, Li et al., 2013). Although data and constraints on N partitioning between mantle minerals and silicate partial melts are lacking, existing data suggest that there may be a strong dependence of fO_2 on rock/melt partitioning of N, with N behaving more and more incompatibly as the conditions get more oxidized (Dasgupta et al., 2022b, Li et al., 2013). Therefore, although N is expected to be highly incompatible during MORB and OIB petrogenesis in the modern Earth, similar partial melting settings at plausibly more reducing Hadean and Archean Earth (Stagno and Aulbach, 2021) might have seen a somewhat less incompatible behavior of N.

1.1.10. Fluxed melting in the MORB and OIB sources and flux of volatiles through MOR and OI settings

1.1.10.1. Modern Earth

The concept of flux melting remains popular for the subduction zone magmatism where hydrous fluid, derived from the subducting lithologies, lowers the melting temperatures and enhances melt productivity of mantle wedge. Such concepts are not generally considered for the melting beneath MORs and intraplate OIs and hotspots. However, the previous section discusses how CO_2-rich and H_2O-bearing melts are generated well below the onset of major melting of mantle peridotite. If mantle heterogeneity such as recycled ocean crusts and continental sediments are considered, the possibility of generation of such volatile-rich melt flux is even higher and melts are generated even deeper (Dasgupta et al., 2006, Spandler et al., 2010, Tsuno and Dasgupta, 2011). Given these CO_2±H_2O-rich melts are of low density, low viscosity, and form interconnected network through mantle matrix, they percolate upward efficiently and has the ability to act as a flux to shallower mantle regions via porous flow. The mantle concentrations (Table 2-5) and the relative degree of incompatibility of the volatiles during

mantle melting dictate the volatile-budget of such melt flux. The effective partition coefficients for major volatile species at the Earth's present-day, relatively oxidized mantle are $D_{CO2} << D_{H2O} < D_S$ at the onset of melting. Hence volatile-induced flux that (Dasgupta et al., 2022b) affect the largest volume of upwelling mantle generate CO_2-rich melts that are H_2O-bearing and S-poor (e.g., Dasgupta et al., 2022). This feature, combined with the fact that the solubility of the key volatile species in basaltic magmas at shallow depths decrease in the order S, H_2O, and CO_2, dictate that the flux of CO_2 during MOR and OI magmatism is the highest among all major volatiles (Table 2-5).

It remains an open question, however, how important the deep volatile-melt flux has been in controlling the flux of CO_2 and other volatiles through MORs and OIs globally. Deepening of the onset of highly incompatible volatile release must affect the mantle volume that gets processed through unit geologic time. Given this, more oxidized oceanic mantle that leads to deeper onset of redox or carbonated melting should lead to greater flux of volatile gases, especially CO_2. Therefore, the debate on the oceanic mantle fO_2 with depth (Eguchi and Dasgupta, 2018b, Gaillard et al., 2015, Stagno et al., 2013) at the present-day mantle is directly tied to the quantitative flux of incompatible volatiles such as CO_2 (Figure 11).

1.1.10.2. The effects of redox and compositional heterogeneity in the MORB and OIB sources

Thus far we mainly focused on the global behavior of major volatiles, their effects on melting depths of peridotite (the dominant upper mantle lithology), with the expected background mantle oxygen fugacity varying as a function of tectonic settings and depth. However, the evidence of mantle heterogeneity both in redox (Cottrell and Kelley, 2013) as well as in major element, lithology or mineralogy in the mantle are also plentiful (Dasgupta et al., 2010, Garapić et al., 2015, Hirschmann and Stolper, 1996, Jackson and Dasgupta, 2008, Le Roux et al., 2011) in the geochemistry of erupted basalts. Furthermore, volatile budget of a given mantle domain is also often coupled to its source compositions. For example, the presence of recycled, altered oceanic crusts may locally elevate the budget of carbon and sulfur well above the budget estimated for the background mantle, as both of these elements are known to deeply recycle into the mantle via subduction (Dasgupta et al., 2004, Duncan and Dasgupta, 2017, Jégo and Dasgupta, 2013, 2014). In addition, various isotopic mantle end-members have also been estimated to contain distinctly different volatile abundance (Table 2-5; Fig. 6; (e.g., Dixon et al., 2002; 2017)). Similarly, recycled crustal lithologies are also more oxidized, i.e., contain a higher Fe^{3+}/Fe_T ratios and therefore can host carbon in the form of carbonates over graphite/diamond to much deeper depths than what is thought for background mantle peridotite (Stagno et al., 2015). In addition, because of distinctly higher abundance of carbon, fO_2 of recycled heterogeneities can also be set by C^0-C^{4+} equilibria rather than Fe^{2+}-Fe^{3+} equilibria (Luth, 1999). Therefore, carbonated or C-involved redox melting of recycled lithologies can take place at depths where the ambient mantle cannot release carbon via melting. Deep melting of recycled lithologies aided by carbonates ± water is indeed thought to be an important process necessary to contribute many features of silica-poor, alkalic OIBs, including elevated CaO and TiO_2 and depleted SiO_2 and Al_2O_3 in primitive alkali OIBs (Gerbode and Dasgupta, 2010, Mallik and Dasgupta, 2013, Mallik

and Dasgupta, 2014). Deep carbonated melting in locally oxidized domain is also thought to be linked to halogen geochemistry of OIBs globally (Kirstein et al., 2023) and is critical in releasing volatiles such as chlorine. Chloride-bearing carbonatitic inclusions in diamonds and carbonate-chloride enrichment in kimberlites are clear testaments that oxidized chloride-carbonate melts are generated at deep mantle (Kamenetsky et al., 2007, Zedgenizov et al., 2007). Laboratory experiments on mixed chloride-carbonate eclogite and peridotite systems also capture broadly some of the compositional variability of (Litasov et al., 2010, Safonov et al., 2011). These types of melts are expected to be generated at least locally in deep MORB and OIB source mantles, although their production may not be a norm everywhere.

1.1.10.3. Ancient Earth MORB and OIB source melting

It remains debated how the mantle fO_2 evolved through time with studies suggesting effectively no change of mantle fO_2 with time (Li and Lee, 2004, Trail et al., 2011) as well some recent studies pointing to as much as 2 log units reduction of fO_2 between 2 and 4 Ga (Nicklas et al., 2018, Stagno and Aulbach, 2021). If the depth-dependence of the ancient mantle fO_2 remained similar to that envisaged for the present-day Earth's mantle, based on continental xenoliths, then the mantle is expected to have reduced form of carbon throughout (Fig. 5). In such a scenario, C-induced melting – either via carbonate melting or via redox melting – is completely suppressed. The onset of melting in such a scenario would be at the nominally anhydrous peridotite solidus (Fig. 12). If this was the case, CO_2 degassing would be greatly limited through MOR or intraplate melting and degassing because CO_2 dissolution in basaltic magma would be limited to what is achieved at graphite saturation (Eguchi and Dasgupta, 2018a), which is significantly muted compared to carbonate dissolution. It is possible that hotter mantle of the Hadean and Archean, which would lead to deeper melting of nominally-volatile free peridotite, can partly offset the lack of carbonated silicate melt generation in terms of CO_2 extraction. Future models of MOR or OI degassing through time, building on studies such as Fuentes et al. (2019), need to consider possible coupled evolution of mantle fO_2 and volatile-induced melting and differential mantle processing. Stagnant to sluggish-lid tectonics coupled with more reduced mantle could have led to diminished outgassing flux of volatiles such as CO_2 in the early Earth. Or at the minimum, the absence of generation of strongly carbonated melts might have offset the effect of hotter mantle, deeper solidus of volatile-free mantle, and greater convective vigor. In other words, despite secular cooling of the mantle, CO_2 outgassing efficiency from the oceanic mantle may have increased through time or at least not diminished.

More reduced mantles of the Archean and Hadean eons, if relevant, could have affected melting induced release of other volatile elements too. For example, flux of N_2 might also have been lesser for more reduced mantle, because of lesser incompatibility of N during mantle melting and higher solubility of N in silicate melts at more reducing conditions. Although for N, the effect might not have been significant as enhanced N dissolution in silicate minerals and melts require strongly reducing conditions, i.e., $\log fO_2 <\sim$IW-2 (Dasgupta et al., 2022b, Libourel et al., 2003). More constraints on mantle volatile abundances and redox in different domains and their possible variation through time are needed to test and refine some of these possibilities.

1.1.11. Outlook

MORB and OIB geochemistry suggest that their mantle sources are distinct both in terms of elemental abundance as well as isotopic compositions of major volatile elements, C, H, S, and N. OIB mantle sources are variably enriched in both primordial and recycled volatiles such as carbon, sulfur, water, and nitrogen. Accordingly, OIB mantle is estimated to have larger range of volatile element budgets. The bulk mantle abundances of various volatiles, therefore, depend on the relative volumes of the OIB vs MORB source mantles. It is possible that the OIB source mantles are preferentially replenished in volatile elements such as carbon and sulfur via subduction-recycling, yet such sources also show primordial volatile signature in abundance.

Sustaining Earth's ocean-atmosphere over geologic time depends on volcanic degassing of major volatiles at MOR and OI settings. In both settings, mantle chiefly melts via decompression, with shallower mantle having the potential to receive CO_2±H_2O-rich melt flux. However, owing to hotter thermal regime responsible for OIB genesis, volatile release takes place at deeper depths. Furthermore, being enriched in volatiles, melts richer in CO_2 and H_2O are generated at the onset of melting for the OIB source. Increased lithospheric thickness suppresses shallow mantle melting for the intraplate settings, leading to extraction of more volatile (CO_2, H_2O)-rich melts, which is consistent with several major and trace element geochemistry of OIBs. Volatile-rich melt generation from the deep OIB source could, however, be suppressed at more reduced mantles with carbon stored as graphite rather than carbonates. Such reduced OIB or MORB source mantles might have been present in the ancient Earth. Extraction efficiency of major volatiles from the Earth's mantle therefore might have varied through time – controlled not only by changing thermal regime, but also by changing redox potential. More constraints are needed for spatial and temporal variability of OIB and MORB source volatile budgets understand Earth's deep volatile cycles better.

Acknowledgments

RD and CA thank Chenguang Sun for some initial discussion on the content of this chapter. RD also acknowledges funding from NSF grant EAR-1763226 and NASA grant 80NSSC18K0828. CA acknowledges support from the French Ministry of Research, INSU-CNRS, and ANR through the IdEx Université de Paris ANR-18-IDEX-0001.

Figures

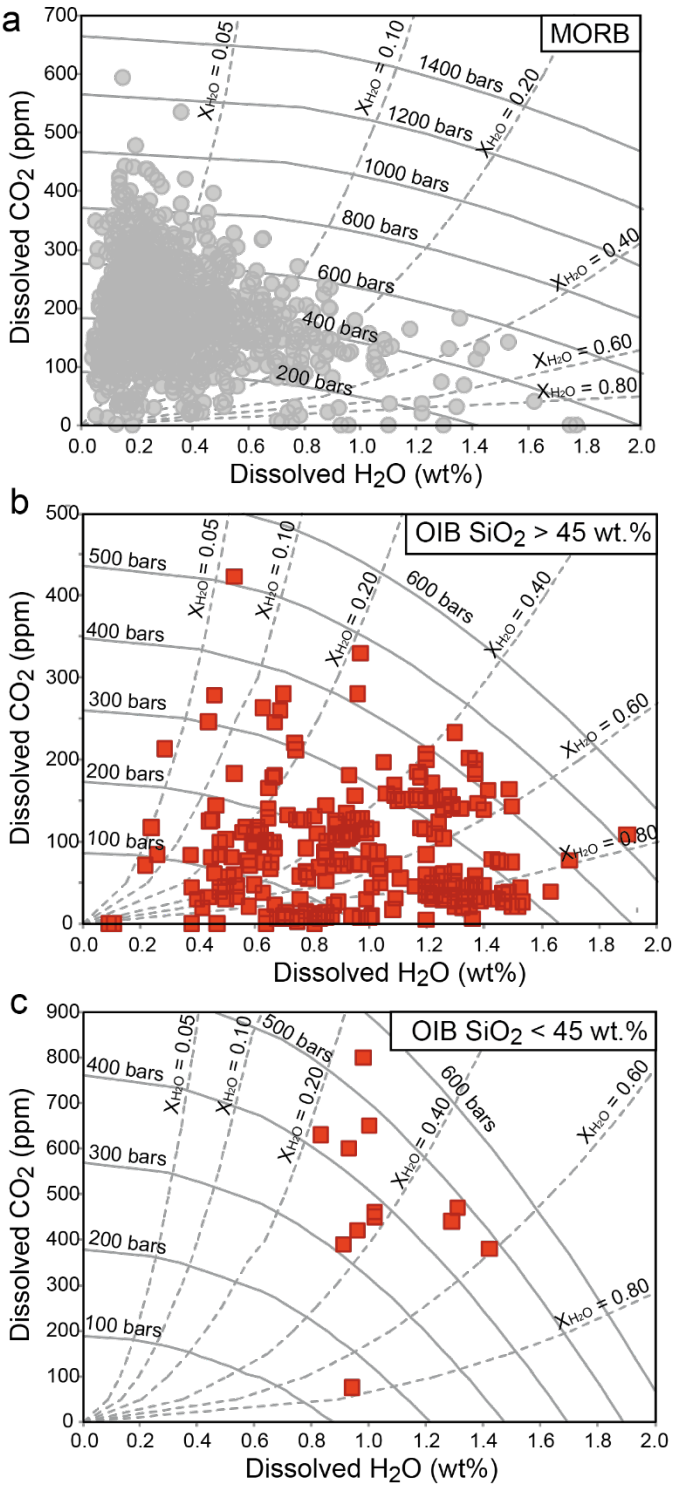

Figure 1. Dissolved CO_2 (ppm by weight) against dissolved H_2O (wt.%) for (A) MORB submarine glasses, (B) hotspot submarine basaltic glasses with SiO_2 >45 wt.% and (C) hotspot submarine basaltic glasses with SiO_2 <45 wt.%. The distinction between hotspot submarine glasses larger and smaller than 45 wt.% SiO_2 has been made to take into account the larger CO_2 solubility in alkalic melts compared to that in melt with tholeiitic composition (Dixon, 1997). The isobars and isopleths have been calculated

with the program VolatileCalc (Newman and Lowenstern, 2002). The figure is redrawn from Aubaud (2022).

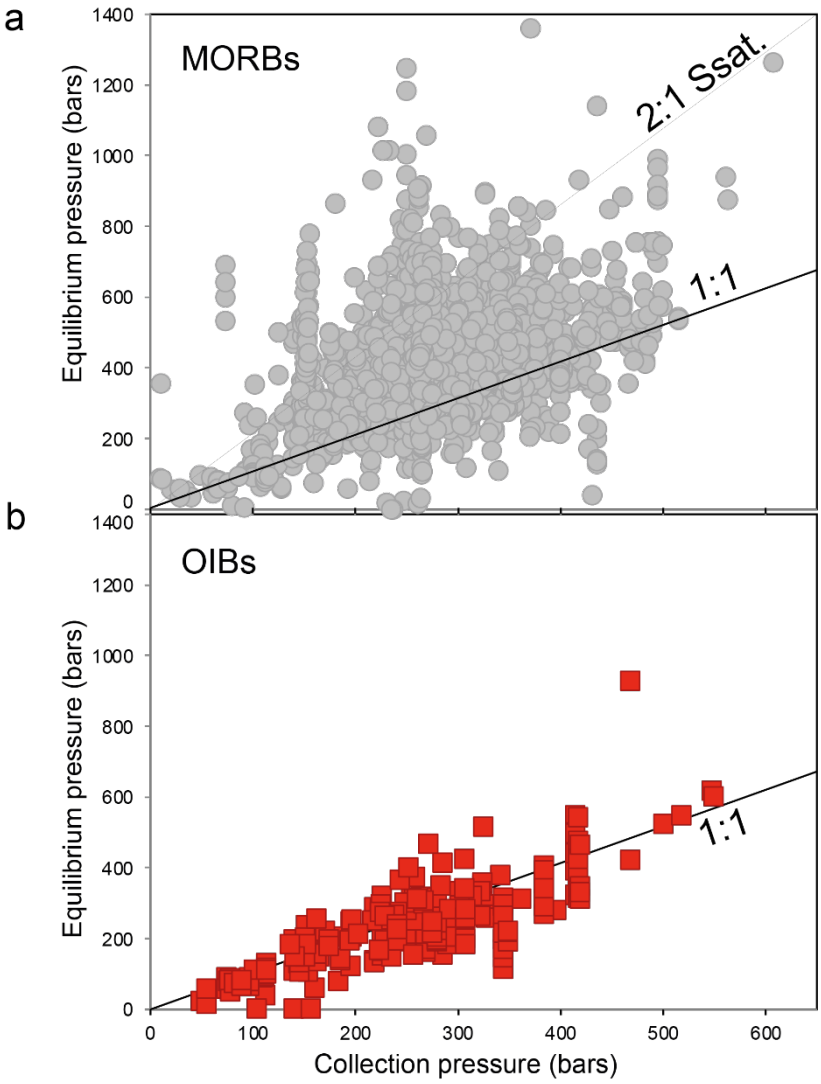

Figure 2. Equilibrium pressure against collection pressure. (A) For MORB submarine glasses, most data points are above the 1:1 equilibrium line. (B) For hotspot submarine basaltic glasses, most samples are located close to the 1:1 equilibrium line. The figure is redrawn from Aubaud (2022).

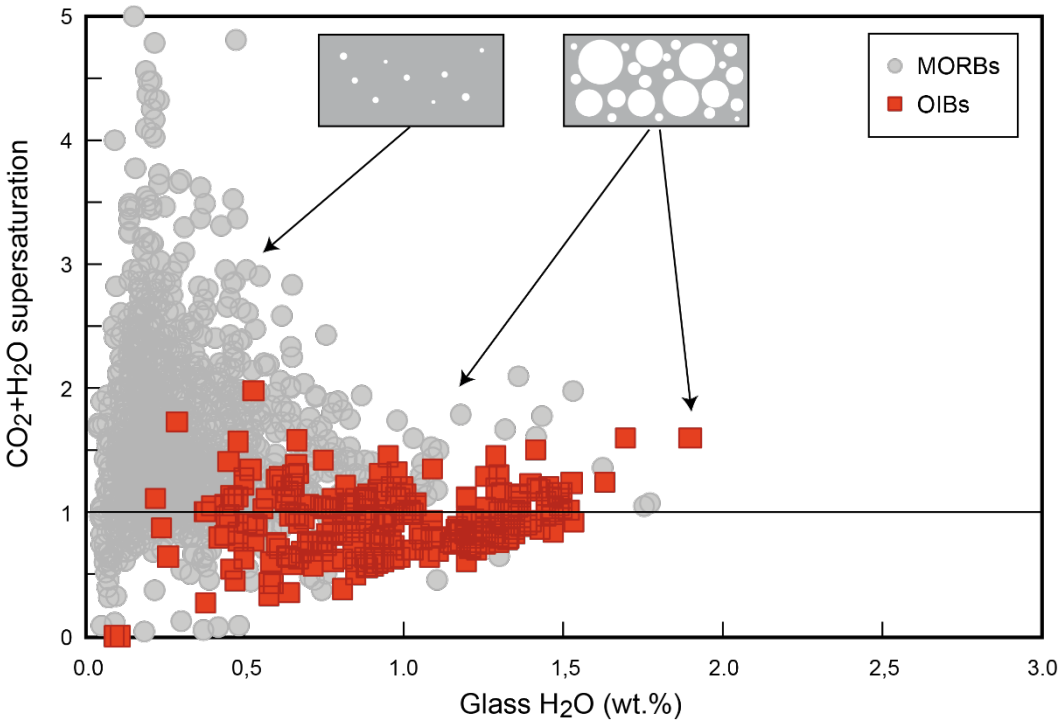

Figure 3. CO_2+H_2O supersaturation in submarine glasses against the dissolved H_2O (in wt.%) of submarine glasses. The black horizontal line is the equilibrium line. Supersaturation occurs mainly in low-H_2O compositions for melts that are vesicle-poor while H_2O-rich melts are essentially in equilibrium with respect to a CO_2+H_2O vapor phase due to higher vesicularity. The figure is redrawn from Aubaud (2022).

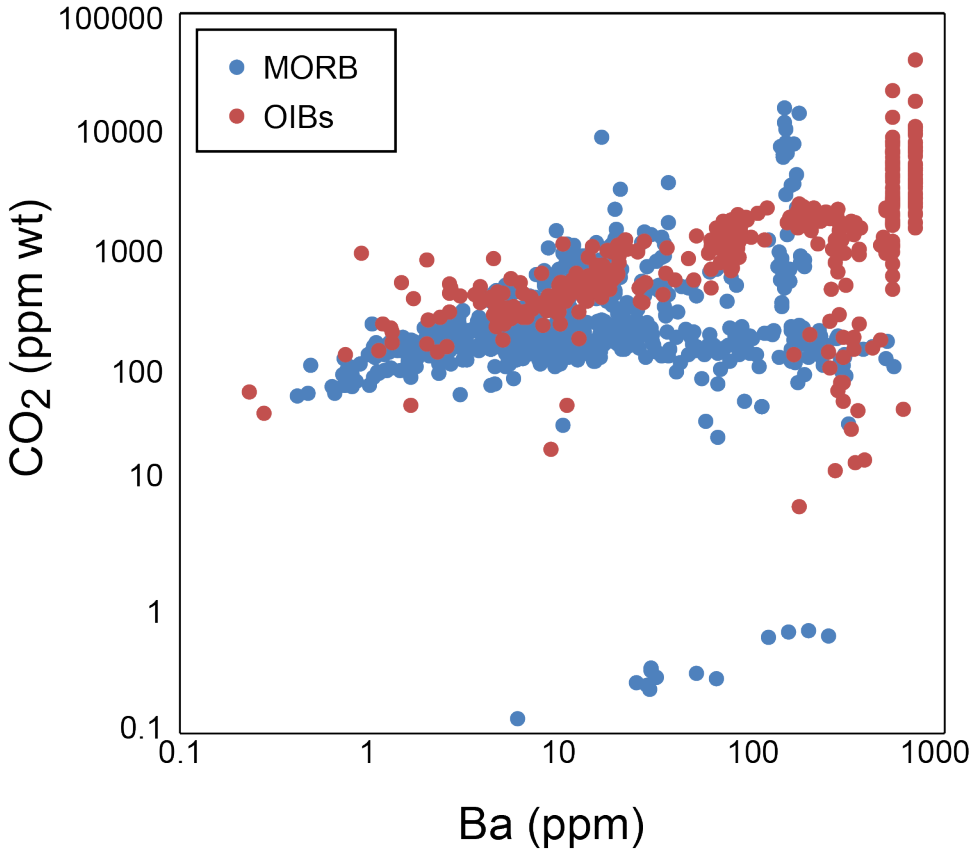

Figure 4. Total CO_2 (ppm by weight) against glass Ba content (ppm by weight) for submarine glasses and glassy melt inclusions from MOR and OI settings. The largest CO_2 contents at any given Ba content represent the least degassed samples while the lowest value essentially reflect degassed values.

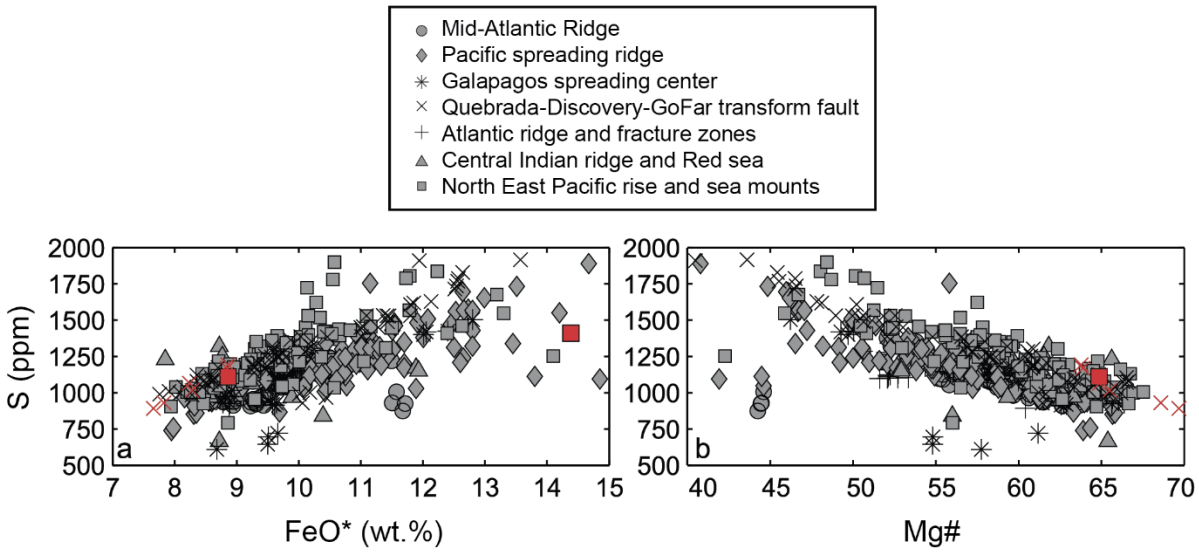

Figure 5: S contents of MORBs plotted as a function of (a) Mg# (molar Mg/(Mg+Fe) × 100) and (b) FeO*. The figure is modified from Ding and Dasgupta (2017). The broad correlation of increasing S contents with increasing FeO* and decreasing Mg# suggests that differentiated MORBs are saturated in immiscible sulfide melts. Data marked in red represent samples that are argued to be CO_2–H_2O vapor-undersaturated based on the comparison between saturation pressure and sample collection pressure (Shimizu et al., 2016).

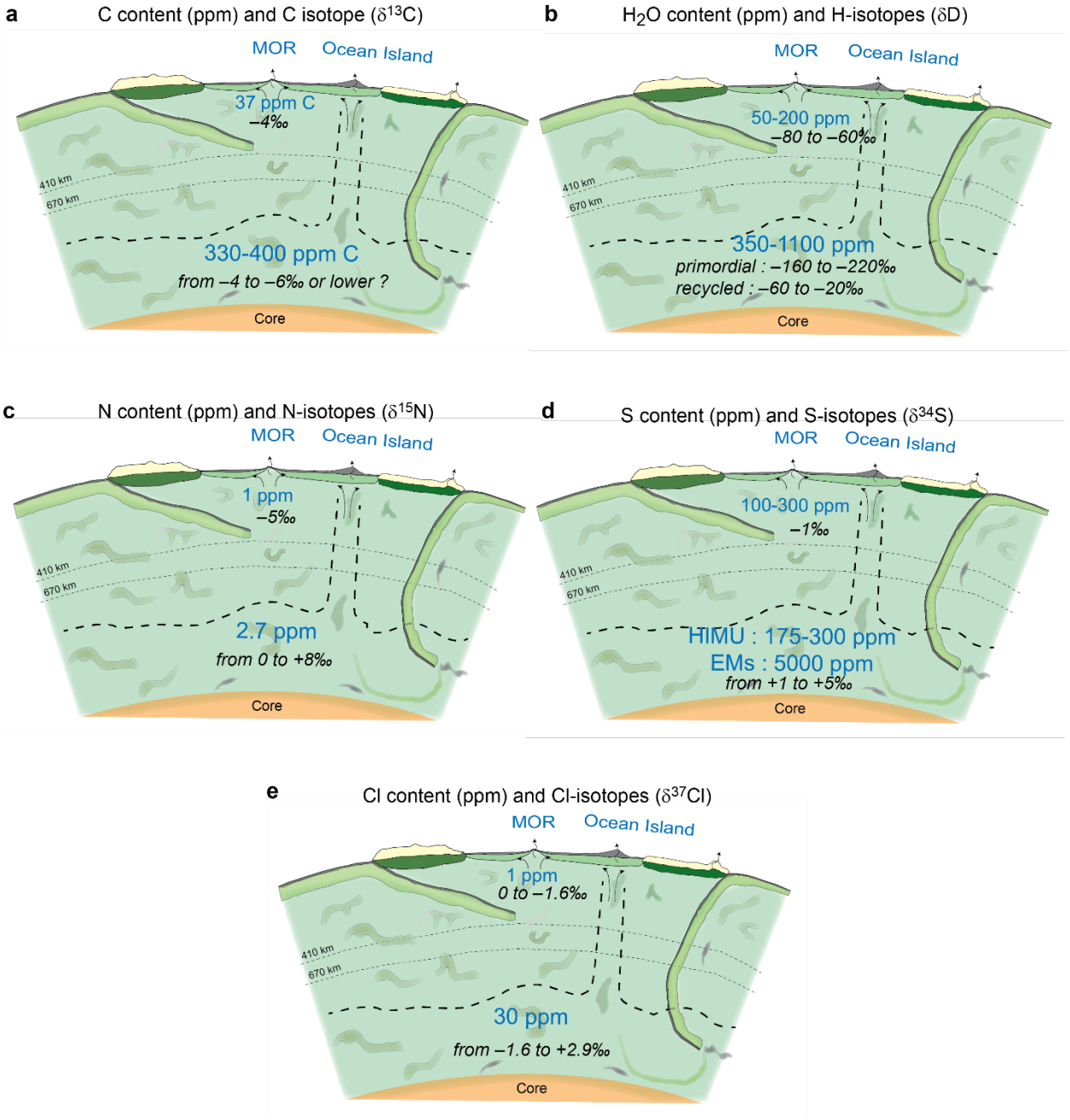

Figure 6: Compiled elemental and isotopic compositions of MORB and OIB source mantles in terms of major volatiles. (a) Carbon, (b) H_2O, (c) Nitrogen, (d) Sulfur, and (e) Chlorine. The isotopic compositions are in black texts and italicized whereas the elemental concentrations are in in blue and in upright texts. OIB sources are assumed to be in the deep mantle based on the higher mantle potential temperatures estimated from majority of the OIBs.

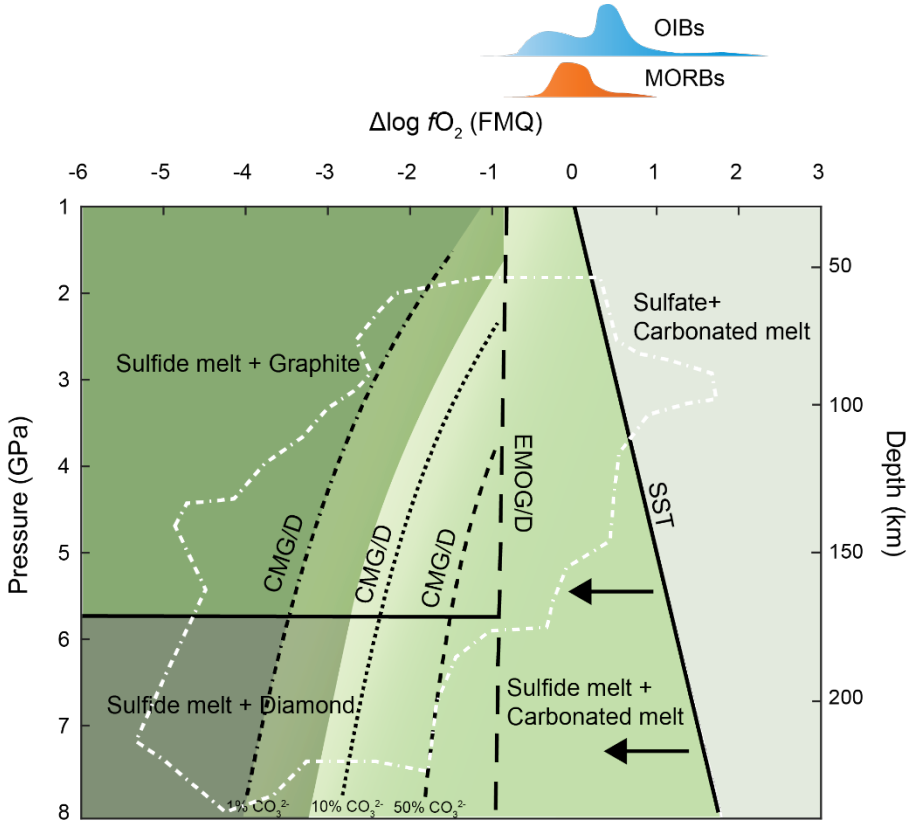

Figure 7: Oxygen fugacity, fO_2 vs depth plot showing primary storage mechanisms of carbon and sulfur beneath mid-ocean ridges (MORs) and ocean islands (OIs). The dashed line marked EMOG/D refers to the fO_2 buffer corresponding to the reaction enstatite (E) + magnesite (M) = olivine (O) + graphite/diamond (G/D) + O_2. Whereas the curves marked CMG/D refer to similar fO_2 buffers as EMOG/D involving carbonated melts rather than magnesite. The three different CMG/D lines refer to the carbonated melt to graphite/diamond transition for different proportion of dissolved carbonate in the melt – from right to left: 50 wt.% CO_3^{2-}, 10 wt.% CO_3^{2-}, and 5 wt.% CO_3^{2-} in the melt. The SST line marks the sulfate to sulfide transition (from right to left) in basaltic melts. The two left pointing arrows indicate that the SST curve may shift to the left if strongly carbonated melts are involved. Shown for reference are the estimates of fO_2 as a function of depth for the continental lithospheric mantle (white dash-dot bounding line; Stagno et al., 2013) and the fO_2s recorded by MORBs (saffron frequency distribution) and OIBs (blue

frequency distribution) from the compilation of Cottrell et al. (2021). The figure is adopted from Figure 1 of Chowdhury and Dasgupta (2020).

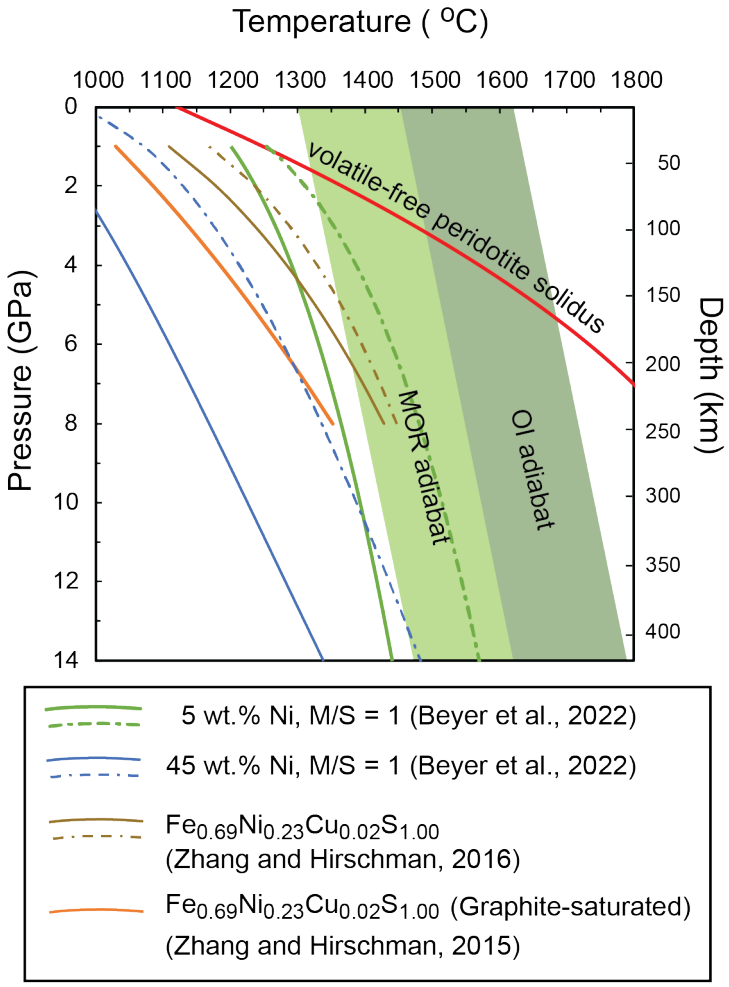

Figure 8: Solidi (solid lines) and liquidi (dash-dot lines) of mantle sulfides in depth-temperature space throughout the Earth's upper mantle compared to the volatile-free peridotite solidus and adiabats applicable for mid-ocean ridge basalt (MORB) and ocean island basalt (OIB) source regions. The volatile-free peridotite solidus is from Hirschmann (2000). The reference for the sulfide compositions and the corresponding experimental studies for the melting are given in the figure legend. The two sulfide compositions from Beyer et al. (2022) span the entire range of sulfide compositions that can be hosted in all mantle lithologies (Ni-rich for peridotite and Ni-poor for eclogite). M/S stands from metal to sulfide ratio. The figure shows that for the MORB source regions, down to ~240 km depth, sulfides in the mantle should be completely molten, especially if hosted in peridotite or at least partially molten, if hosted in eclogite. Hotter OIB source mantle should store sulfur entirely as molten sulfide throughout the upper mantle depths.

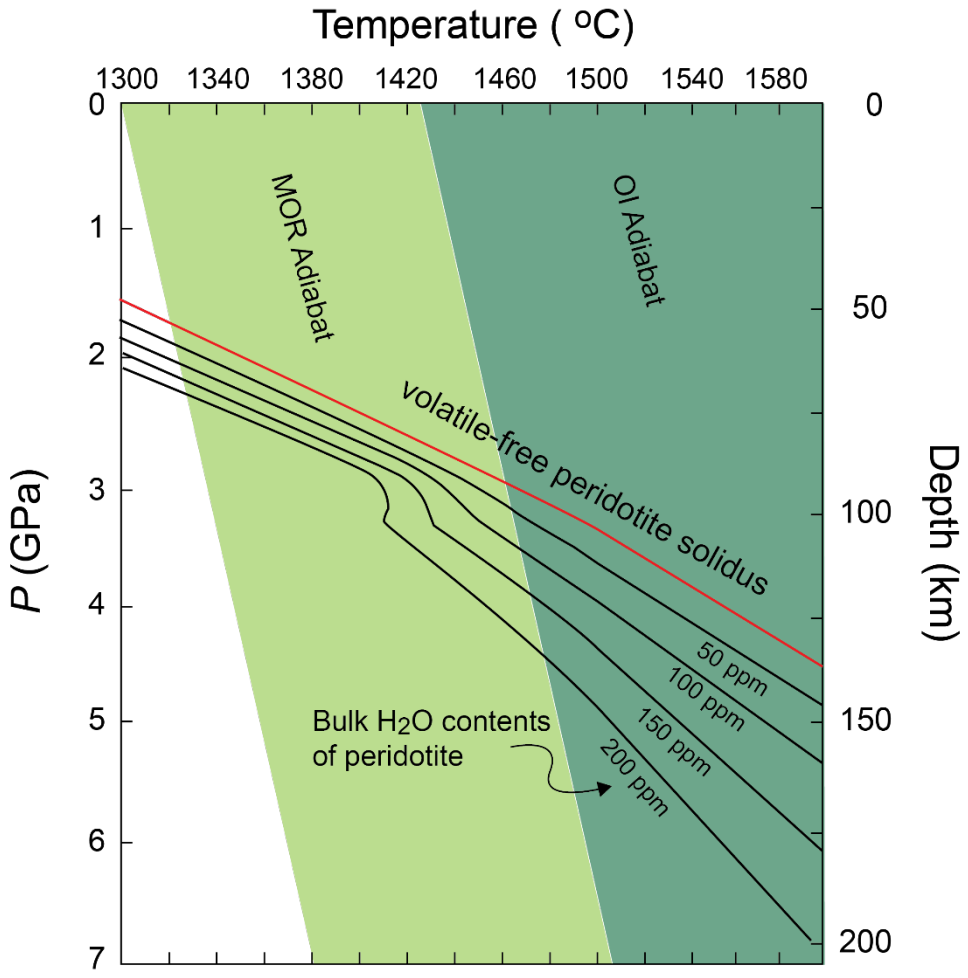

Figure 9: Mantle peridotite solidi as a function of increasing bulk H_2O content from zero (volatile-free peridotite solidus, in red; Hirschmann, 2000) to 200 ppm by weight in *P*-*T* space. The nominally anhydrous solidi (50-200 ppm) are based on the parameterization of O'Leary et al. (2010). Plotted for comparison are the mantle adiabats beneath mid-ocean ridges (MOR) and intraplate ocean islands (OI). Due to greater incompatibility of H_2O in peridotite in the garnet stability field compared to the spinel stability field, hydrous solidi are depressed more compared to the volatile-free solidus for the hotter OIB source regions than the cooler MORB source regions.

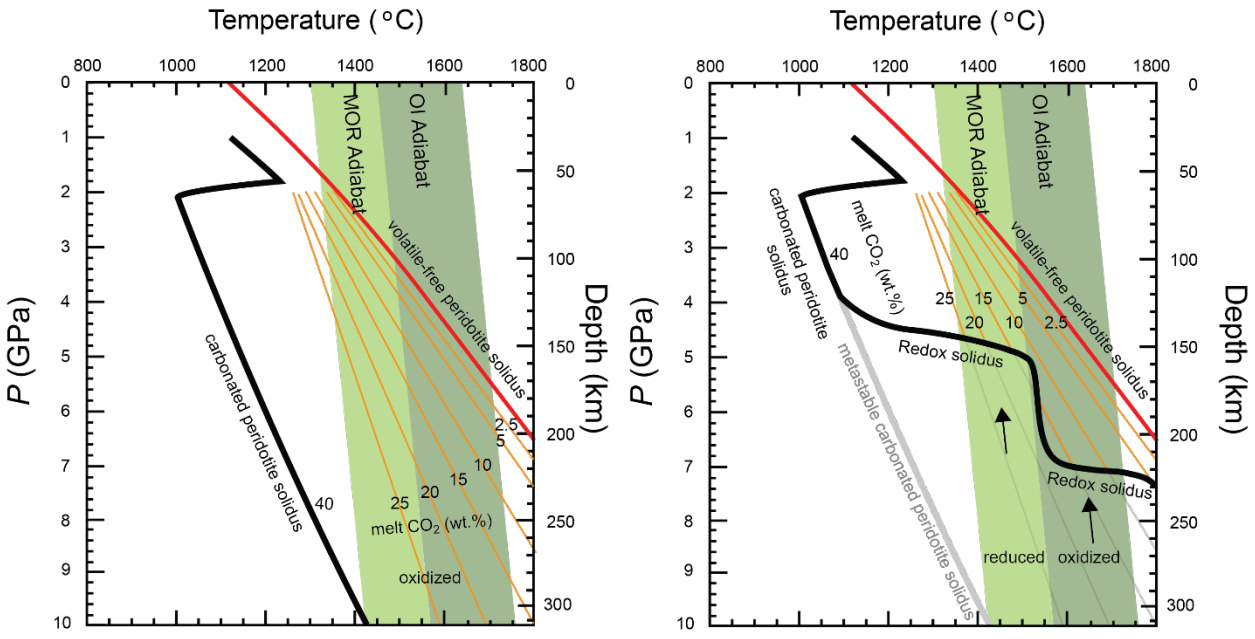

Figure 10: Topology and loci of solidi of carbon-bearing mantle peridotite (thick black line) and evolution of partial melt CO_2 contents (thin yellow-orange lines) as a function of depth and temperature. Also shown for reference are the volatile-free peridotite solidus (Hirschmann, 2000) and the depth-temperature profiles (adiabats) for the MORB and OIB source regions. The left panel shows a melting behavior where the fertile mantle peridotite remains oxidized enough with depth that carbon is present as carbonates. The right panel shows a melting behavior where mantle becomes gradually reduced with depth and the change of carbon speciation and storage from carbonate to graphite/diamond takes place ~5 GPa for the MORB source regions and at ~7 GPa for the OIB source regions. For the case of oxidized mantle to deeper depths (left panel), the cooler MORB source mantle should commence melting ≥300 km and the hotter OIB source mantle should commence melting ≥400 km. This near-solidus melting at the carbonated peridotite solidus generates carbonatitic melt (melt CO_2 content of ~40 wt.%), which evolves to carbonated silicate melts (melt CO_2 contents ≤25 wt.%) that precursor to strongly alkalic magmas at 200-300 km depth. For the cases of gradual reduction with depth (right panel), C-bearing peridotite solidus switches from a carbonated peridotite solidus to a redox solidus. Such a transition from carbonated melting to redox melting (melting aided by oxidation of graphite/diamond to a carbonated melt), if relevant, should occur at a shallower depth for the relatively reduced MORB source mantle and at a deeper depth for the relatively oxidized OIB source mantle. In this latter case, the first formed melt at depth is expected to be a carbonated silicate melt rather than a carbonatitic melt.

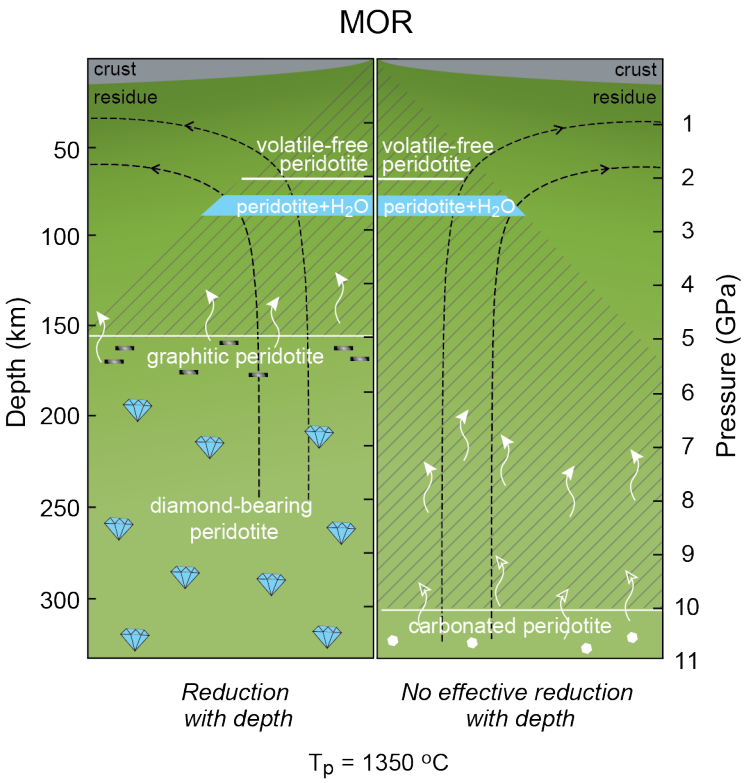

Figure 11: Two possible scenarios of volatile-induced melting beneath present-day mid-ocean ridges (MOR) at mantle potential temperature of 1350 °C. Left: Reduction with depth similar to that estimated for continental mantle lithospheric samples (e.g., Stagno et al., 2013). In this scenario, melting in the upwelling mantle commences via redox melting of graphite-bearing peridotite at ~150 km, with the first-formed melt being carbonated silicate melts (white-filled arrow heads). Right: No effective reduction with depth down to 300 km depth where melting commences at the carbonated peridotite solidus at ~300 km depth, via production of carbonatitic melt (open arrowheads), which evolves to CO_2-rich silicate melts at shallower depths, but yet well below the nominally anhydrous peridotite solidus. The mantle mass that gets processed through the volatile-bearing mantle solidus per unit geologic time is significantly different between the two scenarios and thus should influence flux of CO_2 through MOR systems at present. The depth of graphite to diamond transition is based on Day (2012).

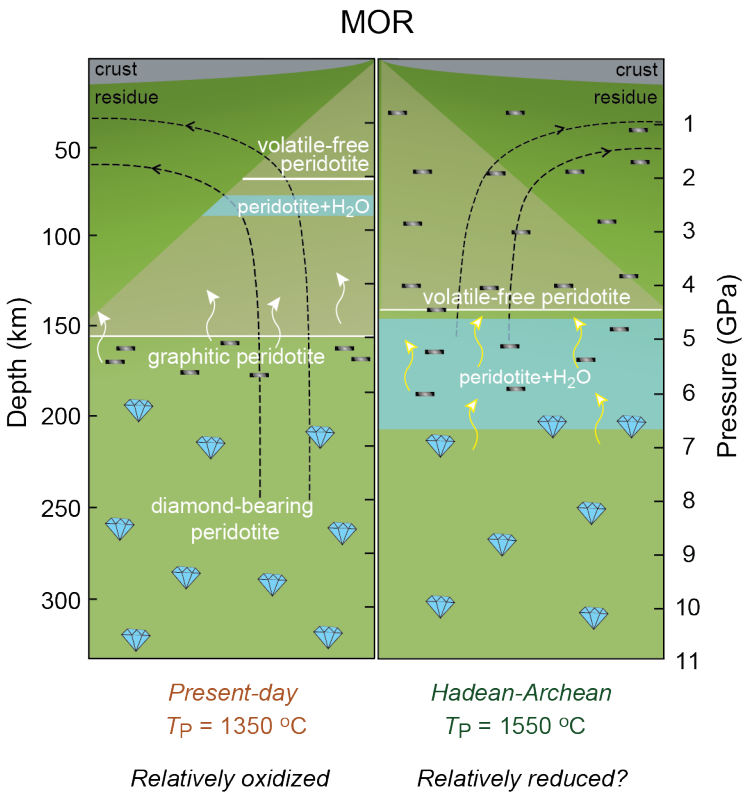

Figure 12: Possible distinction between melting regime beneath MORs at the present-day (left) vs those at Archean-Hadean time, >2 billion years ago (right). The present-day Earth's MORB source mantle is estimated to be relatively oxidized and showing a gradual reduction with depth. The ancient MORB source mantle is estimated to be more reduced by as much as 2 log units and showing similar reduction with depth as argued for the present-day mantle. If this difference is real, the first onset of melting for the present-day MORB source mantle would be via C-involved, redox melting of graphite-bearing peridotite, which would be generate a carbonated silicate partial melt. On the contrary, the onset of melting for the ancient MORB source mantle would be across the nominally anhydrous peridotite solidi (blue band: top with 50 ppm bulk H_2O and bottom with 200 ppm bulk H_2O). The effective ventilation of CO_2 in this latter case should be muted as CO_2 content of mantle melts would be limited to those obtained at graphite saturation. The depth of graphite to diamond transition is based on Day (2012).

References

Ader, M., Thomazo, C., Sansjofre, P., Busigny, V., Papineau, D., Laffont, R., Cartigny, P., Halverson, G.P., 2016. Interpretation of the nitrogen isotopic composition of Precambrian sedimentary rocks: Assumptions and perspectives. Chemical Geology 429, 93-110.

Alard, O., Griffin, W.L., Lorand, J.P., Jackson, S.E., O'Reilly, S.Y., 2000. Non-chondritic distribution of the highly siderophile elements in mantle sulphides. Nature 407, 891-894.

Anderson, K. R., Poland, M. P., 2017. Abundant carbon in the mantle beneath Hawi'i. Nature Geoscience 10, 704-712.

Ariskin, A.A., Danyushevsky, L.V., Bychkov, K.A., McNeill, A.W., Barmina, G.S., Nikolaev, G.S., 2013. Modeling Solubility of Fe-Ni Sulfides in Basaltic Magmas: The Effect of Nickel. Economic Geology 108, 1983-2003.

Asimow, P.D., Langmuir, C.H., 2003. The importance of water to oceanic mantle melting regimes. Nature 421, 815-820.

Aster, E.M., Wallace, P.J., Moore, L.R., Watkins, J., Gazel, E., Bodnar, R.J., 2016. Reconstructing CO2 concentrations in basaltic melt inclusions using Raman analysis of vapor bubbles. Journal of Volcanology and Geothermal Research 323, 148-162.

Aubaud, C., 2022. Carbon stable isotope constraints on CO2 degassing models of ridge, hotspot and arc magmas. Chemical Geology 605, 120962.

Aubaud, C., Hauri, E.H., Hirschmann, M.M., 2004a. Hydrogen partition coefficients between nominally anhydrous minerals and basaltic melts. Geophysical Research Letters 31, L20611, doi:20610.21029/22004GL021341.

Aubaud, C., Hirschmann, M., Withers, A., Hervig, R., 2008. Hydrogen partitioning between melt, clinopyroxene, and garnet at 3 GPa in a hydrous MORB with 6 wt.% H2O. Contributions to Mineralogy and Petrology 156, 607-625.

Aubaud, C., Pineau, F., Hekinian, R., Javoy, M., 2005. Degassing of CO_2 and H_2O in submarine lavas from the Society hotspot. Earth and Planetary Science Letters 235, 511-527.

Aubaud, C., Pineau, F., Hekinian, R., Javoy, M., 2006. Carbon and hydrogen isotope constraints on degassing of CO_2 and H_2O in submarine lavas from the Pitcairn hotspot (South Pacific). Geophysical Research Letters 33, L02308, doi:02310.01029/02005GL024907.

Aubaud, C., Pineau, F., Jambon, A., Javoy, M., 2004b. Kinetic disequilibrium of C, He, Ar and carbon isotopes during degassing of mid-ocean ridge basalts. Earth and Planetary Science Letters 222, 391-406.

Aubaud, C., Pineau, F., Jambon, A., Javoy, M., 2004c. Kinetic disequilibrium of C, He, Ar, and carbon isotopes during degassing of mid-ocean ridge basalts. Earth and Planetary Science Letters 222, 391-406.

Bajgain, S.K., Mookherjee, M., Dasgupta, R., 2021. Earth's core could be the largest terrestrial carbon reservoir. Communications Earth & Environment 2, 165.

Ballhaus, C., Bockrath, C., Wohlgemuth-Ueberwasser, C., Laurenz, V., Berndt, J., 2006. Fractionation of the noble metals by physical processes. Contributions to Mineralogy and Petrology 152, 667-684.

Ballhaus, C., Ellis, D.J., 1996. Mobility of core melts during Earth's accretion. Earth and Planetary Science Letters 143, 137-145.

Barry, P.H., Hilton, D.R., Füri, E., Halldórsson, S.A., Grönvold, K., 2014. Carbon isotope and abundance systematics of Icelandic geothermal gases, fluids and subglacial basalts with

implications for mantle plume-related CO2 fluxes. Geochimica et Cosmochimica Acta 134, 74-99.
Bell, D.R., Rossman, G.R., Moore, R.O., 2004. Abundance and Partitioning of OH in a High-pressure Magmatic System: Megacrysts from the Monastery Kimberlite, South Africa. J. Petrol. 45, 1539-1564.
Bernadou, F., Gaillard, F., Füri, E., Marrocchi, Y., Slodczyk, A., 2021. Nitrogen solubility in basaltic silicate melt - Implications for degassing processes. Chemical Geology 573, 120192.
Berry, A.J., O'Neill, H.S.C., Hermann, J., Scott, D.R., 2007. The infrared signature of water associated with trivalent cations in olivine. Earth and Planetary Science Letters 261, 134-142.
Beyer, C., Bissbort, T., Hartmann, R., Berndt, J., Klemme, S., Fonseca, R.O.C., 2022. High-pressure phase relations in the system Fe–Ni–Cu–S up to 14 GPa: implications for the stability of sulfides in the earth's upper mantle. Contributions to Mineralogy and Petrology 177, 99.
Bezos, A., Humler, E., 2005. The Fe^{3+}/SFe ratios of MORB glasses and their implications for mantle melting. Geochimica et Cosmochimica Acta 69, 711-725.
Bindeman, I.N., Kamenetsky, V.S., Palandri, J., Vennemann, T., 2012. Hydrogen and oxygen isotope behaviors during variable degrees of upper mantle melting: Example from the basaltic glasses from Macquarie Island. Chemical Geology 310-311, 126-136.
Blanchard, I., Rubie, D.C., Jennings, E.S., Franchi, I.A., Zhao, X., Petitgirard, S., Miyajima, N., Jacobson, S.A., Morbidelli, A., 2022. The metal–silicate partitioning of carbon during Earth's accretion and its distribution in the early solar system. Earth and Planetary Science Letters 580, 117374.
Bockrath, C., Ballhaus, C., Holzheid, A., 2004. Fractionation of the platinum-group elements during mantle melting. Science 305, 1951-1953.
Bolfan-Casanova, N., 2005. Water in the Earth's mantle. Mineralogical Magazine 69, 229-257.
Bonifacie, M., Jendrzejewski, N., Agrinier, P., Humler, E., Coleman, M., Javoy, M., 2008. The Chlorine Isotope Composition of Earth's Mantle. Science 319, 1518-1520.
Bonifacie, M., Monnin, C., Jendrzejewski, N., Agrinier, P., Javoy, M., 2007. Chlorine stable isotopic composition of basement fluids of the eastern flank of the Juan de Fuca Ridge (ODP Leg 168). Earth and Planetary Science Letters 260, 10-22.
Boudoire, G., Rizzo, A.L., Di Muro, A., Grassa, F., Liuzzo, M., 2018. Extensive CO2 degassing in the upper mantle beneath oceanic basaltic volcanoes: First insights from Piton de la Fournaise volcano (La Réunion Island). Geochimica et Cosmochimica Acta 235, 376-401.
Boujibar, A., Andrault, D., Bouhifd, M.A., Bolfan-Casanova, N., Devidal, J.-L., Trcera, N., 2014. Metal–silicate partitioning of sulphur, new experimental and thermodynamic constraints on planetary accretion. Earth and Planetary Science Letters 391, 42-54.
Brey, G., Brice, W.R., Ellis, D.J., Green, D.H., Harris, K.L., Ryabchikov, I.D., 1983. Pyroxene-carbonate reactions in the upper mantle. Earth and Planetary Science Letters 62, 63-74.
Bromiley, G.D., Keppler, H., McCammon, C., Bromiley, F.A., Jacobsen, S.D., 2004. Hydrogen solubility and speciation in natural, gem-quality chromian diopside. American Mineralogist 89, 941-949.

Brounce, M., Stolper, E., Eiler, J., 2017. Redox variations in Mauna Kea lavas, the oxygen fugacity of the Hawaiian plume, and the role of volcanic gases in Earth's oxygenation. Proceedings of the National Academy of Sciences 114, 8997-9002.
Brounce, M., Stolper, E., Eiler, J., 2021. The mantle source of basalts from Reunion Island is not more oxidized than the MORB source mantle. Contributions to Mineralogy and Petrology 177, 7.
Bucholz, C.E., Gaetani, G.A., Behn, M.D., Shimizu, N., 2013. Post-entrapment modification of volatiles and oxygen fugacity in olivine-hosted melt inclusions. Earth and Planetary Science Letters 374, 145-155.
Bulanova, G.P., Griffin, W.L., Ryan, C.G., Shestakova, O.Y., Barnes, S.J., 1996. Trace elements in sulfide inclusions from Yakutian diamonds. Contributions to Mineralogy and Petrology 124, 111-125.
Bureau, H., Pineau, F., Metrich, N., Semet, M.P., Javoy, M., 1998. A melt and fluid inclusion study of the gas phase at Piton de la Fournaise volcano (Reunion Island). Chemical Geology 147, 115-130.
Bureau, H., Raepsaet, C., Khodja, H., Carraro, A., Aubaud, C., 2009. Determination of hydrogen content in geological samples using elastic recoil detection analysis (ERDA). Geochimica et Cosmochimica Acta 73, 3311-3322.
Burnard, P., 1999. Eruption dynamics of "popping rock" from vesicle morphologies. Journal of Volcanology and Geothermal Research 92, 247-258.
Burnard, P., Reisberg, L., Colin, A., 2014. An observed link between lithophile compositions and degassing of volatiles (He, Ar, CO2) in MORBs with implications for Re volatility and the mantle C/Nb ratio. Earth and Planetary Science Letters 395, 159-167.
Burton, M., Aiuppa, A., Allard, P., Asensio-Ramos, M., Pardo Cofrdes, A., La Spina, A., Nicholson, E. J., Zanon, V., Barrancos, J., Bittetto, M., Hartley, M., Romero, J. E., Waters, E., Stewart, A., Hernandez, P. A., Lages, J. P., Padron, E., Wood, K., Esse, B., Hayer, C., Cyrzan, K., Rose-Koga, E. F., Schiavi, F., D'Auria, L., Perez, N. M., 2023. Exceptional eruptive CO_2 emissions from intra-plate alkaline magmatism in the Canary volcanic archipelago. Communications Earth & Environment 4, 467, 10.1038/s43247-023-01103-x.
Busigny, V., Cartigny, P., Philippot, P., 2011. Nitrogen isotopes in ophiolitic metagabbros: A re-evaluation of modern nitrogen fluxes in subduction zones and implication for the early Earth atmosphere. Geochimica et Cosmochimica Acta 75, 7502-7521.
Cabral, R.A., Jackson, M.G., Koga, K.T., Rose-Koga, E.F., Hauri, E.H., Whitehouse, M.J., Price, A.A., Day, J.M.D., Shimizu, N., Kelley, K.A., 2014. Volatile cycling of H2O, CO2, F, and Cl in the HIMU mantle: A new window provided by melt inclusions from oceanic hot spot lavas at Mangaia, Cook Islands. Geochemistry, Geophysics, Geosystems 15, 4445-4467.
Cabral, R.A., Jackson, M.G., Rose-Koga, E.F., Koga, K.T., Whitehouse, M.J., Antonelli, M.A., Farquhar, J., Day, J.M.D., Hauri, E.H., 2013. Anomalous sulphur isotopes in plume lavas reveal deep mantle storage of Archaean crust. Nature 496, 490-493.
Callegaro, S., Geraki, K., Marzoli, A., De Min, A., Maneta, V., Baker, D.R., 2020. The quintet completed: The partitioning of sulfur between nominally volatile-free minerals and silicate melts. American Mineralogist 105, 697-707.
Canil, D., 1990. Experimental study bearing on the absence of carbonate in the mantle-derived xenoliths. Geology 18, 1011-1013.

Canil, D., Fellows, S.A., 2017. Sulphide–sulphate stability and melting in subducted sediment and its role in arc mantle redox and chalcophile cycling in space and time. Earth and Planetary Science Letters 470, 73-86.
Cannatelli, C., 2015. Bubbles do matter! American Mineralogist 100, 1335-1336.
Cartigny, P., Jendrzejewski, N., Pineau, F., Petit, E., Javoy, M., 2001. Volatile (C, N, Ar) variability in MORB and the respective roles of mantle source heterogeneity and degassing: the case of the Southwest Indian Ridge. Earth and Planetary Science Letters 194, 241-257.
Cartigny, P., Pineau, F., Aubaud, C., Javoy, M., 2008. Towards a consistent mantle carbon flux estimate: Insights from volatile systematics (H_2O/Ce, δD, CO_2/Nb) in the North Atlantic mantle (14° N and 34° N). Earth and Planetary Science Letters 265, 672-685.
Chaussidon, M., Albarède, F., Sheppard, S.M.F., 1989. Sulphur isotope variations in the mantle from ion microprobe analyses of micro-sulphide inclusions. Earth and Planetary Science Letters 92, 144-156.
Chavrit, D., Humler, E., Grasset, O., 2014. Mapping modern CO2 fluxes and mantle carbon content all along the mid-ocean ridge system. Earth and Planetary Science Letters 387, 229-239.
Chen, Y., Provost, A., Schiano, P., Cluzel, N., 2011. The rate of water loss from olivine-hosted melt inclusions. Contributions to Mineralogy and Petrology 162, 625-636.
Chi, H., Dasgupta, R., Duncan, M., Shimizu, N., 2014. Partitioning of carbon between Fe-rich alloy melt and silicate melt in a magma ocean – Implications for the abundance and origin of volatiles in Earth, Mars, and the Moon. Geochimica et Cosmochimica Acta 139, 447-471.
Chowdhury, P., Dasgupta, R., 2020. Sulfur extraction via carbonated melts from sulfide-bearing mantle lithologies - Implications for deep sulfur cycle and mantle redox. Geochimica et Cosmochimica Acta 269, 376-397.
Chowdhury, P., Dasgupta, R., Phelps, P.R., Costin, G., Lee, C.-T.A., 2022. Oxygen fugacity range of subducting crust inferred from fractionation of trace elements during fluid-present slab melting in the presence of anhydrite versus sulfide. Geochimica et Cosmochimica Acta 325, 214-231.
Christie, D.M., Carmichael, I.S.E., Langmuir, C.H., 1986. Oxidation states of mid-ocean ridge basalt glasses. Earth and Planetary Science Letters 79, 397-411.
Clesi, V., Bouhifd, M.A., Bolfan-Casanova, N., Manthilake, G., Schiavi, F., Raepsaet, C., Bureau, H., Khodja, H., Andrault, D., 2018. Low hydrogen contents in the cores of terrestrial planets. Science Advances 4, e1701876.
Clog, M., Cartigny, P., Aubaud, C. 2012. Experimental evidence for interaction of water vapor and platinum crucibles at high temperatures: Implications for volatiles from igneous rocks and minerals. Geochimica et Cosmochimica Acta 83, 125-137.
Clog, M., Aubaud, C., Cartigny, P., Dosso, L., 2013. The hydrogen isotopic composition and water content of southern Pacific MORB: A reassessment of the D/H ratio of the depleted mantle reservoir. Earth and Planetary Science Letters 381, 156-165.
Cottrell, E., Birner, S.K., Brounce, M., Davis, F.A., Waters, L.E., Kelley, K.A., Oxygen Fugacity Across Tectonic Settings, Magma Redox Geochemistry, 2021, pp. 33-61.
Cottrell, E., Kelley, K.A., 2011. The oxidation state of Fe in MORB glasses and the oxygen fugacity of the upper mantle. Earth and Planetary Science Letters 305, 270-282.

Cottrell, E., Kelley, K.A., 2013. Redox Heterogeneity in Mid-Ocean Ridge Basalts as a Function of Mantle Source. Science 340, 1314-1317.
Craig, H., 1953. The geochemistry of the stable carbon isotopes. Geochimica et Cosmochimica Acta 3, 53-92.
Danyushevsky, L.V., Della-Pasqua, F.N., Sokolov, S., 2000. Re-equilibration of melt inclusions trapped by magnesian olivine phenocrysts from subduction-related magmas: petrological implications. Contributions to Mineralogy and Petrology 138, 68-83.
Danyushevsky, L.V., Falloon, T.J., Sobolev, A.V., Crawford, A.J., Carroll, M., Price, R.C., 1993. The H2O content of basalt glasses from Southwest Pacific back-arc basins. Earth and Planetary Science Letters 117, 347-362.
Dasgupta, R., 2013. Ingassing, Storage, and Outgassing of Terrestrial Carbon through Geologic Time. Reviews in Mineralogy and Geochemistry 75, 183-229.
Dasgupta, R., 2018. Volatile bearing partial melts beneath oceans and continents – where, how much, and of what compositions? American Journal of Science 318, 141–165.
Dasgupta, R., Buono, A., Whelan, G., Walker, D., 2009. High-pressure melting relations in Fe-C-S systems: implications for formation, evolution, and structure of metallic cores in planetary bodies. Geochimica et Cosmochimica Acta 73, 6678-6691.
Dasgupta, R., Chowdhury, P., Eguchi, J., Sun, C., Saha, S., 2022a. Volatile-bearing partial melts in the lithospheric and sub-lithospheric mantle on Earth and other rocky planets. Reviews in Mineralogy and Geochemistry 87, 575-606.
Dasgupta, R., Falksen, E., Pal, A., Sun, C., 2022b. The fate of nitrogen during parent body partial melting and accretion of the inner solar system bodies at reducing conditions. Geochimica et Cosmochimica Acta 336, 291-307.
Dasgupta, R., Grewal, D.S., Origin and early differentiation of carbon and associated life-essential volatile elements on Earth, in: B. Orcutt, Daniel, I., Dasgupta, R., (Ed), Deep Carbon: Past to Present, Cambridge University Press, Cambridge, 2019, pp. 4-39. doi:10.1017/9781108677950.9781108677002.
Dasgupta, R., Hirschmann, M.M., 2006. Melting in the Earth's deep upper mantle caused by carbon dioxide. Nature 440, 659-662.
Dasgupta, R., Hirschmann, M.M., 2007a. Effect of variable carbonate concentration on the solidus of mantle peridotite. American Mineralogist 92, 370-379.
Dasgupta, R., Hirschmann, M.M., 2007b. A modified iterative sandwich method for determination of near-solidus partial melt compositions. II. Application to determination of near-solidus melt compositions of carbonated peridotite. Contributions to Mineralogy and Petrology 154, 647-661.
Dasgupta, R., Hirschmann, M.M., 2010. The deep carbon cycle and melting in Earth's interior. Earth and Planetary Science Letters 298, 1-13.
Dasgupta, R., Hirschmann, M.M., Smith, N.D., 2007a. Partial melting experiments of peridotite + CO_2 at 3 GPa and genesis of alkalic ocean island basalts. J. Petrol. 48, 2093-2124.
Dasgupta, R., Hirschmann, M.M., Smith, N.D., 2007b. Water follows Carbon: CO_2 incites deep silicate melting and dehydration beneath mid-ocean ridges. Geology 35, 135-138. doi:110.1130/G22856A.22851.
Dasgupta, R., Hirschmann, M.M., Stalker, K., 2006. Immiscible transition from carbonate-rich to silicate-rich melts in the 3 GPa melting interval of eclogite + CO_2 and genesis of silica-undersaturated ocean island lavas. J. Petrol. 47, 647-671.

Dasgupta, R., Hirschmann, M.M., Withers, A.C., 2004. Deep global cycling of carbon constrained by the solidus of anhydrous, carbonated eclogite under upper mantle conditions. Earth and Planetary Science Letters 227, 73-85.
Dasgupta, R., Jackson, M.G., Lee, C.-T.A., 2010. Major element chemistry of ocean island basalts – conditions of mantle melting and heterogeneity of mantle source. Earth and Planetary Science Letters 289, 377-392. doi:310.1016/j.epsl.2009.1011.1027.
Dasgupta, R., Mallik, A., Tsuno, K., Withers, A.C., Hirth, G., Hirschmann, M.M., 2013. Carbon-dioxide-rich silicate melt in the Earth's upper mantle. Nature 493, 211-215. doi:210.1038/nature11731.
Dauphas, N., 2017. The isotopic nature of the Earth's accreting material through time. Nature 541, 521.
Day, H.W., 2012. A revised diamond-graphite transition curve. American Mineralogist 97, 52-62.
Delavault, H., Chauvel, C., Thomassot, E., Devey, C.W., Dazas, B., 2016. Sulfur and lead isotopic evidence of relic Archean sediments in the Pitcairn mantle plume. Proceedings of the National Academy of Sciences 113, 12952-12956.
Déruelle, B., Dreibus, G., Jambon, A., 1992. Iodine abundances in oceanic basalts: implications for Earth dynamics. Earth and Planetary Science Letters 108, 217-227.
Des Marais, D.J., Carbon Exchange Between the Mantle and the Crust, and its Effect Upon the Atmosphere: Today Compared to Archean Time, The Carbon Cycle and Atmospheric CO2: Natural Variations Archean to Present, 1985, pp. 602-611.
Des Marais, D.J., Moore, J.G., 1984. Carbon and its isotopes in mid-oceanic basaltic glasses. Earth and Planetary Science Letters 69, 43-57.
Ding, S., Dasgupta, R., 2017. The fate of sulfide during decompression melting of peridotite – implications for sulfur inventory of the MORB-source depleted upper mantle. Earth and Planetary Science Letters 459, 183-195.
Ding, S., Dasgupta, R., 2018. Sulfur inventory of ocean island basalt source regions constrained by modeling the fate of sulfide during decompression melting of a heterogenous mantle. J. Petrol. 59, 1281–1308.
Ding, S., Dasgupta, R., Tsuno, K., 2014. Sulfur concentration of martian basalts at sulfide saturation at high pressures and temperatures – implications for deep sulfur cycle on Mars. Geochimica et Cosmochimica Acta 131, 227-246.
Ding, S., Hough, T., Dasgupta, R., 2018. New high pressure experiments on sulfide saturation of high-FeO* basalts with variable TiO_2 contents – Implications for the sulfur inventory of the lunar interior. Geochimica et Cosmochimica Acta 222, 319-339.
Dixon, J.E., 1997. Degassing of alkalic basalts. American Mineralogist 82, 368-378.
Dixon, J.E., Bindeman, I.N., Kingsley, R.H., Simons, K.K., Le Roux, P.J., Hajewski, T.R., Swart, P., Langmuir, C.H., Ryan, J.G., Walowski, K.J., Wada, I., Wallace, P.J., 2017. Light Stable Isotopic Compositions of Enriched Mantle Sources: Resolving the Dehydration Paradox. Geochemistry, Geophysics, Geosystems 18, 3801-3839.
Dixon, J.E., Clague, D.A., 2001. Volatiles in basaltic glasses from Loihi seamount, Hawaii: evidence for a relatively dry plume component. J. Petrol. 42, 627-654.
Dixon, J.E., Clague, D.A., Wallace, P., Poreda, R., 1997. Volatiles in alkalic basalts from the north arch volcanic field, Hawaii: extensive degassing of deep submarine-erupted alkalic series lavas. J. Petrol. 38, 911-939.

Dixon, J.E., Leist, L., Langmuir, C., Schilling, J.-G., 2002. Recycled dehydrated lithosphere observed in plume-influenced mid-ocean-ridge basalts. Nature 420, 385-389.
Dixon, J.E., Stolper, E., Delaney, J.R., 1988. Infrared spectroscopic measurements of CO2 and H2O in Juan de Fuca Ridge basaltic glasses. Earth and Planetary Science Letters 90, 87-104.
Dixon, J.E., Stolper, E.M., Holloway, J.R., 1995. An experimental study of water and carbon dioxide solubilities in mid-ocean ridge basaltic liquids. Part I: Calibrations and solubility models. J. Petrol. 36, 1607-1631.
Dottin III, J.W., Labidi, J., Jackson, M.G., Farquhar, J., 2021. Sulfur Isotope Evidence for a Geochemical Zonation of the Samoan Mantle Plume. Geochemistry, Geophysics, Geosystems 22, e2021GC009816.
Dottin, J.W., Labidi, J., Lekic, V., Jackson, M.G., Farquhar, J., 2020. Sulfur isotope characterization of primordial and recycled sources feeding the Samoan mantle plume. Earth and Planetary Science Letters 534, 116073.
Dottin, J.W.I., Labidi, J., Jackson, M.G., Woodhead, J., Farquhar, J., 2020. Isotopic Evidence for Multiple Recycled Sulfur Reservoirs in the Mangaia Mantle Plume. Geochemistry, Geophysics, Geosystems 21, e2020GC009081.
Duncan, M.S., Dasgupta, R., 2017. Rise of Earth's atmospheric oxygen controlled by efficient subduction of organic carbon. Nature Geoscience 10, 387-392.
Eggler, D.H., 1978. The effect of CO_2 upon partial melting of peridotite in the system Na_2O-CaO-Al_2O_3-MgO-SiO_2-CO_2 to 35 kb, with an analysis of melting in a peridotite-H_2O-CO_2 system. American Journal of Science 278, 305-343.
Eguchi, J., Dasgupta, R., 2018a. A CO_2 solubility model for silicate melts from fluid saturation to graphite or diamond saturation. Chemical Geology 487, 23-38.
Eguchi, J., Dasgupta, R., 2018b. Redox state of the convective mantle from CO2-trace element systematics of oceanic basalts. Geochemical Perspectives Letters 8, 17-21.
Eguchi, J., Seales, J., Dasgupta, R., 2020. Great Oxidation and Lomagundi events linked by deep cycling and enhanced degassing of carbon. Nature Geoscience 13, 71-76.
Esposito, R., Bodnar, R.J., Danyushevsky, L.V., De Vivo, B., Fedele, L., Hunter, J., Lima, A., Shimizu, N., 2011. Volatile Evolution of Magma Associated with the Solchiaro Eruption in the Phlegrean Volcanic District (Italy). J. Petrol. 52, 2431-2460.
Exley, R.A., Mattey, D.P., Clague, D.A., Pillinger, C.T., 1986. Carbon isotope systematics of a mantle “hotspot”: a comparison of Loihi Seamount and MORB glasses. Earth and Planetary Science Letters 78, 189-199.
Falloon, T.J., Green, D.H., 1989. The solidus of carbonated, fertile peridotite. Earth and Planetary Science Letters 94, 364-370.
Falloon, T.J., Green, D.H., 1990. Solidus of carbonated fertile peridotite under fluid-saturated conditions. Geology 18, 195-199.
Farley, K.A., 1995. Cenozoic variations in the flux of interplanetary dust recorded by ^3He in a deep-sea sediment. Nature 376, 153-156.
Farquhar, J., Bao, H., Thiemens, M., 2000. Atmospheric Influence of Earth's Earliest Sulfur Cycle. Science 289, 756-758.
Fine, G., Stolper, E., 1985. The speciation of carbon dioxide in sodium aluminosilicate glasses. Contributions to Mineralogy and Petrology 91, 105-121.

Fortin, M.-A., Riddle, J., Desjardins-Langlais, Y., Baker, D.R., 2015. The effect of water on the sulfur concentration at sulfide saturation (SCSS) in natural melts. Geochimica et Cosmochimica Acta 160, 100-116.
Frost, D.J., McCammon, C.A., 2008. The Redox State of Earth's Mantle. Annual Review of Earth and Planetary Sciences 36, 389-420.
Fuentes, J.J., Crowley, J.W., Dasgupta, R., Mitrovica, J.X., 2019. The influence of plate tectonic style on melt production and CO_2 outgassing flux at mid-ocean ridges. Earth and Planetary Science Letters 511, 154-163.
Gaetani, G.A., Grove, T.L., 1999. Wetting of mantle olivine by sulfide melt: implications for Re/Os ratios in mantle peridotite and late-stage core formation. Earth and Planetary Science Letters 169, 147-163.
Gaetani, G.A., O'Leary, J.A., Shimizu, N., Bucholz, C.E., Newville, M., 2012. Rapid reequilibration of H2O and oxygen fugacity in olivine-hosted melt inclusions. Geology 40, 915-918.
Gaillard, F., Malki, M., Iacono-Marziano, G., Pichavant, M., Scaillet, B., 2008. Carbonatite melts and electrical conductivity in the asthenosphere. Science 322, 1363-1365.
Gaillard, F., Scaillet, B., Pichavant, M., Iacono-Marziano, G., 2015. The redox geodynamics linking basalts and their mantle sources through space and time. Chemical Geology 418, 217-233.
Garapić, G., Mallik, A., Dasgupta, R., Jackson, M.G., 2015. Oceanic lavas sampling the high-3He/4He mantle reservoir: Primitive, depleted, or re-enriched? American Mineralogist 100, 2066-2081.
Garcia, M.O., Muenow, D.W., Aggrey, K.E., O'Neil, J.R., 1989. Major element, volatile, and stable isotope geochemistry of Hawaiian submarine tholeiitic glasses. Journal of Geophysical Research: Solid Earth 94, 10525-10538.
Geiger, C.A., Rossman, G.R., 2018. IR spectroscopy and OH– in silicate garnet: The long quest to document the hydrogarnet substitution. American Mineralogist 103, 384-393.
Gerbode, C., Dasgupta, R., 2010. Carbonate-fluxed melting of MORB-like pyroxenite at 2·9 GPa and genesis of HIMU ocean island basalts. J. Petrol. 51, 2067-2088.
Gerlach, T.M., 1991. Comment on "Mid-ocean ridge popping rocks: implications for degassing at ridge crests" by P. Sarda and D. Graham. Earth and Planetary Science Letters 105, 566-567.
Gerlach, T.M., Taylor, B.E., 1990. Carbon isotope constraints on degassing of carbon dioxide from Kilauea Volcano. Geochimica et Cosmochimica Acta 54, 2051-2058.
Gerlach, T.M., Thomas, D.M., 1986. Carbon and sulphur isotopic composition of Kilauea parental magma. Nature 319, 480-483.
Ghosh, S., Litasov, K., Ohtani, E., 2014. Phase relations and melting of carbonated peridotite between 10 and 20 GPa: a proxy for alkali- and CO_2-rich silicate melts in the deep mantle. Contributions to Mineralogy and Petrology 167, 1-23.
Ghosh, S., Ohtani, E., Litasov, K., Suzuki, A., Sakamaki, T., 2007. Stability of carbonated magmas at the base of the Earth's upper mantle. Geophysical Research Letters 34.
Graham, D., Sarda, P., 1991. Reply to comment by T.M. Gerlach on "Mid-ocean ridge popping rocks: implications for degassing at ridge crests". Earth and Planetary Science Letters 105, 568-573.

Graham, D.W., Michael, P.J., Truong, T.B., 2023. Carbon isotope composition of basalts from Loihi Seamount: Primordial or recycled carbon in the Hawaiian mantle plume? Earth and Planetary Science Letters 617, 118248.
Grewal, D.S., Dasgupta, R., Holmes, A.K., Costin, G., Li, Y., Tsuno, K., 2019a. The fate of nitrogen during core-mantle separation on Earth. Geochimica et Cosmochimica Acta 251, 87-115.
Grewal, D.S., Dasgupta, R., Hough, T., Farnell, A., 2021. Rates of protoplanetary accretion and differentiation set nitrogen budget of rocky planets. Nature Geoscience 14, 369-376.
Grewal, D.S., Dasgupta, R., Sun, C., Tsuno, K., Costin, G., 2019b. Delivery of carbon, nitrogen and sulfur to the silicate Earth by a giant impact. Science Advances 5, eaau3669, doi:3610.1126/sciadv.aau3669.
Grove, T.L., Chatterjee, N., Parman, S.W., Médard, E., 2006. The influence of H_2O on mantle wedge melting. Earth and Planetary Science Letters 249, 74-89.
Grove, T.L., Till, C.B., Krawczynski, M., 2012. The Role of H_2O in Subduction Zone Magmatism. Annual Review of Earth and Planetary Sciences 40, doi:10.1146/annurev-earth-042711-105310.
Guilhaumou, N., Sautter, V., Dumas, P., 2005. Synchrotron FTIR microanalysis of volatiles in melt inclusions and exsolved particles in ultramafic deep-seated garnets. Chemical Geology 223, 82-92.
Guo, J., Griffin, W.L., O'Reilly, S.Y., 1999. Geochemistry and Origin of Sulphide Minerals in Mantle Xenoliths: Qilin, Southeastern China. J. Petrol. 40, 1125-1149.
Hallis, L.J., Huss, G.R., Nagashima, K., Taylor, G.J., Halldórsson, S.A., Hilton, D.R., Mottl, M.J., Meech, K.J., 2015. Evidence for primordial water in Earth's deep mantle. Science 350, 795-797.
Hanyu, T., Yamamoto, J., Kimoto, K., Shimizu, K., Ushikubo, T., 2020. Determination of total CO2 in melt inclusions with shrinkage bubbles. Chemical Geology 557, 119855.
Hartley, M.E., Maclennan, J., Edmonds, M., Thordarson, T., 2014. Reconstructing the deep CO2 degassing behaviour of large basaltic fissure eruptions. Earth and Planetary Science Letters 393, 120-131.
Hartley, M.E., Shorttle, O., Maclennan, J., Moussallam, Y., Edmonds, M., 2017. Olivine-hosted melt inclusions as an archive of redox heterogeneity in magmatic systems. Earth and Planetary Science Letters 479, 192-205.
Hauri, E., 2002. SIMS analysis of volatiles in silicate glasses, 2: isotopes and abundances in Hawaiian melt inclusions. Chemical Geology 183, 115-141.
Hauri, E., Wang, J., Dixon, J.E., King, P.L., Mandeville, C., Newman, S., 2002. SIMS analysis of volatiles in silicate glasses 1. Calibration, matrix effects and comparisons with FTIR. Chemical Geology 183, 99-114.
Hauri, E.H., Cottrell, E., Kelley, K.A., Tucker, J.M., Shimizu, K., Voyer, M.L., Marske, J., Saal, A.E., Carbon in the Convecting Mantle, in: B.N. Orcutt, I. Daniel, R. Dasgupta, (Eds), Deep Carbon: Past to Present, Cambridge University Press, Cambridge, 2019, pp. 237-275.
Hauri, E.H., Gaetani, G.A., Green, T.H., 2006. Partitioning of water during melting of the Earth's upper mantle at H_2O-undersaturated conditions. Earth and Planetary Science Letters 248, 715-734.
Hauri, E.H., Maclennan, J., McKenzie, D., Gronvold, K., Oskarsson, N., Shimizu, N., 2017. CO2 content beneath northern Iceland and the variability of mantle carbon. Geology 46, 55-58.

Hekinian, R., Chaigneau, M., Cheminee, J.L., 1973. Popping Rocks and Lava Tubes from the Mid-Atlantic Rift Valley at 36° N. Nature 245, 371-373.
Hekinian, R., Pineau, F., Shilobreeva, S., Bideau, D., Gracia, E., Javoy, M., 2000. Deep sea explosive activity on the Mid-Atlantic Ridge near 34°50′N: Magma composition, vesicularity and volatile content. Journal of Volcanology and Geothermal Research 98, 49-77.
Helo, C., Longpre, M.-A., Shimizu, N., Clague, D.A., Stix, J., 2011. Explosive eruptions at mid-ocean ridges driven by CO_2-rich magmas. Nature Geoscience 4, 260-263.
Herzberg, C., Asimow, P.D., 2008. Petrology of some oceanic island basalts: PRIMELT2.XLS software for primary magma calculation. Geochemistry Geophysics Geosystems 9, Q09001, doi:09010.01029/02008GC002057.
Hirose, K., 1997. Partial melt compositions of carbonated peridotite at 3 GPa and role of CO_2 in alkali-basalt magma generation. Geophysical Research Letters 24, 2837-2840.
Hirschmann, M.M., 2000. The mantle solidus: experimental constraints and the effect of peridotite composition. Geochemistry Geophysics Geosystems 1, 2000GC000070.
Hirschmann, M.M., 2006. Water, melting, and the deep Earth H_2O cycle. Annual Review of Earth and Planetary Sciences 34, 629-653.
Hirschmann, M.M., 2016. Constraints on the early delivery and fractionation of Earth's major volatiles from C/H, C/N, and C/S ratios. American Mineralogist 101, 540-553.
Hirschmann, M.M., 2018. Comparative deep Earth volatile cycles: The case for C recycling from exosphere/mantle fractionation of major (H2O, C, N) volatiles and from H2O/Ce, CO2/Ba, and CO2/Nb exosphere ratios. Earth and Planetary Science Letters doi:10.1016/j.epsl.2018.1008.1023.
Hirschmann, M.M., Stolper, E.M., 1996. A possible role of garnet pyroxenite in the origin of the "garnet signature" in the MORB. Contrib. Mineral. Petrol. 124, 185-208.
Hirschmann, M.M., Tenner, T., Aubaud, C., Withers, A.C., 2009. Dehydration melting of nominally anhydrous mantle: The primacy of partitioning. Physics of the Earth and Planetary Interiors 176, 54-68. doi:10.1016/j.pepi.2009.1004.1001.
Hirth, G., Kohlstedt, D.L., 1996. Water in the oceanic upper mantle: implications for rheology, melt extraction and the evolution of the lithosphere. Earth and Planetary Science Letters 144, 93-108.
Holloway, J.R., 1998. Graphite-melt equilibria during mantle melting: constraints on CO_2 in MORB magmas and the carbon content of the mantle. Chemical Geology 147, 89-97.
Holzheid, A., Grove, T.L., 2002. Sulfur saturation limits in silicate melts and their implications for core formation scenarios for terrestrial planets. American Mineralogist 87, 227-237.
Hughes, E.C., Buse, B., Kearns, S.L., Blundy, J.D., Kilgour, G., Mader, H.M., 2019. Low analytical totals in EPMA of hydrous silicate glass due to sub-surface charging: Obtaining accurate volatiles by difference. Chemical Geology 505, 48-56.
Ihinger, P.D., Hervig, R.L., McMillan, P.F., 1994. Analytical methods for volatiles in glasses. Reviews in Mineralogy and Geochemistry 30, 67-121.
Ito, E., Harris, D.M., Anderson, A.T., 1983. Alteration of oceanic crust and geologic cycling of chlorine and water. Geochimica et Cosmochimica Acta 47, 1613-1624.
Jackson, C.R.M., Cottrell, E., Du, Z., Bennett, N.R., Fei, Y., 2021. High pressure redistribution of nitrogen and sulfur during planetary stratification. Geochemical Perspectives Letters 18, 37-42.

Jackson, M.G., Dasgupta, R., 2008. Compositions of HIMU, EM1, and EM2 from global trends between radiogenic isotopes and major elements in ocean island basalts. Earth and Planetary Science Letters 276, 175-186. doi:110.1016/j.epsl.2008.1009.1023.
Jacobsen, S.D., Jiang, F., Mao, Z., Duffy, T.S., Smyth, J.R., Holl, C.M., Frost, D.J., 2008. Effects of hydration on the elastic properties of olivine. Geophysical Research Letters 35.
Jambon, A., Déruelle, B., Dreibus, G., Pineau, F., 1995. Chlorine and bromine abundance in MORB: the contrasting behaviour of the Mid-Atlantic Ridge and East Pacific Rise and implications for chlorine geodynamic cycle. Chemical Geology 126, 101-117.
Jambon, A., Weber, H., Braun, O., 1986. Solubility of He, Ne, Ar, Kr and Xe in a basalt melt in the range 1250–1600°C. Geochemical implications. Geochimica et Cosmochimica Acta 50, 401-408.
Jambon, A., Zimmerman, J.L., 1990. Water in oceanic basalts: evidence for dehydration of recycled crust. Earth and Planetary Science Letters 101, 323-331.
Jambon, A., Zimmermann, J.L., 1987. Major volatiles from a North Atlantic MORB glass and calibration to He: A size fraction analysis. Chemical Geology 62, 177-189.
Javoy, M., 1997. The major volatile elements of the Earth: Their origin, behavior, and fate. Geophysical Research Letters 24, 177-180.
Javoy, M., 1998. The birth of the Earth's atmosphere: the behaviour and fate of its major elements. Chemical Geology 147, 11-25.
Javoy, M., Pineau, F., 1991. The volatiles record of a “popping” rock from the Mid-Atlantic Ridge at 14°N: chemical and isotopic composition of gas trapped in the vesicles. Earth and Planetary Science Letters 107, 598-611.
Javoy, M., Pineau, F., Allègre, C.J., 1982. Carbon geodynamic cycle. Nature 300, 171-173.
Javoy, M., Pineau, F., Iiyama, I., 1978. Experimental determination of the isotopic fractionation between gaseous CO2 and carbon dissolved in tholeiitic magma. Contributions to Mineralogy and Petrology 67, 35-39.
Jégo, S., Dasgupta, R., 2013. Fluid-present melting of sulfide-bearing ocean-crust: Experimental constraints on the transport of sulfur from subducting slab to mantle wedge. Geochimica et Cosmochimica Acta 110, 106-134.
Jégo, S., Dasgupta, R., 2014. The fate of sulfur during fluid-present melting of subducting basaltic crust at variable oxygen fugacity. J. Petrol. 55, 1019-1050. doi:1010.1093/petrology/egu1016.
Jenner, F.E., O'Neill, H.S.C., 2012. Analysis of 60 elements in 616 ocean floor basaltic glasses. Geochemistry, Geophysics, Geosystems 13.
John, T., Layne, G.D., Haase, K.M., Barnes, J.D., 2010. Chlorine isotope evidence for crustal recycling into the Earth's mantle. Earth and Planetary Science Letters 298, 175-182.
Johnson, A., Dasgupta, R., Costin, G., Tsuno, K., submitted. Electron probe microanalysis of trace sulfur in basaltic glasses and silicate minerals. American Mineralogist.
Johnson, B., Goldblatt, C., 2015. The nitrogen budget of Earth. Earth-Science Reviews 148, 150-173.
Jones, M.P., Soule, S.A., Liao, Y., Brodsky, H., Le Roux, V., Klein, F., 2020. Quantitative vesicle analyses and total CO2 reconstruction in mid-ocean ridge basalts. Journal of Volcanology and Geothermal Research 407, 107109.
Jones, M.P., Wanless, V.D., Soule, S.A., Kurz, M.D., Mittelstaedt, E., Fornari, D.J., Curtice, J., Klein, F., Le Roux, V., Brodsky, H., Péron, S., Schwartz, D.M., 2019. New constraints

on mantle carbon from Mid-Atlantic Ridge popping rocks. Earth and Planetary Science Letters 511, 67-75.
Jugo, P.J., Luth, R.W., Richards, J.P., 2005. Experimental data on the speciation of sulfur as a function of oxygen fugacity in basaltic melts. Geochimica et Cosmochimica Acta 69, 497-503.
Jugo, P.J., Wilke, M., Botcharnikov, R.E., 2010. Sulfur K-edge XANES analysis of natural and synthetic basaltic glasses: Implications for S speciation and S content as function of oxygen fugacity. Geochimica et Cosmochimica Acta 74, 5926-5938.
Kagoshima, T., Sano, Y., Takahata, N., Maruoka, T., Fischer, T.P., Hattori, K., 2015. Sulphur geodynamic cycle. Scientific Reports 5, 8330.
Kamenetsky, V.S., Kamenetsky, M.B., Sharygin, V.V., Golovin, A.V., 2007. Carbonate-chloride enrichment in fresh kimberlites of the Udachnaya-East pipe, Siberia: A clue to physical properties of kimberlite magmas? Geophysical Research Letters 34.
Karki, B.B., Ghosh, D.B., Karato, S.-i., 2021. Behavior and properties of water in silicate melts under deep mantle conditions. Scientific Reports 11, 10588.
Katz, R.F., Spiegelman, M., Langmuir, C.H., 2003. A new parameterization of hydrous mantle melting. Geochemistry Geophysics Geosystems 4, 1073, doi:1010.1029/2002GC000433.
Kendrick, M.A., Jackson, M.G., Hauri, E.H., Phillips, D., 2015. The halogen (F, Cl, Br, I) and H2O systematics of Samoan lavas: Assimilated-seawater, EM2 and high-3He/4He components. Earth and Planetary Science Letters 410, 197-209.
Kendrick, M.A., Jackson, M.G., Kent, A.J.R., Hauri, E.H., Wallace, P.J., Woodhead, J., 2014. Contrasting behaviours of CO2, S, H2O and halogens (F, Cl, Br, and I) in enriched-mantle melts from Pitcairn and Society seamounts. Chemical Geology 370, 69-81.
Kendrick, M.A., Kamenetsky, V.S., Phillips, D., Honda, M., 2012a. Halogen systematics (Cl, Br, I) in Mid-Ocean Ridge Basalts: A Macquarie Island case study. Geochimica et Cosmochimica Acta 81, 82-93.
Kendrick, M.A., Woodhead, J.D., Kamenetsky, V.S., 2012b. Tracking halogens through the subduction cycle. Geology 40, 1075-1078.
Kent, A.J.R., 2008. Melt Inclusions in Basaltic and Related Volcanic Rocks. Reviews in Mineralogy and Geochemistry 69, 273-331.
Kent, A.J.R., Clague, D.A., Honda, M., Stolper, E.M., Hutcheon, I.D., Norman, M.D., 1999a. Widespread assimilation of a seawater-derived component at Loihi Seamount, Hawaii. Geochimica et Cosmochimica Acta 63, 2749-2761.
Kent, A.J.R., Norman, M.D., Hutcheon, I.D., Stolper, E.M., 1999b. Assimilation of seawater-derived components in an oceanic volcano: evidence from matrix glasses and glass inclusions from Loihi seamount, Hawaii. Chemical Geology 156, 299-319.
Keppler, H., Cialdella, L., Couffignal, F., Wiedenbeck, M., 2022. The solubility of N2 in silicate melts and nitrogen partitioning between upper mantle minerals and basalt. Contributions to Mineralogy and Petrology 177, 83.
Keppler, H., Golabek, G., 2019. Graphite floatation on a magma ocean and the fate of carbon during core formation. Geochemical Perspectives Letters 11, 12-17.
Keppler, H., Wiedenbeck, M., Shcheka, S.S., 2003. Carbon solubility in olivine and the mode of carbon storage in the Earth's mantle. Nature 424, 414-416.
Kingsley, R.H., Schilling, J.-G., Dixon, J.E., Swart, P., Poreda, R., Simons, K., 2002. D/H ratios in basalt glasses from the Salas y Gomez mantle plume interacting with the East Pacific

Rise: Water from old D-rich recycled crust or primordial water from the lower mantle? Geochemistry, Geophysics, Geosystems 3, 1-26.
Kirstein, L.A., Walowski, K.J., Jones, R.E., Burgess, R., Fitton, J.G., De Hoog, J.C.M., Savov, I.P., Kalnins, L.M., F, E.I.M., 2023. Volatiles and Intraplate Magmatism: a Variable Role for Carbonated and Altered Oceanic Lithosphere in Ocean Island Basalt Formation. J. Petrol. 64.
Kohlstedt, D.L., Keppler, H., Rubie, D.C., 1996. Solubility of water in the a, b and g phases of $(Mg,Fe)_2SiO_4$. Contributions to Mineralogy and Petrology 123, 345-357.
Koleszar, A.M., Saal, A.E., Hauri, E.H., Nagle, A.N., Liang, Y., Kurz, M.D., 2009. The volatile contents of the Galapagos plume; evidence for H2O and F open system behavior in melt inclusions. Earth and Planetary Science Letters 287, 442-452.
Kono, Y., Kenney-Benson, C., Hummer, D., Ohfuji, H., Park, C., Shen, G., Wang, Y., Kavner, A., Manning, C.E., 2014. Ultralow viscosity of carbonate melts at high pressures. Nature Communications 5.
Kushiro, I., Syono, Y., Akimoto, S.-i., 1968. Melting of a peridotite nodule at high pressures and high water pressures. Journal of Geophysical Research 73, 6023-6029.
Kyser, T.K., O'Neil, J.R., 1984. Hydrogen isotope systematics of submarine basalts. Geochimica et Cosmochimica Acta 48, 2123-2133.
Labidi, J., Cartigny, P., 2016. Negligible sulfur isotope fractionation during partial melting: Evidence from Garrett transform fault basalts, implications for the late-veneer and the hadean matte. Earth and Planetary Science Letters 451, 196-207.
Labidi, J., Cartigny, P., Birck, J.L., Assayag, N., Bourrand, J.J., 2012. Determination of multiple sulfur isotopes in glasses: A reappraisal of the MORB δ34S. Chemical Geology 334, 189-198.
Labidi, J., Cartigny, P., Hamelin, C., Moreira, M., Dosso, L., 2014. Sulfur isotope budget (32S, 33S, 34S and 36S) in Pacific–Antarctic ridge basalts: A record of mantle source heterogeneity and hydrothermal sulfide assimilation. Geochimica et Cosmochimica Acta 133, 47-67.
Labidi, J., Cartigny, P., Jackson, M.G., 2015. Multiple sulfur isotope composition of oxidized Samoan melts and the implications of a sulfur isotope 'mantle array' in chemical geodynamics. Earth and Planetary Science Letters 417, 28-39.
Labidi, J., Cartigny, P., Moreira, M., 2013. Non-chondritic sulphur isotope composition of the terrestrial mantle. Nature 501, 208.
Labidi, J., Dottin, J.W., Clog, M., Hemond, C., Cartigny, P., 2022. Near-zero 33S and 36S anomalies in Pitcairn basalts suggest Proterozoic sediments in the EM-1 mantle plume. Earth and Planetary Science Letters 584, 117422.
Lamadrid, H.M., Moore, L.R., Moncada, D., Rimstidt, J.D., Burruss, R.C., Bodnar, R.J., 2017. Reassessment of the Raman CO2 densimeter. Chemical Geology 450, 210-222.
Lane, S.J., Dalton, J.A., 1994. Electron-microprobe analysis of geological carbonates. American Mineralogist 79, 745-749.
Langmuir, C.H., Klein, E.M., Plank, T., Petrological systematics of mid-ocean ridge basalts: constraints on melt generation beneath ocean ridges, in: J. Phipps Morgan, D.K. Blackman, J.M. Sinton, (Eds), Mantle flow and melt generation at mid-ocean ridges 71, American Geophysical Union, Washington, DC, 1992, pp. 183-280.

Laporte, D., Toplis, M.J., Seyler, M., Devidal, J.-L., 2004. A new experimental technique for extracting liquids from peridotite at very low degrees of melting: application to partial melting of depleted peridotite. Contrib. Mineral. Petrol. 146, 463-484.
Lara, M., Dasgupta, R., 2022. Carbon recycling efficiency in subduction zones constrained by the effects of H2O-CO2 fluids on partial melt compositions in the mantle wedge. Earth and Planetary Science Letters 588, 117578.
Lara, M., Dasgupta, R., 2023. Effects of H2O–CO2 Fluids, Temperature, and Peridotite Fertility on Partial Melting in Mantle Wedges and Generation of Primary Arc Basalts. J. Petrol. 64.
le Roux, P.J., Shirey, S.B., Hauri, E.H., Perfit, M.R., Bender, J.F., 2006. The effects of variable sources, processes and contaminants on the composition of northern EPR MORB (8–10°N and 12–14°N): Evidence from volatiles (H2O, CO2, S) and halogens (F, Cl). Earth and Planetary Science Letters 251, 209-231.
Le Roux, V., Dasgupta, R., Lee, C.T.A., 2011. Mineralogical heterogeneities in the Earth's mantle: Constraints from Mn, Co, Ni and Zn partitioning during partial melting. Earth and Planetary Science Letters 307, 395-408.
Le Voyer, M., Kelley, K.A., Cottrell, E., Hauri, E.H., 2017. Heterogeneity in mantle carbon content from CO2-undersaturated basalts. Nature Communications 8, 14062.
Lécuyer, C., Gillet, P., Robert, F., 1998. The hydrogen isotope composition of seawater and the global water cycle. Chemical Geology 145, 249-261.
Lee, C.-T.A., Jiang, H., Dasgupta, R., Torres, M., A framework for understanding whole Earth carbon cycling, in: B.N. Orcutt, I. Daniel, R. Dasgupta, (Eds), Deep Carbon: Past to Present, Cambridge University Press, Cambridge, UK, 2019, pp. 313-357.
Lee, C.-T.A., Luffi, P., Chin, E.J., Bouchet, R., Dasgupta, R., Morton, D.M., Le Roux, V., Yin, Q.-z., Jin, D., 2012. Copper systematics in arc magmas and implications for crust-mantle differentiation. Science 336, 64-68.
Lee, C.-T.A., Luffi, P., Plank, T., Dalton, H., Leeman, W.P., 2009. Constraints on the depths and temperatures of basaltic magma generation on Earth and other terrestrial planets. Earth and Planetary Science Letters 279, 20-33.
Li, C., Ripley, E., 2005. Empirical equations to predict the sulfur content of mafic magmas at sulfide saturation and applications to magmatic sulfide deposits. Mineralium Deposita 40, 218-230.
Li, J.-L., Schwarzenbach, E.M., John, T., Ague, J.J., Huang, F., Gao, J., Klemd, R., Whitehouse, M.J., Wang, X.-S., 2020. Uncovering and quantifying the subduction zone sulfur cycle from the slab perspective. Nature Communications 11, 514.
Li, Y., Audétat, A., 2015. Effects of temperature, silicate melt composition, and oxygen fugacity on the partitioning of V, Mn, Co, Ni, Cu, Zn, As, Mo, Ag, Sn, Sb, W, Au, Pb, and Bi between sulfide phases and silicate melt. Geochimica et Cosmochimica Acta 162, 25-45.
Li, Y., Dasgupta, R., Tsuno, K., Monteleone, B., Shimizu, N., 2016. Carbon and sulfur budget of the silicate Earth explained by accretion of differentiated planetary embryos. Nature Geosci 9, 781-785.
Li, Y., Wiedenbeck, M., Monteleone, B., Dasgupta, R., Costin, G., Gao, Z., Lu, W., 2023. Nitrogen and carbon fractionation in planetary magma oceans and origin of the superchondritic C/N ratio in the bulk silicate Earth. Earth and Planetary Science Letters 605, 118032.

Li, Y., Wiedenbeck, M., Shcheka, S., Keppler, H., 2013. Nitrogen solubility in upper mantle minerals. Earth and Planetary Science Letters 377-378, 311-323.
Li, Z.-X.A., Lee, C.-T.A., 2004. The constancy of upper mantle fO2 through time inferred from V/Sc ratios in basalts. Earth and Planetary Science Letters 228, 483-493.
Libourel, G., Marty, B., Humbert, F., 2003. Nitrogen solubility in basaltic melt. Part I. Effect of oxygen fugacity. Geochimica et Cosmochimica Acta 67, 4123-4135.
Litasov, K.D., Safonov, O.G., Ohtani, E., 2010. Origin of Cl-bearing silica-rich melt inclusions in diamonds: Experimental evidence for an eclogite connection. Geology 38, 1131-1134.
Liu, J., Rudnick, R.L., Walker, R.J., Gao, S., Wu, F., Piccoli, P.M., 2010. Processes controlling highly siderophile element fractionations in xenolithic peridotites and their influence on Os isotopes. Earth and Planetary Science Letters 297, 287-297.
Longpré, M. A., Stix, J., Klügel, A., Shimizu, N. 2017. Mantle to surface degassing of carbon- and sulfur-rich alkaline magma at El Hierro, Canary Islands. Earth and Planetary Science Letters 460, 268-280.
Lorand, J.-P., Luguet, A., 2016. Chalcophile and Siderophile Elements in Mantle Rocks: Trace Elements Controlled By Trace Minerals. Reviews in Mineralogy and Geochemistry 81, 441-488.
Lorand, J.-P., Luguet, A., Alard, O., 2013. Platinum-group element systematics and petrogenetic processing of the continental upper mantle: A review. Lithos 164-167, 2-21.
Lowenstern, J.B., 2015. Bursting the bubble of melt inclusions†. American Mineralogist 100, 672-673.
Luguet, A., Lorand, J.-P., Seyler, M., 2003. Sulfide petrology and highly siderophile element geochemistry of abyssal peridotites: a coupled study of samples from the Kane Fracture Zone (45°W 23°20N, MARK area, Atlantic Ocean). Geochimica et Cosmochimica Acta 67, 1553-1570.
Lupton, J.E., Craig, H., 1975. Excess ^{3}He in oceanic basalts: Evidence for terrestrial primordial helium. Earth and Planetary Science Letters 26, 133-139.
Luth, R.W., Carbon and carbonates in the mantle, in: Y. Fei, Bertka, C. M., Mysen, B. O., (Ed), Mantle Petrology: Field Observations and High Pressure Experimentation: A Tribute to Francis R. (Joe) Boyd 6, The Geochemical Society, 1999, pp. 297-316.
Lux, G., 1987. The behavior of noble gases in silicate liquids: Solution, diffusion, bubbles and surface effects, with applications to natural samples. Geochimica et Cosmochimica Acta 51, 1549-1560.
Machida, S., Hirano, N., Kimura, J.-I., 2009. Evidence for recycled plate material in Pacific upper mantle unrelated to plumes. Geochimica et Cosmochimica Acta 73, 3028-3037.
Macpherson, C., Mattey, D., 1994. Carbon isotope variations of CO2 in Central Lau Basin basalts and ferrobasalts. Earth and Planetary Science Letters 121, 263-276.
Mallik, A., Dasgupta, R., 2013. Reactive infiltration of MORB-eclogite-derived carbonated silicate melt into fertile peridotite at 3 GPa and genesis of alkalic magmas. J. Petrol. 54, 2267-2300.
Mallik, A., Dasgupta, R., 2014. Effect of variable CO_2 on eclogite-derived andesite-lherzolite reaction at 3 GPa – Implications for mantle source characteristics of alkalic ocean island basalts. Geochemistry, Geophysics, Geosystems 15, 1533-1557.
Mann, U., Schmidt, M.W., 2015. Melting of pelitic sediments at subarc depths: 1. Flux vs. fluid-absent melting and a parameterization of melt productivity. Chemical Geology 404, 150-167.

Marty, B., 1995. Nitrogen content of the mantle inferred from N_2–Ar correlation in oceanic basalts. Nature 377, 326-329.
Marty, B., 2012. The origins and concentrations of water, carbon, nitrogen and noble gases on Earth. Earth and Planetary Science Letters 313–314, 56-66.
Marty, B., Almayrac, M., Barry, P.H., Bekaert, D.V., Broadley, M.W., Byrne, D.J., Ballentine, C.J., Caracausi, A., 2020. An evaluation of the C/N ratio of the mantle from natural CO2-rich gas analysis: Geochemical and cosmochemical implications. Earth and Planetary Science Letters 551, 116574.
Marty, B., Dauphas, N., 2003. The nitrogen record of crust–mantle interaction and mantle convection from Archean to Present. Earth and Planetary Science Letters 206, 397-410.
Marty, B., Jambon, A., 1987. $C/^3He$ in volatile fluxes from the solid Earth: implications for carbon geodynamics. Earth and Planetary Science Letters 83, 16-26.
Marty, B., Tolstikhin, I.N., 1998. CO_2 fluxes from mid-ocean ridges, arcs and plumes. Chemical Geology 145, 233-248.
Marty, B., Zimmermann, L., 1999. Volatiles (He, C, N, Ar) in mid-ocean ridge basalts: assesment of shallow-level fractionation and characterization of source composition. Geochimica et Cosmochimica Acta 63, 3619-3633.
Mathez, E.A., 1976. Sulfur solubility and magmatic sulfides in submarine basalt glass. Journal of Geophysical Research 81, 4269-4276.
Matsyuk, S.S., Langer, K., 2004. Hydroxyl in olivines from mantle xenoliths in kimberlites of the Siberian platform. Contributions to Mineralogy and Petrology 147, 413-437.
Mattey, D.P., 1991. Carbon dioxide solubility and carbon isotope fractionation in basaltic melt. Geochimica et Cosmochimica Acta 55, 3467-3473.
Mattey, D.P., 1991. Carbon dioxide solubility and carbon isotope fractionation in basaltic melt. Geochimica et Cosmochimica Acta 55, 3467-3473.
Mattey, D.P., Carr, R.H., Wright, I.P., Pillinger, C.T., 1984. Carbon isotopes in submarine basalts. Earth and Planetary Science Letters 70, 196-206.
Matthews, S., Shorttle, O., Maclennan, J., Rudge, J.F., 2021. The global melt inclusion C/Ba array: Mantle variability, melting process, or degassing? Geochimica et Cosmochimica Acta 293, 525-543.
Matthews, S., Shorttle, O., Rudge, J.F., Maclennan, J., 2017. Constraining mantle carbon: CO2-trace element systematics in basalts and the roles of magma mixing and degassing. Earth and Planetary Science Letters 480, 1-14.
McGovern, P.J., Schubert, G., 1989. Thermal evolution of the Earth: effects of volatile exchange between atmosphere and interior. Earth and Planetary Science Letters 96, 27-37.
McKenzie, D., Jackson, J., Priestley, K., 2005. Thermal structure of oceanic and continental lithosphere. Earth and Planetary Science Letters 233, 337-349.
Métrich, N., Berry, A.J., O'Neill, H.S.C., Susini, J., 2009. The oxidation state of sulfur in synthetic and natural glasses determined by X-ray absorption spectroscopy. Geochimica et Cosmochimica Acta 73, 2382-2399.
Michael, P., 1995. Regionally distinctive sources of depleted MORB: Evidence from trace elements and H2O. Earth and Planetary Science Letters 131, 301-320.
Michael, P.J., Cornell, W.C., 1998. Influence of spreading rate and magma supply on crystallization and assimilation beneath mid-ocean ridges: Evidence from chlorine and major element chemistry of mid-ocean ridge basalts. Journal of Geophysical Research: Solid Earth 103, 18325-18356.

Michael, P.J., Graham, D.W., 2015. The behavior and concentration of CO2 in the suboceanic mantle: Inferences from undegassed ocean ridge and ocean island basalts. Lithos 236–237, 338-351.
Michael, P.J., Schilling, J.-G., 1989. Chlorine in mid-ocean ridge magmas: Evidence for assimilation of seawater-influenced components. Geochimica et Cosmochimica Acta 53, 3131-3143.
Miller, G.H., Rossman, G.R., Harlow, G.E., 1987. The natural occurrence of hydroxide in olivine. Physics and Chemistry of Minerals 14, 461-472.
Miller, W.G.R., Maclennan, J., Shorttle, O., Gaetani, G.A., Le Roux, V., Klein, F., 2019. Estimating the carbon content of the deep mantle with Icelandic melt inclusions. Earth and Planetary Science Letters 523, 115699.
Minarik, W.G., Ryerson, F.J., Watson, E.B., 1996. Textural Entrapment of Core-Forming Melts. Science 272, 530-533.
Mironov, N., Portnyagin, M., Botcharnikov, R., Gurenko, A., Hoernle, K., Holtz, F., 2015. Quantification of the CO2 budget and H2O–CO2 systematics in subduction-zone magmas through the experimental hydration of melt inclusions in olivine at high H2O pressure. Earth and Planetary Science Letters 425, 1-11.
Mookherjee, M., Karato, S.-i., 2010. Solubility of water in pyrope-rich garnet at high pressures and temperature. Geophysical Research Letters 37.
Moore, L.R., Gazel, E., Tuohy, R., Lloyd, A.S., Esposito, R., Steele-MacInnis, M., Hauri, E.H., Wallace, P.J., Plank, T., Bodnar, R.J., 2015. Bubbles matter: An assessment of the contribution of vapor bubbles to melt inclusion volatile budgets†. American Mineralogist 100, 806-823.
Mosenfelder, J.L., Deligne, N.I., Asimow, P.D., Rossman, G.R., 2006. Hydrogen incorporation in olivine from 2-12 GPa. American Mineralogist 91, 285-294.
Moussallam, Y., Longpré, M.-A., McCammon, C., Gomez-Ulla, A., Rose-Koga, E.F., Scaillet, B., Peters, N., Gennaro, E., Paris, R., Oppenheimer, C., 2019. Mantle plumes are oxidised. Earth and Planetary Science Letters 527, 115798.
Moussallam, Y., Georgeais, G., Rose-Koga, E. F., Koga, K. T., Hartley, M. E., Sciallet, B., Oppenheimer, C., Peters, N., 2023. CO_2-undersaturated melt inclusions from the South West Indian Ridge record surprisingly uniform redox conditions. Geochemistry, Geophysics, Geosystems 24(12), e2023GC011235.
Neave, D.A., Maclennan, J., Edmonds, M., Thordarson, T., 2014. Melt mixing causes negative correlation of trace element enrichment and CO2 content prior to an Icelandic eruption. Earth and Planetary Science Letters 400, 272-283.
Newman, S., Epstein, S., Stolper, E., 1988. Water, carbon dioxide, and hydrogen isotopes in glasses from the ca. 1340 A.D. eruption of the Mono Craters, California: Constraints on degassing phenomena and initial volatile content. Journal of Volcanology and Geothermal Research 35, 75-96.
Newman, S., Lowenstern, J.B., 2002. VolatileCalc: a silicate melt–H_2O–CO_2 solution model written in Visual Basic for excel. Computers and Geosciences 28, 597-604.
Newton, R.C., Sharp, W.E., 1975. Stability of forsterite + CO_2 and its bearing on the role of CO_2 in the mantle. Earth and Planetary Science Letters 26, 239-244.
Ni, H., Keppler, H., Behrens, H., 2011. Electrical conductivity of hydrous basaltic melts: implications for partial melting in the upper mantle. Contributions to Mineralogy and Petrology 162, 637-650.

Nicklas, R.W., Puchtel, I.S., Ash, R.D., 2018. Redox state of the Archean mantle: Evidence from V partitioning in 3.5–2.4 Ga komatiites. Geochimica et Cosmochimica Acta 222, 447-466.
Nielsen, S.G., Shimizu, N., Lee, C.-T.A., Behn, M.D., 2014. Chalcophile behavior of thallium during MORB melting and implications for the sulfur content of the mantle. Geochemistry, Geophysics, Geosystems 15, 4905-4919.
O'Leary, J.A., Gaetani, G.A., Hauri, E.H., 2010. The effect of tetrahedral Al^{3+} on the partitioning of water between clinopyroxene and silicate melt. Earth and Planetary Science Letters 297, 111-120.
O'Neill, H.S.C., The Thermodynamic Controls on Sulfide Saturation in Silicate Melts with Application to Ocean Floor Basalts, in: R. Moretti, D.R. Neuville, (Eds), Magma Redox Geochemistry, Geophysical Monograph, 2021, pp. 177-213.
O'Neill, H.S.C., Mavrogenes, J.A., 2002. The sulfide capacity and the sulfur content at sulfide saturation of silicate melts at 1400°C and 1 bar. J. Petrol. 43, 1049-1087.
Okumura, S., Hirano, N., 2013. Carbon dioxide emission to Earth's surface by deep-sea volcanism. Geology 41, 1167-1170.
Patten, C., Barnes, S.-J., Mathez, E.A., 2012. Textural variations in MORB sulfide droplets due to differences in crystallization history. The Canadian Mineralogist 50, 675-692.
Piani, L., Marrocchi, Y., Rigaudier, T., Vacher, L.G., Thomassin, D., Marty, B., 2020. Earth's water may have been inherited from material similar to enstatite chondrite meteorites. Science 369, 1110-1113.
Pineau, F., Javoy, M., 1983. Carbon isotopes and concentrations in mid-oceanic ridge basalts. Earth and Planetary Science Letters 62, 239-257.
Pineau, F., Javoy, M., 1994. Strong degassing at ridge crests: The behaviour of dissolved carbon and water in basalt glasses at 14°N, Mid-Atlantic Ridge. Earth and Planetary Science Letters 123, 179-198.
Pineau, F., Shilobreeva, S., Hekinian, R., Bidiau, D., Javoy, M., 2004. Deep-sea explosive activity on the Mid-Atlantic Ridge near 34º 50' N: a stable isotope (C, H, O) study. Chemical Geology 211, 159-175.
Pintér, Z., Foley, S.F., Yaxley, G.M., Rosenthal, A., Rapp, R.P., Lanati, A.W., Rushmer, T., 2021. Experimental investigation of the composition of incipient melts in upper mantle peridotites in the presence of CO2 and H2O. Lithos 396-397, 106224.
Plank, T., Manning, C.E., 2019. Subducting carbon. Nature 574, 343-352.
Poreda, R., Schilling, J.G., Craig, H., 1986. Helium and hydrogen isotopes in ocean-ridge basalts north and south of Iceland. Earth and Planetary Science Letters 78, 1-17.
Rauch, M., Keppler, H., 2002. Water solubility in orthopyroxene. Contributions to Mineralogy and Petrology 143, 525-536.
Richet, P., Polian, A., 1998. Water as a dense icelike component in silicate glasses. Science 281, 396-398.
Rison, W., Craig, H., 1983. Helium isotopes and mantle volatiles in Loihi Seamount and Hawaiian Island basalts and xenoliths. Earth and Planetary Science Letters 66, 407-426.
Rohrbach, A., Ghosh, S., Schmidt, M.W., Wijbrans, C.H., Klemme, S., 2014. The stability of Fe–Ni carbides in the Earth's mantle: Evidence for a low Fe–Ni–C melt fraction in the deep mantle. Earth and Planetary Science Letters 388, 211-221.
Rohrbach, A., Schmidt, M.W., 2011. Redox freezing and melting in the Earth's deep mantle resulting from carbon-iron redox coupling. Nature 472, 209-212.

Romano, C., Mungall, J.E., Sharp, T., Dingwell, D.B., 1996. Tensile strengths of hydrous vesicular glasses; an experimental study. American Mineralogist 81, 1148-1154.
Rosenthal, A., Hauri, E.H., Hirschmann, M.M., 2015. Experimental determination of C, F, and H partitioning between mantle minerals and carbonated basalt, CO_2/Ba and CO_2/Nb systematics of partial melting, and the CO_2 contents of basaltic source regions. Earth and Planetary Science Letters 412, 77-87.
Saal, A.E., Hauri, E., Langmuir, C.H., Perfit, M.R., 2002. Vapour undersaturation in primitive mid-ocean-ridge basalt and the volatile content of Earth's upper mantle. Nature 419, 451-455.
Saal, A.E., Hauri, E.H., Lo Casio, M., Van Orman, J.A., Rutherford, M.C., Cooper, R.F., 2008. Volatile content of lunar volcanic glasses and the presence of water in the Moon's interior. Nature 454, 192-195.
Saal, A.E., Hauri, E.H., Van Orman, J.A., Rutherford, M.J., 2013. Hydrogen Isotopes in Lunar Volcanic Glasses and Melt Inclusions Reveal a Carbonaceous Chondrite Heritage. Science 340, 1317-1320.
Safonov, O.G., Kamenetsky, V.S., Perchuk, L.L., 2011. Links between Carbonatite and Kimberlite Melts in Chloride–Carbonate–Silicate Systems: Experiments and Application to Natural Assemblages. J. Petrol. 52, 1307-1331.
Saha, S., Dasgupta, R., 2019. Phase Relations of a Depleted Peridotite fluxed by a CO_2-H_2O fluid– Implications for the Stability of Partial Melts versus Volatile-bearing Mineral Phases in the Cratonic Mantle. Journal of Geophysical Research: Solid Earth 124, 10089-10106.
Sano, Y., Takahata, N., Nishio, Y., Fischer, T.P., Williams, S.N., 2001. Volcanic flux of nitrogen from the Earth. Chemical Geology 171, 263-271.
Sarafian, E., Gaetani, G.A., Hauri, E.H., Sarafian, A.R., 2017. Experimental constraints on the damp peridotite solidus and oceanic mantle potential temperature. Science 355, 942-945.
Sarda, P., Graham, D., 1990. Mid-ocean ridge popping rocks: implications for degassing at ridge crests. Earth and Planetary Science Letters 97, 268-289.
Schilling, J.G., Unni, C.K., Bender, M.L., 1978. Origin of chlorine and bromine in the oceans. Nature 273, 631-636.
Shannon, M.C., Agee, C.B., 1996. High pressure constraints on percolative core formation. Geophysical Research Letters 23, 2717-2720.
Sharp, Z.D., Barnes, J.D., Brearley, A.J., Chaussidon, M., Fischer, T.P., Kamenetsky, V.S., 2007. Chlorine isotope homogeneity of the mantle, crust and carbonaceous chondrites. Nature 446, 1062-1065.
Shaw, C.S.J., 1997. Origin of sulfide blebs in variably metasomatized mantle xenoliths, Quaternary West Eifel volcanic field, Germany. The Canadian Mineralogist 35, 1453-1463.
Shcheka, S.S., Wiedenbeck, M., Frost, D.J., Keppler, H., 2006. Carbon solubility in mantle minerals. Earth and Planetary Science Letters 245, 730-742.
Shi, C.Y., Zhang, L., Yang, W., Liu, Y., Wang, J., Meng, Y., Andrews, J.C., Mao, W.L., 2013. Formation of an interconnected network of iron melt at Earth's lower mantle conditions. Nature Geoscience 6, 971-975.
Shi, L., Lu, W., Kagoshima, T., Sano, Y., Gao, Z., Du, Z., Liu, Y., Fei, Y., Li, Y., 2022. Nitrogen isotope evidence for Earth's heterogeneous accretion of volatiles. Nature Communications 13, 4769.

Shimizu, K., Saal, A.E., Hauri, E.H., Perfit, M.R., Hékinian, R., 2019. Evaluating the roles of melt-rock interaction and partial degassing on the CO2/Ba ratios of MORB: Implications for the CO2 budget in the Earth's depleted upper mantle. Geochimica et Cosmochimica Acta 260, 29-48.

Shimizu, K., Saal, A.E., Hauri, E.H., Sinton, J.M., Janney, P.E., Geshi, N., Hékinian, R., 2023. High-C content and CO2/Ba ratio of the Earth's enriched upper mantle. Geochimica et Cosmochimica Acta 343, 161-179.

Shimizu, K., Saal, A.E., Myers, C.E., Nagle, A.N., Hauri, E.H., Forsyth, D.W., Kamenetsky, V.S., Niu, Y., 2016. Two-component mantle melting-mixing model for the generation of mid-ocean ridge basalts: Implications for the volatile content of the Pacific upper mantle. Geochimica et Cosmochimica Acta 176, 44-80.

Simons, K., Dixon, J., Schilling, J.-G., Kingsley, R., Poreda, R., 2002. Volatiles in basaltic glasses from the Easter-Salas y Gomez seamount chain and easter microplate: implications for geochemical cycling of volatile elements. Geochemistry Geophysics Geosystems 3.

Sleep, N.H., Zahnle, K., 2001. Carbon dioxide cycling and implications for climate on ancient earth. Journal of Geophysical Research 106, 1373-1399.

Smythe, D.J., Wood, B.J., Kiseeva, E.S., 2017. The S content of silicate melts at sulfide saturation: New experiments and a model incorporating the effects of sulfide composition. American Mineralogist 102, 795-803.

Sobolev, A.V., Chaussidon, M., 1996. H_2O concentrations in primary melts from supra-subduction zones and mid-ocean ridges: Implications for H_2O storage and recycling in the mantle. Earth and Planetary Science Letters 137, 45-55.

Spandler, C., Yaxley, G., Green, D., Scott, D., 2010. Experimental phase and melting relations of metapelite in the upper mantle: implications for the petrogenesis of intraplate magmas. Contributions to Mineralogy and Petrology doi:10.1007/s00410-00010-00494-00412.

Spilliaert, N., Métrich, N., Allard, P., 2006. S–Cl–F degassing pattern of water-rich alkali basalt: Modelling and relationship with eruption styles on Mount Etna volcano. Earth and Planetary Science Letters 248, 772-786.

Stagno, V., Aulbach, S., Redox Processes Before, During, and After Earth's Accretion Affecting the Deep Carbon Cycle, Magma Redox Geochemistry, 2021, pp. 19-32.

Stagno, V., Frost, D.J., McCammon, C.A., Mohseni, H., Fei, Y., 2015. The oxygen fugacity at which graphite or diamond forms from carbonate-bearing melts in eclogitic rocks. Contributions to Mineralogy and Petrology 169, 16.

Stagno, V., Ojwang, D.O., McCammon, C.A., Frost, D.J., 2013. The oxidation state of the mantle and the extraction of carbon from Earth's interior. Nature 493, 84-88.

Stalder, R., 2004. Influence of Fe, Cr and Al on hydrogen incorporation in orthopyroxene. European Journal of Mineralogy 16, 703 - 711.

Stalder, R., Skogby, H., 2002. Hydrogen incorporation in enstatite. European Journal of Mineralogy 14, 1139-1144.

Stolper, E., 1982. The speciation of water in silicate melts. Geochimica et Cosmochimica Acta 46, 2609-2620.

Stolper, E., Asimow, P., 2007. Insights into mantle melting from graphical analysis of one-component systems. American Journal of Science 307, 1051-1139.

Stroncik, N.A., Haase, K.M., 2004. Chlorine in oceanic intraplate basalts: Constraints on mantle sources and recycling processes. Geology 32, 945-948.

Sun, C., Dasgupta, R., 2019. Slab-mantle interaction, carbon transport, and kimberlite generation in the deep upper mantle. Earth and Planetary Science Letters 506, 38-52.
Sun, C., Dasgupta, R., 2020. Thermobarometry of CO2-rich, silica-undersaturated melts constrains cratonic lithosphere thinning through time in areas of kimberlitic magmatism. Earth and Planetary Science Letters 550, 116549.
Sun, C., Dasgupta, R., 2023. Carbon budget of Earth's deep mantle constrained by petrogenesis of silica-poor ocean island basalts. Earth and Planetary Science Letters 611, 118135.
Sun, Z., Xiong, X., Wang, J., Liu, X., Li, L., Ruan, M., Zhang, L., Takahashi, E., 2020. Sulfur abundance and heterogeneity in the MORB mantle estimated by copper partitioning and sulfur solubility modelling. Earth and Planetary Science Letters 538, 116169.
Taracsak, Z., Hartley, M. E., Burgess, R., Edmonds, M., Iddon, F., Longpré, M.A., 2019. High fluxes of deep volatiles from ocean island volcanoes: Insights from El Hierro, Canary Islands. Geochimica et Cosmochimica Acta 258, 19-36.
Tenner, T.J., Hirschmann, M.M., Humayun, M., 2012. The effect of H_2O on partial melting of garnet peridotite at 3.5 GPa. Geochem. Geophys. Geosyst. 13, Q03016.
Till, C., Grove, T., Withers, A., 2012. The beginnings of hydrous mantle wedge melting. Contributions to Mineralogy and Petrology 163, 669-688.
Trail, D., Watson, E.B., Tailby, N.D., 2011. The oxidation state of Hadean magmas and implications for early Earth's atmosphere. Nature 480, 79-82.
Tsuno, K., Dasgupta, R., 2011. Melting phase relation of nominally anhydrous, carbonated pelitic-eclogite at 2.5-3.0 GPa and deep cycling of sedimentary carbon. Contributions to Mineralogy and Petrology 161, 743-763.
Tsuno, K., Dasgupta, R., 2012. The effect of carbonates on near-solidus melting of pelite at 3 GPa: Relative efficiency of H_2O and CO_2 subduction. Earth and Planetary Science Letters 319–320, 185-196.
Tsuno, K., Dasgupta, R., 2015. Fe–Ni–Cu–C–S phase relations at high pressures and temperatures – The role of sulfur in carbon storage and diamond stability at mid- to deep-upper mantle. Earth and Planetary Science Letters 412, 132-142.
Tsuno, K., Grewal, D.S., Dasgupta, R., 2018. Core-mantle fractionation of carbon in Earth and Mars: The effects of sulfur. Geochimica et Cosmochimica Acta 238, 477-495.
Tucker, J.M., Hauri, E.H., Pietruszka, A.J., Garcia, M.O., Marske, J.P., Trusdell, F.A., 2019. A high carbon content of the Hawaiian mantle from olivine-hosted melt inclusions. Geochimica et Cosmochimica Acta 254, 156-172.
Tucker, J.M., Mukhopadhyay, S., Gonnermann, H.M., 2018. Reconstructing mantle carbon and noble gas contents from degassed mid-ocean ridge basalts. Earth and Planetary Science Letters 496, 108-119.
Ulmer, P., 2001. Partial melting in the mantle wedge - the role of H_2O in the genesis of mantle-derived 'arc-related' magmas. Physics of the Earth and Planetary Interiors 127, 215-232.
van Hinsberg, V.J., Berlo, K., Migdisov, A.A., Williams-Jones, A.E., 2016. CO2-fluxing collapses metal mobility in magmatic vapou. Geochemical Perspectives Letters 2, 169-177.
von Aulock, F.W., Kennedy, B.M., Schipper, C.I., Castro, J.M., E. Martin, D., Oze, C., Watkins, J.M., Wallace, P.J., Puskar, L., Bégué, F., Nichols, A.R.L., Tuffen, H., 2014. Advances in Fourier transform infrared spectroscopy of natural glasses: From sample preparation to data analysis. Lithos 206-207, 52-64.

Wallace, M.E., Green, D.H., 1988. An experimental determination of primary carbonatite magma composition. Nature 335, 343-346.
Wallace, P. J. 1998. Pre-eruptive H_2O and CO_2 contents of mafic magmas from the submarine to emergent shield stages of Gran Canaria. In: Proceedings of the Ocean Drilling Program, Scientific Results, Weaver, P.P.E., Schmincke, H.-U., Firth, J. V., Duffield, W. (Eds.) 175, 411-420.
Wallace, P., Carmichael, I.S.E., 1992. Sulfur in basaltic magmas. Geochimica et Cosmochimica Acta 56, 1863-1874.
Wallace, P.J., 1998. Water and partial melting in mantle plumes: Inferences from the dissolved H2O concentrations of Hawaiian basaltic magmas. Geophysical Research Letters 25, 3639-3642.
Wallace, P.J., Carmichael, I.S.E., 1994. S speciation in submarine basaltic glasses as determined by measurements of SKα X-ray wavelength shifts. American Mineralogist 79, 161-167.
Wallace, P.J., Edmonds, M., 2011. The Sulfur Budget in Magmas: Evidence from Melt Inclusions, Submarine Glasses, and Volcanic Gas Emissions. Reviews in Mineralogy and Geochemistry 73, 215-246.
Wallace, P.J., Kamenetsky, V.S., Cervantes, P., 2015. Melt inclusion CO2 contents, pressures of olivine crystallization, and the problem of shrinkage bubbles. American Mineralogist 100, 787-794.
Wanamaker, B.J., Wong, T.-F., Evans, B., 1990. Decrepitation and crack healing of fluid inclusions in San Carlos olivine. Journal of Geophysical Research: Solid Earth 95, 15623-15641.
Wang, C., Hirama, J., Nagasaka, T., Ban-Ya, S., 1991. Phase Equilibria of Liquid Fe-S-C Ternary System. ISIJ International 31, 1292-1299.
Wang, W., Kelley, K.A., Li, Z., Chu, F., Dong, Y., Chen, L., Dong, Y., Li, J., 2021. Volatile Element Evidence of Local MORB Mantle Heterogeneity Beneath the Southwest Indian Ridge, 48°–51°E. Geochemistry, Geophysics, Geosystems 22, e2021GC009647.
Wanless, V.D., Behn, M.D., Shaw, A.M., Plank, T., 2014. Variations in melting dynamics and mantle compositions along the Eastern Volcanic Zone of the Gakkel Ridge: insights from olivine-hosted melt inclusions. Contributions to Mineralogy and Petrology 167, 1005.
Wanless, V.D., Shaw, A.M., 2012. Lower crustal crystallization and melt evolution at mid-ocean ridges. Nature Geoscience 5, 651-655.
Wanless, V.D., Shaw, A.M., Behn, M.D., Soule, S.A., Escartín, J., Hamelin, C., 2015. Magmatic plumbing at Lucky Strike volcano based on olivine-hosted melt inclusion compositions. Geochemistry, Geophysics, Geosystems 16, 126-147.
Watenphul, A., Wunder, B., Wirth, R., Heinrich, W., 2010. Ammonium-bearing clinopyroxene: A potential nitrogen reservoir in the Earth's mantle. Chemical Geology 270, 240-248.
Watson, B.E., 1991. Diffusion of dissolved CO2 and Cl in hydrous silicic to intermediate magmas. Geochimica et Cosmochimica Acta 55, 1897-1902.
Witham, F., Blundy, J., Kohn, S.C., Lesne, P., Dixon, J., Churakov, S.V., Botcharnikov, R., 2012. SolEx: A model for mixed COHSCl-volatile solubilities and exsolved gas compositions in basalt. Computers & Geosciences 45, 87-97.
Woodland, A.B., Girnis, A.V., Bulatov, V.K., Brey, G.P., Höfer, H.E., 2019. Experimental study of sulfur solubility in silicate–carbonate melts at 5–10.5 GPa. Chemical Geology 505, 12-22.

Workman, R.K., Hauri, E., Hart, S.R., Wang, J., Blusztajn, J., 2006. Volatile and trace elements in basaltic glasses from Samoa: Implications for water distribution in the mantle. Earth and Planetary Science Letters 241, 932-951.
Wykes, J.L., O'Neill, H.S.C., Mavrogenes, J.A., 2015. The Effect of FeO on the Sulfur Content at Sulfide Saturation (SCSS) and the Selenium Content at Selenide Saturation of Silicate Melts. J. Petrol. 56, 1407-1424.
Wyllie, P.J., 1978. Mantle Fluid Compositions Buffered in Peridotite-CO_2-H_2O by Carbonates, Amphibole, and Phlogopite. The Journal of Geology 86, 687-713.
Wysoczanski, R., Tani, K., 2006. Spectroscopic FTIR imaging of water species in silicic volcanic glasses and melt inclusions: An example from the Izu-Bonin arc. Journal of Volcanology and Geothermal Research 156, 302-314.
Yaxley, G.M., Ghosh, S., Kiseeva, E.S., Mallik, A., Spandler, C., Thomson, A.R., Walter, M.J., CO2-Rich Melts in Earth, in: B.N. Orcutt, I. Daniel, R. Dasgupta, (Eds), Deep Carbon: Past to Present, Cambridge University Press, Cambridge, 2019, pp. 129-162.
Yoshioka, T., Wiedenbeck, M., Shcheka, S., Keppler, H., 2018. Nitrogen solubility in the deep mantle and the origin of Earth's primordial nitrogen budget. Earth and Planetary Science Letters 488, 134-143.
Zedgenizov, D.A., Ragozin, A.L., Shatsky, V.S., 2007. Chloride-carbonate fluid in diamonds from the eclogite xenolith. Doklady Earth Sciences 415, 961-964.
Zhang, Y., Zindler, A., 1993. Distribution and evolution of carbon and nitrogen in Earth. Earth and Planetary Science Letters 117, 331-345.
Zhang, Z., Hastings, P., Von der Handt, A., Hirschmann, M.M., 2018. Experimental determination of carbon solubility in Fe-Ni-S melts. Geochimica et Cosmochimica Acta 225, 66-79.
Zhang, Z., Hirschmann, M.M., 2016. Experimental constraints on mantle sulfide melting up to 8 GPa. American Mineralogist 101, 181-192.
Zhang, Z., Lentsch, N., Hirschmann, M.M., 2015. Carbon-saturated monosulfide melting in the shallow mantle: solubility and effect on solidus. Contributions to Mineralogy and Petrology 170, 47.
Zhang, Z., Qin, T., Pommier, A., Hirschmann, M.M., 2019. Carbon storage in Fe-Ni-S liquids in the deep upper mantle and its relation to diamond and Fe-Ni alloy precipitation. Earth and Planetary Science Letters 520, 164-174.